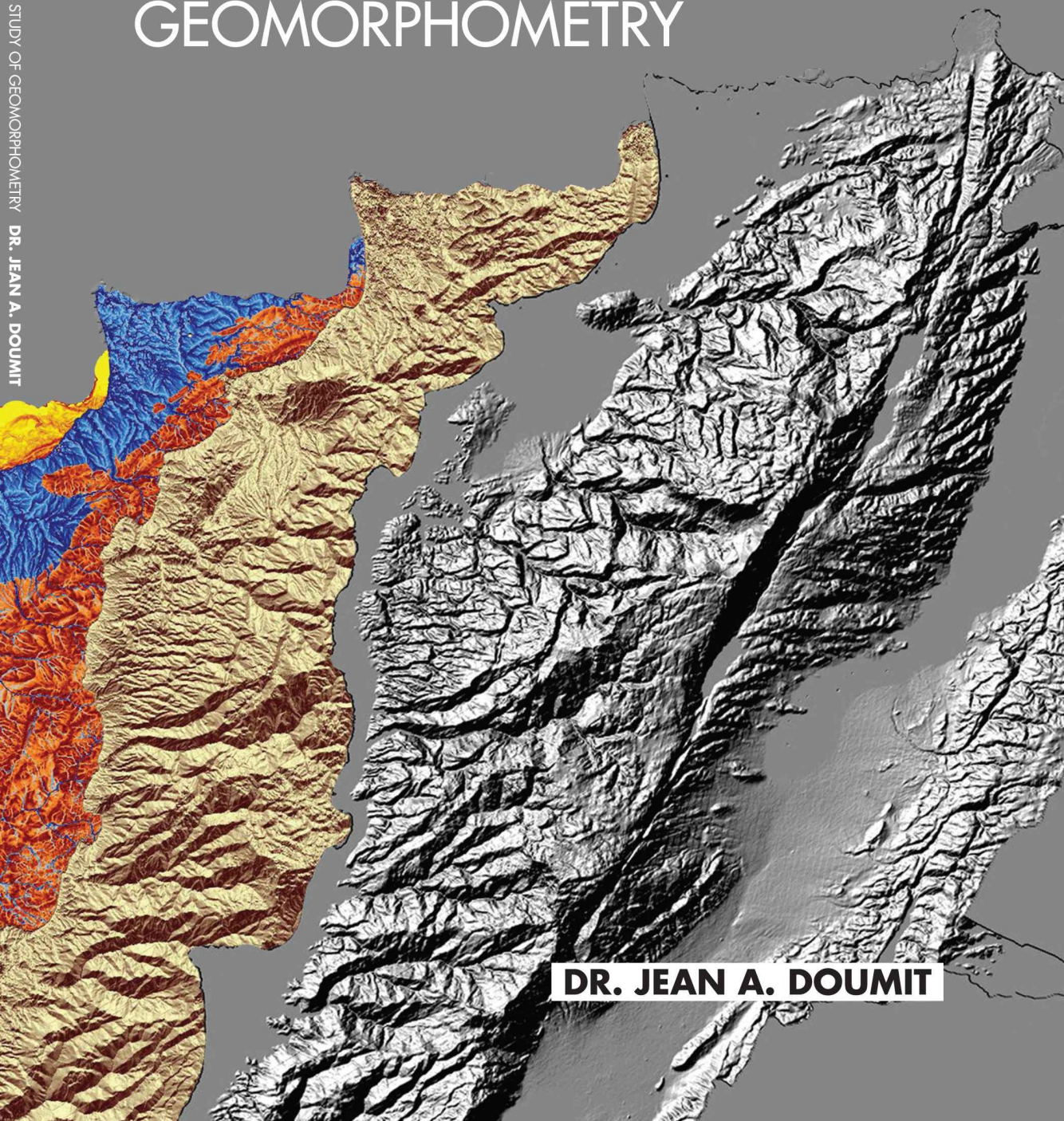


# DIGITAL TERRAIN ANALYSIS OF LEBANON: A STUDY OF GEOMORPHOMETRY



**DR. JEAN A. DOUMIT**

Lebanese University  
Kuban State University

# **Digital Terrain Analysis of Lebanon: A Study of Geomorphometry**

**Dr. Jean A. Doumit**

Reviewed by Prof. Dr. Anatoly V. Pogorelov

2017

УДК 551.4(1/9)

**Jean A. Doumit**

Digital Terrain Analysis of Lebanon: A Study of Geomorphometry. – Krasnodar: Kuban State University, 2017. – 161 p. – 150 copies.

This book present the results of Lebanese terrain quantitative analysis based on digital models. Terrain analysis applied for the extraction and analysis of geomorphological elements from digital elevation models. Shuttle Radar Topography Mission (SRTM) and Global Digital Elevation Map (GDEM) are used for GIS linear and areal morphological structure analysis and discretization of the Earth's surface according to its curvature with the extraction of primary terrain morphological elements.

Methods and results of this book enlarge the possibilities of subsequent genetic, historic and geodynamic terrain interpretations by applying Geographical Information Systems (GIS) and Digital Elevation Models (DEM) and their uses in geosciences.

УДК 551.4(1/9)  
© Doumit J.A., 2017

## **Acknowledgements**

This book is dedicated to all Geomatics Engineers and Earth Scientists, of which three must be singled out for special mention: Professor Pogorelov Anatoly Valerievich as the best scientific advisor, the department of Geoinformatics at Kuban State University (Russia), and the department of Geography at the Lebanese University.

I would also like to express my gratitude to all who helped me take this book from a vision to an actualization, especially my parents for their constant support.

## Preface

Terrain analysis or geomorphometry is a process to extract and measure the forms of the land surface. Such measurements and forms have found wide applications since the origin of Digital mapping and especially Digital Models. This has been the case across various disciplines such as mapping, remote sensing, civil engineering, geology, geomorphology, military engineering, land planning, and communications. It is encouraging that more literature is now available in this discipline. This book was written with the intention to add to and benefit this field of study.

I am pleased to present you with this 1st edition of this book. This study is a terrain analysis of the Lebanese territory. It studies the disclosure of morphological terrain structure, based on Digital Elevation Models. In its nine chapters, this book carries out several tasks: the comparison between two digital elevation models, morphological structure analysis of the Lebanese territory by extraction of terrain structural lines, estimation of fractal dimensions, and the calculation of morphometric parameters. All the results are new on the merits for the Lebanese territory, with GIS database creation, containing the raw data derived from digital models of structural lines and morphometric variables. There is also calculation of statistical indicators of morphometric variable distribution and a discretization of the Earth's surface according to its curvature with the extraction of primary terrain morphological elements. The purpose of this study is to help and guide students in their research, and introduce them to digital models and their uses in geosciences. Digital models adopted by GIS technology can lead to a treasure of information. My message to the readers is: "Use new technology".

## Introduction

People have lived on Earth, and have learned to cope with its terrain. Civil engineers design and erect buildings on it, geologists try to study its underlying construction, and geo-morphologists find interest in its shape and the processes by which the landscape was formed. Topographic scientists are more concerned with measuring and describing the land's surface and presenting it in various ways. These listed specialists have a common interest, which is the desire the surface of the terrain be represented conveniently and with certain accuracy. Essentially, a map is a scientific generalization and abstraction of features on a terrain. Since the middle of the 20th century, various digital terrain representation techniques have been developed, along with the development of computing technology, modern mathematics, and computer graphics. Nowadays, the use of the computer has become a significant landmark in the era of information. Indeed, computers have become an important means for the representation of digital terrain surface.

Geomorphometry is the science of quantitative land-surface analysis (Pike, 2000). It is a modern, analytical-cartographic approach to representing earth topography by the computer manipulation of terrain elevations (Tobler, 1976, 2000). Geomorphometry is an interdisciplinary field that has evolved from mathematics, Earth computer sciences (Figure 1). Although geomorphometry ranges from geography and geomorphology to soil science and military engineering, it is no longer just a collection of numerical techniques but an important discipline (Pike, 1995).

We can see from Figure 1 that geomorphometry could be the source of environmental and earth sciences. In this book, geomorphometry is primarily the computer characterization and terrain analysis of the Lebanese territory. It is inextricably linked with geoinformatics, various branches of engineering, and most of the earth and environmental sciences (Figure 1). Geomorphometry is the science of quantitative land-surface analysis. A mix of earth and computer science, engineering, and mathematics, it is a new field paralleling analytical cartography and GIS. It evolved directly from geomorphology and quantitative terrain analysis. Terrain analysis is not only associated with land form, hydrographic features, soil, vegetation, and geology but also with the socio-economic aspects of an area (Li et al., 2005).

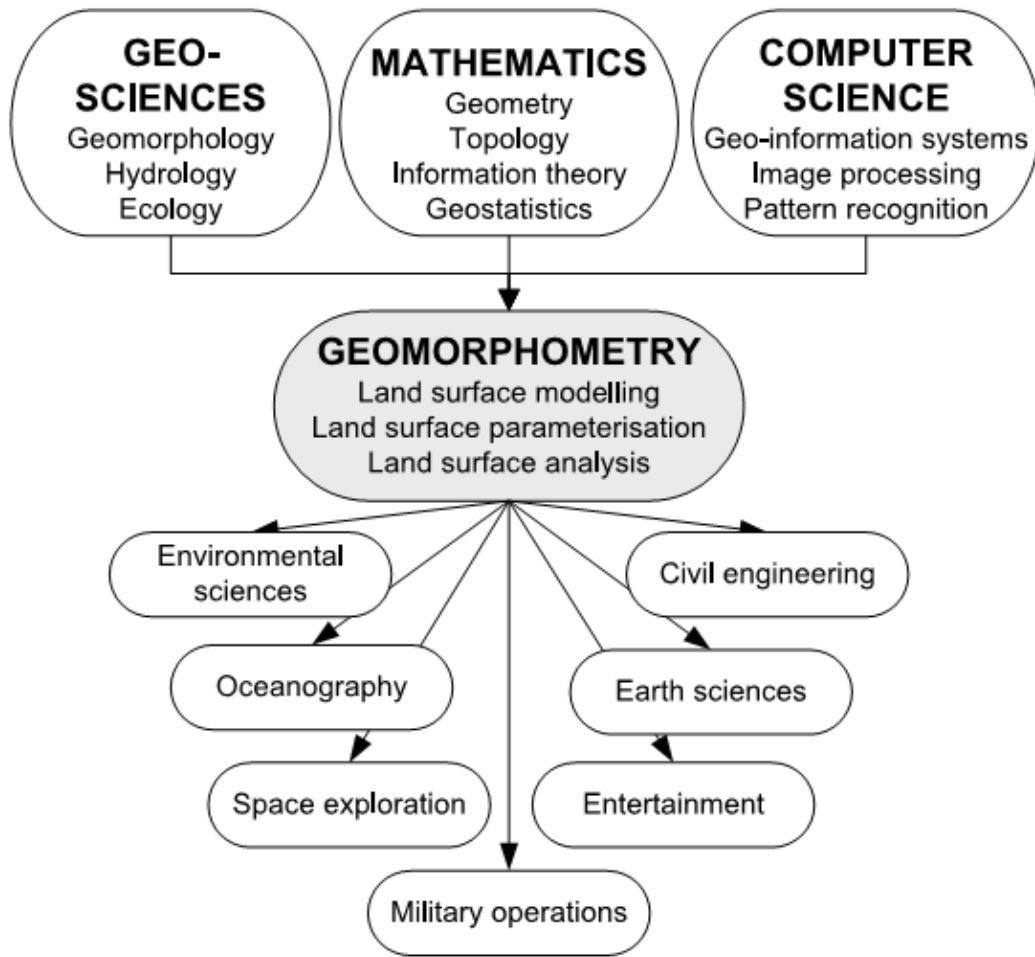


**Figure 1** *Geomorphometry and Its Relation to Other Disciplines* (Pike, 1995)

Digital elevation model (DEM) is the main data most commonly input to geomorphometry. In this book, DEM refers to a gridded set of points in Cartesian space attributed with elevation values that approximate Earth's ground surface to define parameter and object. Derived from DEM, land surface parameters are a descriptive measurement of the surface form (e.g. slope, aspect, curvature etc...) these quantities can be obtained from a DEM by a series of mathematical operations, or morphometric algorithms. In this study, a somewhat different classification, that reflects the purpose and type of analysis will be followed.

Digital terrain surfaces can be represented mathematically and graphically.

A mathematical model represents a situation, object, or phenomenon in mathematical terms. In other words, a mathematical model is a model whose components are mathematical concepts, such as constants, variables, functions, equations, inequalities, etc. Terrain models have always appealed to military

personnel, planners, landscape architects, civil engineers, as well as other experts in various earth sciences. The term terrain means different things to specialists in different areas and so does the term Digital Elevation Model (DEM). Our ancestors studied the globe terrain from topographic maps, with the evolution of science and technology, and the appearance of Geographical Information Systems (GIS), remote sensing and photogrammetry. This technology provides us with a very powerful generator of terrain analysis such as elevation, slope, slope form, and other more complicated geomorphological features that are used to depict relief of a terrain, such as hydrographic features.

All this geographical data was very difficult to process with only topographic maps and without computers. This is why I was inspired to write a book about terrain analysis and provide structural analysis to help students and specialists better understand the earth terrain and the best ways to deal with it.

In Lebanon, and in several other countries, there is a scarcity of geographical data for analysis and studies. In this book, a solution has been found for this problem, which involves integrating DEM free of charge from the internet in a GIS system to create a very huge geomorphological and hydrological database which constitutes a foundation base for both applied and theoretical research.

Not knowing the earth surface morphology, consequently, makes it impossible to quantitatively validate the terrain contribution to the geofield and landscape region structure. Moreover, Lebanese territory represents special geomorphologic properties, which make it an ideal focus of study and analysis.

Earth surface terrain is generally a main object of geomorphology. The subject of this book is a terrain analysis of the Lebanese territory, under which it is understood that there is some procedure of change of terrain conditions, defined as a combination of its elements and their appropriate geometric forms. Terrain analysis has been sustained by procedure ‘discretization’ of the terrain surface by means of extraction of its elementary parts. The aim of this study is the disclosure of morphological terrain structure of the Lebanese territory, based on digital techniques. To achieve this aim, several tasks were carried out:

- To make a comparison between two digital elevation models, Shuttle Radar Topographic mission (SRTM) and ASTER Global Digital Elevation Model (ASTER GDEM), for the morphological structure analysis of the Lebanese territory.
- To build a model of structural lines of the Lebanese terrain (thalwegs and watersheds) for the analysis of ‘horizontal’ and ‘vertical’ relations between the components of the river system.
- To estimate the parameters of the fractal dimension of erosion network elements.

- To build a model of the erosion network with the list of thalwegs corresponding to DEM spatial precision.
- To execute the automated calculation of the standard morphometric parameters (hypometry, slope and aspects, stream density and relief energy) according to the data of DEM and to map these parameters.
- On the basis of morphometric variables to analyze the morphological structure of the terrain – using statistical methods of data processing.

To calculate and analyze the spatial distribution of curvature parameters of the earth surface with following discretization of the surface – structural element extraction as a form of morphologically uniform terrain.

The methodological basis of this book lie in the works of Russian geomorphology school representatives (A.N. Lastochkin, Y.G. Simonov, A.I. Spiridonov, D.A. Timofeev, G.F. Ufimtsev, N.A. Florencov, P.A. Sharyi et al.). The theories of geo-informatics and digital elevations are based on the following: A.M. Berlyant, I.K. Lurie, V.S. Tikunov, A.V. Koshkarev, B.A. Nowakowski and al. In preparation of the general methodological approaches of this book, I have relied on works of A.G. Isachenko, Y.G. Puzachenko, E.G. Kolomyca and other authors. Conceptually, this book is based on a ‘geometric approach’ in earth surface description, better known in English as geomorphometry, quantitative morphology, and quantitative terrain analysis.

The description of morphological structure has been carried out by calculating and mapping the variables in a Geographic Information System (GIS). With that, there was the usage of general and specific methods of geo-informatics, oriented to solve the tasks of morphometric analysis, using statistical methods, including geostatistical approaches. The main software used in the research includes ArcGIS (ESRI Inc., USA), SAGA (Germany), and MicroDEM (USA). The listed software supports a versatility of terrain analysis algorithms, which greatly reduces the complexity of the study.

In this, monography, new approaches in regional geomorphological analysis have been implemented, with a focus on complex calculations of morphometric changes according to the DEM in a GIS environment. Methodological novelty lies in the development and application of algorithms for automated calculation, and mapping morphometric parameters and morphological elements. All the results of terrain analysis of the Lebanese territory are new on the merits. Among them:

1. GIS data base creation, containing the raw data derived from digital models of structural lines and morphometric variables, calculation algorithms, the results of statistical processing sets of variables in the form of tables and charts, as well as other related materials.

2. Hypsometric analysis of the Lebanese territory.

3. Construction of models of structural lines of the Earth's surface, mapping morphometric parameters (slope, aspect, stream density, relief energy, curvature of the earth's surface, fractal dimension, etc.).

4. Calculation of statistical indicators of morphometric variable distribution in Lebanese territory, and their interpretation in terms of their impact on surface flow.

5. A comparative analysis of the terrain morphological structure of watersheds, according to an erosion network model (thalwegs different order), distribution of plan and profile curvature, the elementary forms of the surface, morphological elements and fractal dimension.

6. Discretization and proper sampling of the Earth's surface according to its curvature, and extraction of primary terrain morphological elements.

# Chapter 1: Digital Elevation Modeling

People are interested in the place where they live. Geologists study the layers of the earth, geo-morphologists are interested in its shape, architects and civil engineers design and construct buildings on it, and topographic scientists are concerned with measuring and describing its surface and presenting it in different ways. Despite these differences in expertise and interest, these specialists intend the surface of the terrain to be represented conveniently and with certain accuracy. Maps have played as important a role in the development of society and they have been used to represent the environments during the history of civilization. Modern maps employ a well-designed symbol system and a well-established mathematical basis for representation so that they possess a very powerful tool for deriving thematic maps. The introduction of mathematical, numerical, and digital techniques to terrain modeling owes much to the activities of photogrammetrists. C. Miller and R. Laflamme (1958) of Massachusetts Institute of Technology (MIT) introduced the concept of the digital terrain model. The definition given by them is as follows: «The digital terrain model (DTM) is simply a statistical representation of the continuous surface of the ground by a large number of selected points with known X, Y, Z coordinates in an arbitrary coordinate field» (Li et al., 2005).

Compared to traditional analog representation, a DTM has the following specific features:

1. A variety of representation forms – Various forms of representations can be easily produced digitally, such as topographic maps, vertical and cross sections, and 3-D animation.
2. No accuracy loss of data over time – As time goes by, paper maps may be deformed, but the DTM can keep its precision owing to the use of digital medium.
3. Greater feasibility of automation and real-time processing – In digital form, data integration and updating are more flexible than in analog form.
4. Multi-scale representation – DTM can be arranged in different resolutions, corresponding to representations at different scales.

Despite its obvious advantages as listed above, these advantages offset at least three disadvantages. The size of the grid mesh will often affect the storage requirements. Square grids will often skip important details of the land surface in flat areas (Moore et al., 1991). The computed upslope flow paths will tend to zigzag across the landscape and increase the difficulty of calculating specific catchment areas accurately (Zevenbergen and Throne, 1987; Moore et al., 1991). The effective use of Digital Elevation Models, however, requires more effort than

the interpretation of traditional paper maps. Just as terrain information extraction from a contour map requires the techniques of map reading, interpretation, and measurement, deriving terrain features and measurements from a DEM also demands information extraction methods and techniques based on digital representation of the terrain. Most of the currently available digital elevation data sets are the product of photogrammetric data capture (Moore et al., 1991). These sources rely on the stereoscopic interpretation of aerial photographs, satellite, or by digitizing contour lines on topographic maps and conducting ground survey. This digital elevation data is usually organized into one of three data structures: regular grids, triangulated irregular networks, and contours depending on the preferred method of analysis.

Digital elevation models are an accepted and widespread method of modelling the ground surface topography or terrain that provide quantitative elevation data for many applications in topographic and landcover studies, geomorphology, etc., at both large and small scales (Miliaresis, 2008; Kokkas, 2007).

Surveyors study DTM from the viewpoint of terrain representation and are especially interested in the topography of and objects in the terrain. Specialists in other geosciences combine the non-topographic information with topographic information to construct the DTM according to their own specific needs. For example, C. Miller and R. Laflamme (1958) used the DTM in highway design. Generally, from a DTM we could extract the following four groups of:

1. Landforms, such as elevation, slope, slope curvature, aspect, and the other more complicated geomorphological features.
2. Terrain features, such as hydrographic features (i.e. rivers, lakes, coast lines), transportation networks (i.e. roads, railways, paths), settlements, boundaries, etc.
3. Natural resources and environments, such as soil, vegetation, geology, climate, etc.
4. Socioeconomic data, such as the population distribution in an area, industry, agriculture, and capital income, etc.

Digital models of topographic elevation data form an integral part of geographic information systems (GIS) and are most often used for: hydrological modeling, delineation and analysis of watersheds and drainage networks, soil erosion, sediment transportation modeling, geomorphological evaluation of landforms, civil engineering and military applications, visibility analysis, and 3D analysis. Digital elevation models provide an opportunity to characterize, quantitatively, land surface in terms of slope gradient and curvature. Analysis of directional aspect data is crucial in image processing, hydrology, and climatic

studies. Image analysis methods are often applied to grey-scale terrain models, thus losing the inherent geometric information of digital terrain models (Simpson and Anders, 1992). Accordingly, available software designed for the specific needs of each field of study in many cases does not offer all the operations required for consistent digital terrain analysis. GIS software can easily perform most of the analyses, digital terrain analysis requires the use of an integrated system of many analytical and software tools. The objective of this study is to present some basics for consistent use of digital terrain analysis methods in a GIS environment.

Digital elevation model (DEM) has become the key input to geomorphometry, ever since the United States Geological Survey (USGS) first began distribution of 3-arc-second DEMs in 1974 (Allder et al., 1982). In this book, DEM refers to a gridded set of points with elevation values that approximate Earth's ground surface.

Finally, we define parameter and object, derived from DEM – entities fundamental to modern geomorphometry (Mark and Smith, 2004). A land surface parameter is a descriptive measure of surface form (e.g. slope, aspect, wetness index) and a discrete spatial feature (e.g. watershed line, drainage network), represented by raster images or vector maps. Geomorphometry is commonly implemented in five steps:

1. Sampling the land surface (height measurements).
2. Generating a surface model from the sampled heights.
3. Correcting errors and artifacts in the surface model.
4. Deriving land-surface parameters and objects.
5. Applying the resulting parameters and objects.

DEMs provide either bare earth (ground) – termed as digital terrain models (DTMs) – or elevations with respect to the reflective surface, which may be vegetation, human-made features, etc. – termed as digital surface models (DSMs). DEMs have been used, and are currently in use, within a great number of applications, from drainage modeling (Niemann, 1991) to improving classification of remotely sensed imagery (Warner et al., 1994). Indeed, work describing the use of DEMs for improving image classification has been available for at least the last two decades (Hutchinson, 1982).

The DSM elevations are more accurate, containing data which may be vegetation, human-made features, etc., as well as several additional substantial editing steps (e.g. filling voids, modifying elevations over oceans, lakes, and lake islands) (Slater et al., 2006).

With all digital geospatial data sets, users must be aware of certain characteristics of the data, such as resolution, accuracy, method of production and any resulting artifacts, in order to better judge its suitability for a specific

application. A characteristic of the data that renders it unsuitable for one application may have no relevance as a limiting factor for its use in a different application (NASA/JPL, 2005). The region of study covers the Lebanese country, Southwest Asia, bounded by the Mediterranean Sea (W), Syria (N, E), and occupied Palestine (S). The Shuttle Radar Topography Mission (SRTM) and the Advanced Spaceborne Thermal Emission and Reflection Radiometer (ASTER) Global Digital Elevation Model (GDEM) datasets provides DSM elevation data for the majority of Earth's land surface (Rodriguez, Morris, Belz, 2006).

## 1.01 Shuttle Radar Topography Mission (SRTM)

The Space Shuttle Endeavour during an 11-day mission in February of 2000, known as "Shuttle Radar Topography Mission (SRTM)", obtained elevation data on a near-global scale (between  $60^{\circ}$  N and  $56^{\circ}$  S latitude) (T.G. Farr and Kobrick 2009). It produced digital topographic data on a 3 arc-second grid, which roughly translates to a 90-meter horizontal spatial resolution and an absolute horizontal and vertical accuracy is given as equal to 20 meters (circular error at 90% confidence) and 16 meters (linear error at 90% confidence) respectively (Finished SRTM data).

The SRTM finished DSM of the study area is given in geographic coordinates (using as horizontal datum the WGS84 ellipsoid). The SRTM DSM grid values are provided in terms of orthometric heights with respect to the geoid model computed from the EGM96 geopotential model (NASA/JPL, 2005).

Since SRTM data became widely available, many studies have utilized them for applications in topography (Falorni et al., 2005; Koch and Lohmann, 2000), geomorphology (Guth, 2003; Stock et al., 2002; Pogorelov, Doumit, 2008), vegetation cover studies (Kellndorfer et al., 2004), and urban studies (Gamba et al., 2002). SRTM data verification was performed using various altimetry data (Helm et al., 2002; Sun et al., 2003) and digital elevation models (Jarvis et al., 2004; Muller, 2005; Smith and Sandwell, 2003).

The Digital Elevation Model that has been derived from the February 2000 Shuttle Radar Topography Mission (SRTM) has been one of the most important publicly available new spatial data sets. However, the 'finished' grade version of the data (also referred to as Version 2) contains regions of no-data (voids), specifically over large water bodies such as lakes and rivers, and in areas where radar-specific problems prevented the production of reliable elevation data (Figure 1.1). These areas include mountainous regions where the radar shadow effect is prominent, such as the Himalayas and Andes, as well as certain land surfaces, such as bare sand or rock conditions as found in the Sahara Desert. SRTM data produced a number of gaps which due to lack of contrast in the radar image, a methodology

based on spatial filtering was developed to correct this phenomenon (Dowding et al., 2004; Jarvis et al., 2004).

The SRTM data sets of Lebanon at 33 to 34 degree Northing and 35 to 36 degree Easting produced a number of voids at mountainous zones with a total area of 23 square kilometers inside the Lebanese boundary (Figure 1.1).

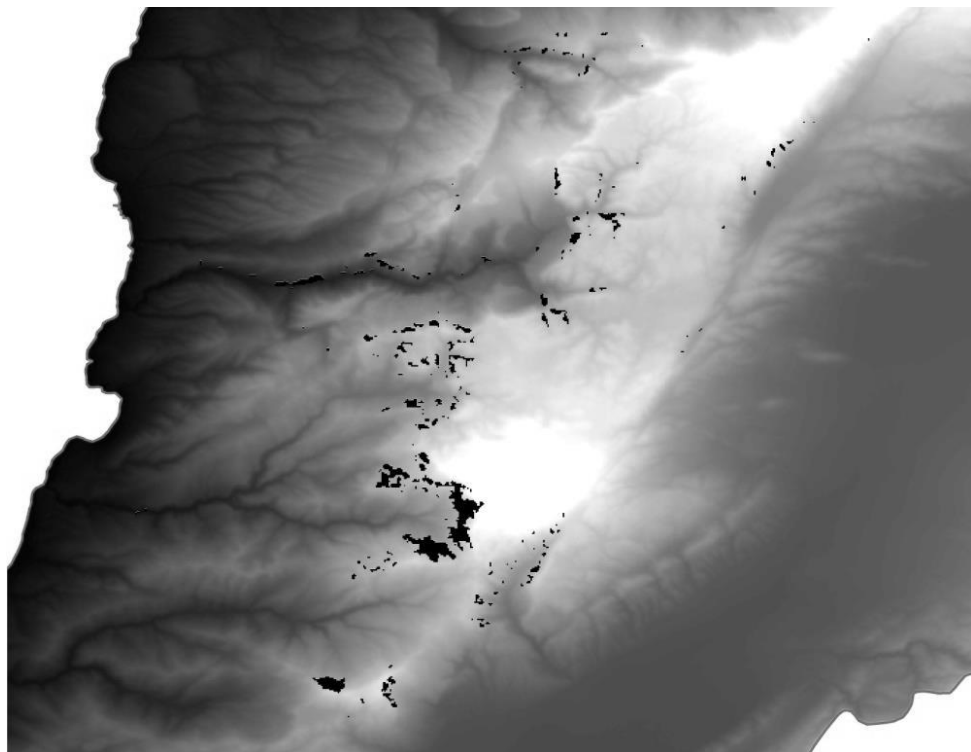


**Figure 1.1** SRTM DSM of the Lebanese Territory  
(with dark areas corresponding to voids)

The gaps occur in various places, most often in areas where data has only been recorded once or very few times. This is mostly the case in regions near the equator – places where the surface material apparently results in very low radar reflectance. This seems to be especially the case in sand deserts and water surfaces, as well as areas with steep slopes like high mountain regions and deep valleys. These voids can be filled using a range of interpolation algorithms in conjunction with other sources of elevation data. This obviously leads to huge inaccuracies in areas with large height differences in the data voids. Another possible solution is to fill the voids with data from other sources. This, however, only leads to usable results if the data is of comparable quality. The widely used GTopo30 hardly leads to better results than simple interpolation.

An alternative way to fill voids is to use computer tools and scripts like “SRTM Fill” and “Voids Killer” which use the automatic interpolation method between datasets. These methods cannot give an accurate solution thus they are usually used to enhance the visualization of the relief. They can be used in geographical analysis only in the case of short interpolation distance or to fill voids with small dimensions.

Algorithm can patch moderate-sized NULL holes in flat or sloping terrain. It cannot, however, replace features that are entirely missing, such as putting back an entire mountain. Large areas of NULL data will be filled with data interpolated from their surrounding edges, which may create unpleasant streaks or platforms in the resulting data.

There is little guidance available on the most appropriate void-filling method. Contrary to some previous findings, the best methods can actually be generalized, such as: kriging or inverse distance weighting interpolation for small and medium size voids in relatively flat low-lying areas, spline interpolation for small and medium-sized voids in high-altitude and dissected terrain, triangular irregular network or inverse distance weighting interpolation for large voids in very flat areas, and an advanced spline method for large voids in other terrains (Reuter, Nelson, Jarvis, 2007). The final seamless SRTM dataset with voids filled in, known as version 4, which we used in our study, is available at the website of Consultative Group for International Agriculture Research Consortium for Spatial Information. This latest version represents a significant improvement from previous versions, using new interpolation algorithms and better auxiliary DEM's. The CGIAR-CSI are confident that this is now the highest quality SRTM dataset<sup>1</sup>.

Dr. Andy Jarvis and Edward Guevara of the CIAT Agroecosystems Resilience project, Dr. Hannes Isaak Reuter (JRC-IES-LMNH) and Dr. Andy Nelson (JRC-IES-GEM) have further processed the original DEMs to fill in these no-data voids. This involved the production of vector contours and points, and the re-interpolation of these derived contours back into a raster DEM. These interpolated DEM values are then used to fill in the original no-data holes within the SRTM data. These processes were implemented using Arc/Info and an AML script<sup>2</sup>.

The SRTM dataset version 4 of the Lebanese territory contains areas or pixels of negative value, which need a correction. By applying some geospatial methods, we arrived at resolving the problem without affecting the resolution of the datasets. After the conversion of the DEM into points of elevation and removing

---

<sup>1</sup> Available via <http://srtm.cgiar.org/>

<sup>2</sup> <http://srtm.cgiar.org>

the negative value, an interpolation was done to build a new dataset empty of artifacts.

## 1.02 Global Digital Elevation Map (GDEM)

The topography of the land surface is one of the most fundamental geophysical measurements of the Earth, and it is a dominant controlling factor in virtually all physical processes that occur on the land surface. Topography of the land surface also significantly controls processes within the overlying atmosphere, and it reflects the processes within the underlying lithosphere. Consequently, topographic information is important across the full spectrum of earth sciences and the availability of an up-to-date, high resolution (1-arc-sec or less) global DEM has been a priority for earth scientists for a long time. The ASTER GDEM, with 30 meter grid postings and produced from a consistent primary data source, is expected to meet the requirements of many users for global topographic information.

The Ministry of Economy, Trade, and Industry (METI) of Japan and the United States National Aeronautics and Space Administration (NASA) released Version 1 of the Advanced Space borne Thermal Emission and Reflection Radiometer (ASTER) Global Digital Elevation Model (GDEM). The methodology used to produce the ASTER GDEM involved automated processing of the entire 1.5-million-scene ASTER archive, including stereo-correlation to produce 1,264,118 individual scene-based ASTER DEMs, cloud masking to remove cloudy pixels, stacking all cloud-screened DEMs, removing residual bad values and outliers, averaging selected data to create final pixel values, and then correcting residual anomalies before partitioning the data into  $1^0$ -by- $1^0$  tiles. It is referenced to as the WGS84/EGM96 geoids. In June 2009, the first version of ASTER GDEM was announced<sup>3</sup>.

Pre-production estimated accuracies for this global product were 20 meters at 95% confidence for vertical data and 30 meters at 95% confidence for horizontal data (ASTER GDEM 2009) with a standard deviation of 18 meters for the test area with outliers, predominately found in the areas of complex terrain rather than in the valley floors. It also recorded a -2.3 meter shift of re-projection artifacts and the artifacts that are clearly related to linear and curvilinear boundaries between different stacks. Such artifacts appear as straight lines, pits, bumps, mole runs, and other geometric shapes. Anomalous elevations associated with these artifacts can range from 1 meter or 2 meters to more than 100 meters. It will be worth checking

---

<sup>3</sup> [www.ersdac.or.jp](http://www.ersdac.or.jp)

if SRTM data (90 m) could help to identify and remove the spikes from the DEM. The CGIAR-CSI SRTM-DEM Version 4 might better suit ones needs until the ASTER GDEM is improved (<http://technology.slashgeo.org>).

Statistically, the GDEM appears to generally meet its pre-production estimated vertical accuracy of  $\pm 20\text{m}$  at 95% confidence. The ASTER GDEM contains anomalies and artifacts that will reduce its usability for certain applications, because they can introduce large elevation errors on local scales. However, in spite of its flaws, the GDEM will be a very useful product for many applications, including those requiring a true global DEM (<http://www.ersdac.or.jp>). METI and NASA acknowledge that Version 1 of the ASTER GDEM should be viewed as ‘experimental’ or ‘research grade’ because there are known inaccuracies and artifacts in the data set, and it is advised to use the product with awareness of its limitations. The data is provided ‘as is’ and neither NASA nor METI/ERSDAC are responsible for any damages resulting from its.

## 1.03 Data Set Comparisons

Many scientists provide comparisons between ASTER GDEM and SRTM datasets.

Steve Metzler found that in some cases, the ASTER GDEM dataset missed islands that other datasets (such as Google Earth) clearly showed, and in other cases, it added islands where none exist. Cloudy areas also give it problems, and unfortunately, the problems don’t merely result in SRTM 3 being substituted for bad ASTER data, but also cause spurious land features to be created where defective ASTER data wasn’t recognized.

In some science research of the Amazon region, a number of problems were found in the ASTER GDEM data. In addition numerous spurious hills rising to hundreds of meters were found where none existed. Moreover, some river channels of the Amazon do not have the correct hydrological flow, but have sections that jump around in height, which resulted in the observation that lower river sections may be higher than sections further up the river (S. Metzler, 2009.).

The Open Topography team member Ramon Arrowsmith has a preliminary comparison of the ASTER GDEM data with 90m Shuttle Radar Topography Mission (SRTM) data on his blog. Ramon notes that due to various artifacts and high-frequency noise, the GDEM data may not be as impressive as one would hope, relative to the SRTM data (R. Arrowsmith, 2009). Initial studies to validate and characterize the ASTER GDEM confirm that pre-production accuracy estimates are generally achieved for most of the global land surface. Version 1 of

the ASTER GDEM contains certain residual anomalies and artifacts that affect the accuracy of the product and may be impediments to effective utilization for certain applications. Consequently, METI and NASA acknowledge that Version 1 of the ASTER GDEM should be viewed as ‘experimental’ or ‘research grade’. Nevertheless, they are confident that the ASTER GDEM represents an important contribution to the global earth observation community.

The hydrologic consistency of SRTM data might imply that SRTM data was post-processed, while ASTER GDEM version 1 available was not ([www.ersdac.or.jp](http://www.ersdac.or.jp)). In addition, GDEM offers an alternative data source for high relief areas where SRTM has large amounts of missing data. This is possible because the ASTER instrument senses the IR spectrum while SRTM is a radar instrument. ASTER can also have missing data, but for different reasons. As a result, they may not occur in the same place. However, the most surprising thing about the data is that it apparently does not represent a resolution improvement over SRTM, despite the vastly increased sampling rate (30 m for GDEM versus 90 m for SRTM).

In addition to the resolution issues, the ASTER scientists have expended a lot of effort to determine the vertical accuracy of the dataset. The stated accuracy is 7-14 m stated in terms of standard deviation. This should mean that 99% of GDEM data will fall within +/- 42m maximum of the actual elevation. Vertical accuracy was determined by subtracting GDEM elevation values from those of other datasets, including the NED and SRTM plus comparison with control points. A lot of attention has been focused on anomalies as well. These can result from sensing and processing errors and may take the form of pits and spikes. Further errors can occur around bodies of water and data may be completely missing around areas of persistent cloud cover (<http://www.terrainmap.com>). Both the SRTM and GDEM datasets of the Lebanese territory were compared to 50 geodetic points or ground elevation points taken from the topographic maps. The ground geodetic points were randomly distributed inside regions of different topography like Brital, Beino, Bikfaya, Srifa and Deir el Ahmar. As known the most accurate elevation datasets are the geodetic ones. Table 1.1 below shows the statistic values of the SRTM and GDEM datasets compared with 50 elevation points.

In the majority of the values, the SRTM datasets are more similar to the geodetic points than the GDEMs especially in the hilly and mountainous areas. It is the same case in canopy surfaces, but in the bore lands the GDEM is more similar. Statistics are very comparable, and the frequency distributions of elevations in both datasets are negatively skewed while they follow the normal distribution (skew < 0.5) and as show in Table 1.1, the kurtosis value of the SRTM and the GDEM appears to be not leptokurtic (kurtosis < 1.5). Both of these statistics are extremely

good results. The difference interval between the SRTM datasets and the sample geodetic points is -23 to 46 meters, while the GDEM one is -31 to 66 meters which is very high, contrary to that of the SRTM.

**Table 1.1 Statistic Values of the Elevation Datasets**

Statistic Values of the Elevation Datasets										
	Number of values	Min	Max	Mean	Std. Dev.	Skewness	Kurtosis	1-st Quartile	Median	3-nd Quartile
<b>Geodetic points</b>	50	267	1731	921.3	391.5	0.014	-0.90	522	1010	1157
<b>SRTM</b>	50	247	1731	913.1	394.3	-0.002	-0.90	503	1009	1139
<b>GDEM</b>	50	233	1736	907	397.3	-0.003	-0.89	470	1002	1141

## 1.04 Errors in Digital Elevation Models

The effect errors in a DEM are often not evaluated by DEM users. Elevation values in DEMs are subject to three types of errors: blunders, systematic errors, and random errors. Blunders are vertical errors associated with the data collection process. These errors exceed the maximum absolute error permitted, and as such, are easily identified and removed prior to release of the data.

Systematic errors are the result of procedures or systems used in the DEM generation process and follow fixed patterns that can cause bias or artifacts in the final DEM product. When the cause is known or if they can be identified, systematic errors can be eliminated or reduced. Random errors result from mistakes, such as inaccurate surveying or improper recording of elevation information. Many studies have investigated methods to identify systematic errors in DEMs (Brown and Bara, 1994). They used semivariograms and fractal dimensions to analytically confirm the presence and structure of systematic errors in DEMs, and suggested filtering as a means to reduce the error (Theobald, 1989). The sources of DEMs and DEM data structure were reviewed to identify how bias and errors are produced in DEM generation (Polidori et al., 1991).

Gyasi-Agyei et al. (1995) investigated the effect of vertical resolution on derived geomorphological parameters. Random errors result from accidental or unknown combinations of mistakes and identification of these errors is beyond the control of the DEM user. Random errors remain in the data after blunders and systematic errors are removed (USGS, 1997). Measure of vertical accuracy in

USGS DEMs is provided by the USGS in the form of the Root Mean Square Error (RMSE) statistic. The RMSE value is typically calculated through the use of a reference dataset. The reference set of points and the same points derived from the DEM production process are compared and the difference calculated for each point. These differences are then squared, the mean of the squared differences calculated, and the root of this mean value used as the error value (Zukowskyj et al., 2000). Typically the statistical measure Root Mean Square Error is used to define the error present in the output datasets. Error analysis of many datasets is also confusing to some end-users, in that error statistics are not widely or fully understood. At the forefront of this problem is the widely used measure of error, Root Mean Squared Error.

The RMSE for DEMs is calculated by comparing the DEM with elevation points that reflect the ‘most probable’ elevations at those locations (obtained from field control, aero-triangulated test points, spot elevations, or points on contours from existing source maps) (Zukowskyj et al., 2000).

The RMSE is expressed as:

$$RMSE = \sqrt{\frac{\sum_{i=1}^N (y_i - y_j)^2}{N - 1}}$$

Where  $y_i$  is an elevation from the DEM,  $y_j$  is the ‘true’ known or measured elevation of a test point and  $N$  is the number of sample points. The RMSE statistic is essentially a standard deviation and is thus based on the assumption that errors in the DEM are random and normally distributed. In this case  $y_j$  is the geodetic elevation points,  $y_i$  is the SRTM and GDEM datasets and  $N$  is the number of sample points taken with a value of 50. Root Mean Square Errors of the altitudinal difference between these DEMs and ground survey data for the 50 sample points of the Lebanese ground were 17.7 meters for SRTM and 22.8 meters for GDEM.

## 1.05 DEM Error Constitutes Uncertainty

Error is the departure of a measurement from its true value. Often, in geographic analysis or analysis of complex natural systems using spatial data, we do not know or do not have access to the true value. Uncertainty is a measure of what we do not know. Uncertainty exists in spatial databases. Unfortunately, the exact nature and location of this error cannot be precisely determined. Sources of uncertainty error in DEM datasets include (Burrough, 1986):

1. Data errors due to the age of data, incomplete density of observations, or results of spatial sampling.

2. Measurement errors such as positional inaccuracy, data entry faults, or observer bias.

3. Processing errors such as numerical errors in the computer, interpolation errors or classification and generalization problems.

It is a practical impossibility to obtain information on the exact source and amount of error in a particular DEM.

A lot of methods and studies light at the uncertainty error in a DEM as simulated errors in a grid DEM and determine that small errors introduced into the database significantly affect the quality of extracted hydrologic features (Lee et al., 1992, 1996). The effect of simulated changes in elevation differs at various levels of spatial autocorrelation on slope and aspect calculations (Hunter and Goodchild, 1997). Uncertainty errors can only be evaluated with a surface of higher accuracy data – a truth surface – such as data obtained from a GPS survey (or other) (Ehlschlaeger, 1998).

## 1.06 Non-Spatial DEM Characterization

The moments of a distribution (mean, standard deviation, skewness and kurtosis) provide basic descriptions of a distribution and are often referred to as descriptive statistics. The standard deviation provides a measure of dispersion of the data a DEM of very rough terrain could have the same standard deviation as a smoothly sloping surface. The histogram and its associated measures of skew and kurtosis quantify the normality of a distribution of elevations. The histogram can provide an indication of the presence of inconsistencies within the DEM. Skew is a measure of the shape of the frequency distribution. A positive or negative skew indicates that the data is not normally distributed. Kurtosis is a measure of the degree of flatness or peaks of the distribution. These statistics include the RMSE, mean absolute difference, and standard deviation of difference. The RMSE statistic is provided by the USGS to indicate vertical data accuracy. This statistic is rarely incorporated in reports of results of data analyses that utilize DEMs. One drawback of the RMSE is that the statistic has no spatial dimension. Although it provides information about the overall accuracy of a DEM, uncertainty varies spatially across a surface (Wood, 1996).

Other precision indices have been applied to DEMs to address the problem associated with the RMSE and its assumption of a normally distributed error (Li, 1988; Desmet, 1997). Another measure of accuracy is the mean absolute difference between interpolated and true values and the standard deviation of these

differences. The mean absolute difference is a measure of the ‘shift’ of the surface and the standard deviation represents the measure of dispersion of this shift. Therefore, the accuracy can be reported as mean absolute difference  $\pm$  the standard deviation of difference (Li, 1988).

$$\text{Mean Absolute Difference} (\bar{\Delta z}) = \frac{\sum |y_j \text{ observed} - y_i \text{ interpolated}|}{N}$$

$$\text{Standard Deviation of Difference} (\rho) = \sqrt{\frac{\sum_{i=1}^N (|y_j \text{ oberved} - y_i \text{ interpolated}| - \bar{\Delta z})^2}{N-1}}$$

In the results of our calculations in the Lebanese territory, we came to a satisfying conclusion by calculating the RMSE, mean absolute difference, and standard deviation of difference. Table 1.2 shows the SRTM and GDEM relief with ground geodetic points.

**Table 1.2 SRTM and GDEM errors based on topographic maps**

	<b>Root Mean Square Error (RMSE)</b>	<b>Mean Absolute Difference (<math>\bar{\Delta z}</math>)</b>	<b>Standard Deviation of Difference (<math>\rho</math>)</b>
SRTM	17.7 m	8 m	15.6 m
GDEM	22.8 m	15 m	17.7 m

The results of RMSE show that the SRTM datasets are more accurate than those of the GDEM. An accuracy ratio attempts to remove the effects of relative relief by dividing the RMSE by a surface’s standard deviation. This standardization allows comparison between different terrain surfaces (Wood, 1996).

The purpose of this methodology is to provide a suite of methods for evaluating the effect of uncertainty in DEMs and selected derived topographic parameters. Until now, DEM users would often apply the DEM as a truth surface rather than as a model, but it is not safe to make this judgment without a thorough evaluation. The determination as to whether DEM uncertainty will impact a particular application rooted in DEM data cannot be made without quantitative evaluation of DEM uncertainty. Relating to this study, users can determine whether uncertainty in the DEM will affect results from specific analyses that utilize data derived from a DEM. This research provides the DEM user with a suite of methods

to assist in this assessment. Use of this tool could result in more responsible use of DEM and derived data. Our studies showed that the accuracy of DEM SRTM compared to DEM ASTER GDEM for the analyzed area (territory of Lebanon) is sufficient to perform complex morphometric and dimensional calculations on landscape maps.

## Chapter 2: Terrain Representation

The utility of a map is highly enhanced if the relative position of the points is represented both horizontally and vertically. On a map, the relative vertical positions of the points can be represented by shading, hachures, spot heights or contour lines. Contour lines are a unique, useful and straightforward way to represent topography. They are by far the most quantitative of the cartographic techniques for representing continuous surfaces (Kennelly, 2002).

A contour is an imaginary line of constant elevation on the ground surface. It may be thought of as the trace formed by the intersection of a level surface with the ground surface. On a given map the successive contour lines represent elevations differing by a fixed vertical distance called the contour interval, which depends upon the nature of the terrain. A contour interval chosen for a flat ground will be highly unsuitable for undulating ground. For flat ground, a small contour interval is chosen whereas for undulating and broken ground, greater contour interval should be adopted. The contour interval is normally inversely proportional to the scale of the map. If the scale is large, the contour interval should be small. If the scale is small, the contour interval should be large. In the topographic maps, the configuration of the terrain is represented by drawing contours at constant vertical distance. A knowledge of contour characteristics helps in identifying the natural features of the area from the given map and in avoiding mistakes in plotting the contours correctly. Contour lines cannot begin or end on the plan. Contours deflect uphill at valley lines and downhill at ridgelines. Contour lines in U-shape cross a ridge and V-shape cross a valley. The concavity in contour lines is towards higher ground in the case of a ridge and towards lower ground in the case of a valley.

The methods of locating contours, therefore, depend upon the instruments used to determine the horizontal as well as vertical position of several points in the area. Field methods are divided into direct and indirect methods. In the direct method, the contour is traced on the ground by using surveying instruments (Chandra, 2002). In the indirect method, a sufficient number of points are located and given spot levels. Contours in between spot levels are interpolated by traditional methods like: grid, cross-section, and radial line methods.

With the appearance of GIS and CAD technologies, more accurate interpolation methods appear. These technologies yield to Triangulated irregular networks (TIN) and Digital Elevation Models (DEM). Application of an interpolation method should be determined by the nature of input data, availability of computer resources, the characteristics of the modeled surface, and the objective of modeling (Lam, 1983). For random points, kriging is usually considered the most efficient method (El-Sheemy et al., 2005). If the characteristics of the modeled

surface are known, then the interpolation function best representing the surface should be selected. Interpolation from contour lines should avoid splines around contour; therefore they seem to be improper in most cases. Kriging also seems to be less appropriate for contour data source (El-Sheimy et al., 2005). Linear interpolation methods, such as Triangulated irregular network (TIN), offer good results for contour source data. Triangulation inserts flats for closed contours at hill tops (peaks), however, and it can truncate valley bottoms and ridge tops where contours strongly curve. This feature disables the estimation of gradient at the truncated flat areas. Hilltops can be cured by adding spot heights or by interpolating locally for the flat tops. Flat valleys and ridges can be adjusted by using constraints in the algorithm ensuring that the three points of triangular facets do not fall on the same contour line.

In digital terrain analysis of morphostructural studies, first and second-order derivatives are frequently used (Florinsky, 2000) and therefore, it is a requirement that the fitted function should be continuous in the first two derivatives. This contradicts the idea that break-lines must also be included for tectonic analysis (McCullagh, 1988). For example, TINs are efficient in the representation of areas with uniform slope or aspect, which are essential in identification of tectonically induced erosional morphology of spurs and pediments in mountain fronts (Riley and Moore, 1993).

## 2.01 Analytical Hillshading

Hillshading is a technique where a lighting effect is added to a map based on elevation model of the landscape. The hillshading is related to the sun's effects – illumination, shading and shadows – on the relief (hills and canyons). This is a very important tool that people can use to identify the terrain parameters and provide a suitable way to get a 3-D effect without changing from a 2-D perspective. Compute Hillshade is used to determine the hypothetical illumination of a surface as part of an analysis step or for graphical display. Compute Hillshade can be used to determine the length of time and intensity of the sun in a given location. For a graphical display, Compute Hillshade can greatly enhance the relief of a surface (Susam, 2002). The azimuth is expressed in positive degrees from 0 to 360, measured clockwise from the north. The altitude is expressed in positive degrees, with 0 degrees at the horizon and 90 degrees directly overhead.

Analytical hillshading uses variations in shades of gray colors to give two-dimensional maps a three-dimensional appearance. Most analytical hillshading uses the Lambertian assumption. This assumption states that apparent brightness of a matte surface will vary with the cosine of the angle  $\theta$  between the illumination ( $I$ )

and the surface normal (SN) vector. In Figure 2.1, the angle  $\theta$  can vary from  $0^\circ$  to  $90^\circ$ . At  $0^\circ$ , the illumination vector is perpendicular to the surface resulting in a strongly illuminated white surface. At  $90^\circ$ , the illumination vector is parallel to a surface resulting in a non-illuminated black surface (P. Kennelly, 2002). Several cartographers have automated this procedure using the angle  $\theta$  with GIS (Peucker et al., 1975; Peucker, 1980; Yoeli, 1976). P. Kennelly and A.J. Kimerling (2001) suggest an alternative GIS implementation, using the angle  $\theta$ .

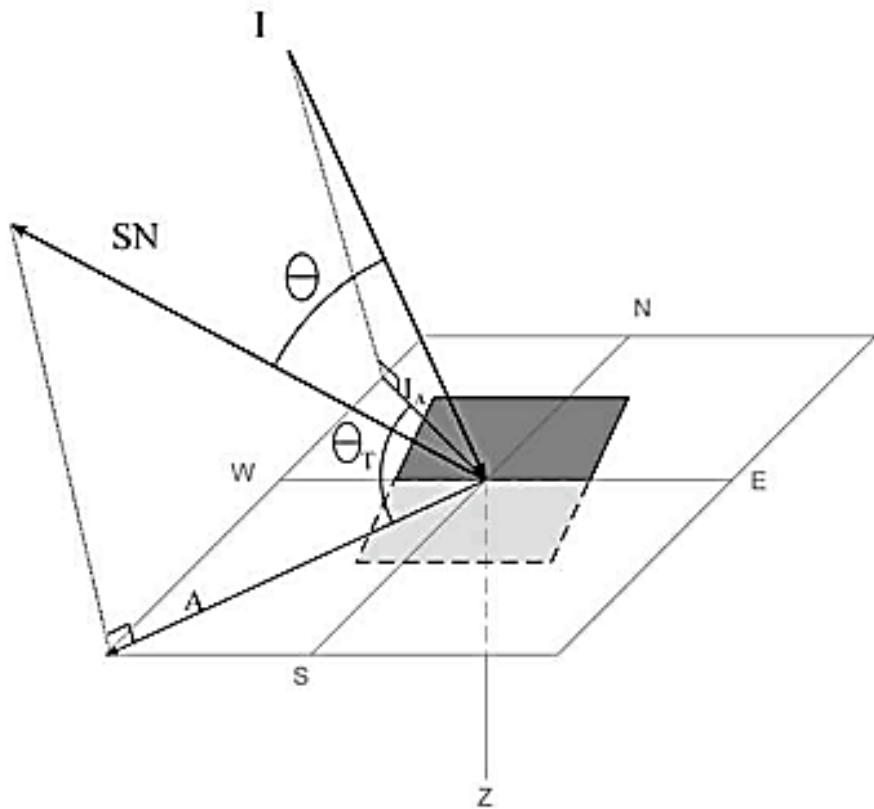


**Figure 2.1** Illumination ( $I$ ) and Surface Normal (SN)

Line thickness is proportional to the cosine of twice the angle  $\theta$   
Vertical projections of vectors  $I$  and  $SN$  onto a horizontal plane

Shaded relief effect is derived from a digital elevation model (DEM), which is a raster dataset of elevation values. DEMs and hillshades are separate datasets – a DEM contains actual elevation values while a hillshade, though also a raster, contains brightness values. These two data layers can be used on their own or in combination. In a Digital Elevation Model, the Hillshade function obtains the hypothetical illumination of a surface by determining illumination values for each cell in a raster. It does this by setting a position for a hypothetical light source and

calculating the illumination values of each cell in relation to neighboring cells. To calculate the shade value, the altitude and azimuth of the illumination values, they will need to be processed with slope and aspect to determine the final hillshade value for each cell. The algorithm for calculating the Hillshade value is:

$$\text{Hillshade} = 255 * \{[\cos(\text{Zenith}_{\text{rad}}) * \cos(\text{Slope}_{\text{rad}})] + [\sin(\text{Zenith}_{\text{rad}}) * \sin(\text{Slope}_{\text{rad}}) * \cos(\text{Azimuth}_{\text{rad}} - \text{Aspect}_{\text{rad}})]\}$$

The altitude of the illumination source is specified in degrees above horizontal. However, the formula for calculating the Hillshade value requires the angle be represented in radians, and be the deflection from the vertical. The direction straight up from the surface (directly overhead) is labelled the 'Zenith'. The zenith angle is measured from the zenith point to the direction of the illumination source, and is the  $90^0$  complement to the altitude.

$$\begin{aligned}\text{Zenith}_{\text{deg}} &= 90 - \text{Altitude} \\ \text{Zenith}_{\text{rad}} &= \text{Zenith}_{\text{deg}} * \pi / 180\end{aligned}$$

The direction of the illumination source, azimuth, is specified in degrees. The Hillshade formula requires this angle to be in units of radians. First, the azimuth angle is changed from its geographic unit (compass direction) to a mathematic unit (right angle). Next, the azimuth angle is converted to radians. Change azimuth angle measure:

$$\begin{aligned}\text{Azimuth}_{\text{math}} &= 360.0 - \text{Azimuth} + 90 \\ \text{Note that if } \text{Azimuth}_{\text{math}} &\geq 360, \text{ then:} \\ \text{Azimuth}_{\text{math}} &= \text{Azimuth}_{\text{math}} - 360.0 \\ \text{Azimuth}_{\text{rad}} &= \text{Azimuth}_{\text{math}} * \pi / 180.0\end{aligned}$$

As shown in Figure 2.2 a, we created an analytical hillshading grid from the DEM, with an azimuth value of  $330^0$  and an altitude angle of  $30^0$  and Figure 2.2 b with an azimuth of  $315^0$  and an altitude angle of  $45^0$ , these tow hillshade maps show the sun's effects – illumination and shadows – on the relief especially on Al Yammouneh fault and the Bekaa valley. In Figure 2.2 b the contrast is very high, and in Figure 2.2 a, the contrast is very low and the darkness is high. From these maps, we can distinguish that the darkness decreases with the azimuth value.

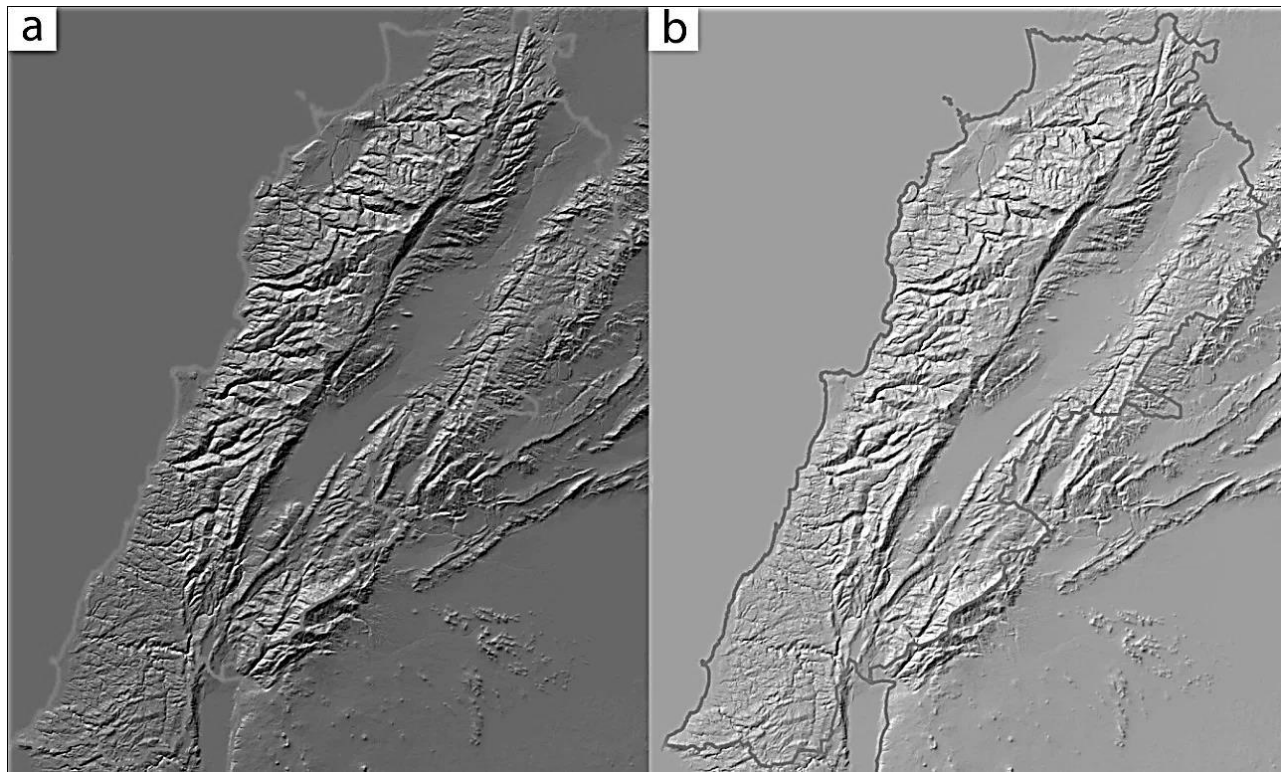


**Figure 2.2** a) Hillshade map with an azimuth of  $330^\circ$  and an altitude angle of  $30^\circ$   
 b) An azimuth of  $315^\circ$  and an altitude angle of  $45^\circ$

## 2.02 Slope

Slope is one of the most fundamental measures of landscape characteristics and first vertical derivative of elevation (Evans, 1972). Slope refers to the angle of inclination of a land surface above the horizontal. Slope steepness is measured as rise over run (Figure 2.3). In the field, slope is commonly measured for a site with clinometers in a matter of seconds. Slope may be calculated from paper topographic maps by measuring rise over run for a particular area. Both of these measures may yield accurate expressions of slope. Slope stability is:

$$\text{Percent slope} = \left( \frac{\text{rise}}{\text{run}} \right) \times 100 = \left( \frac{100}{200} \right) \times 100 = 50\% \text{ slope}$$

$$\text{Degree slope} = \tan^{-1} \left( \frac{\text{rise}}{\text{run}} \right) = \tan^{-1} \left( \frac{100}{200} \right) = 26.6^\circ \text{ slope}$$

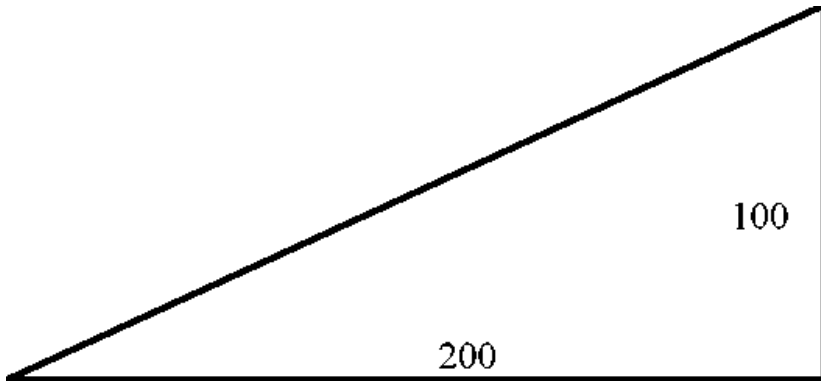


**Figure 2.3 Methods of Calculating Slope**

The standard measure of rise over run can be used to determine percent slope steepness. The inverse tangent of rise over run can be used to determine slope steepness in degrees. Slope can be calculated by geographic information systems through many mathematical formulae (Chang and Tsai, 1991; Peucker et al., 1979; Green and Sibson, 1978; McCullagh and Ross, 1980; McKenna, 1987; Scarlatos, 1989). The accuracy of each method of slope calculation varies, and is dependent on the quality and scale of the base DEM. Chang and Tsai (1991) and Hammer et al. (1995) studied the effects of different scales of DEMs and slope calculation methods on slope accuracy. They found little differences existed between these methods. As DEM raster size increased, or scale increased, slope accuracy decreased. Walsh et al. (1987) attributed poor slope computation accuracy on low resolution DEMs (3 arc-second). Computed slope values, as expected, showed greater error in areas of high relief than areas with low relief (Chang and Tsai, 1991). In DEM, slope is defined as the rate of elevation change in a cell's  $3 \times 3$  neighborhoods. Here, we are interested in the degree angle of the slope identified as the angle defined by rise (vertical distance change) and run (horizontal distance change). It is obtained by computing the partial derivative components in  $x$ ,  $y$  direction for each point.

The most common method for calculating slope in a geographic information system raster is to compute the “spatial derivative” (Burrough and McDonnell, 1998; Carter, 1990). The derivative expresses the rate of change of the data. The first derivative of elevation is the slope and is calculated as follows:

$$\text{Slope \%} = 100 * \sqrt{\left(\frac{\Delta Z_x}{\Delta X}\right)^2 + \left(\frac{\Delta Z_y}{\Delta Y}\right)^2} \quad (2a)$$

$$\text{Slope } ^\circ = \arctan \sqrt{\left(\frac{\Delta Z_x}{\Delta X}\right)^2 + \left(\frac{\Delta Z_y}{\Delta Y}\right)^2} \quad (2b)$$

Where:  $\Delta Z_x$  = change in elevation in the x direction,  $\Delta Z_y$  = change in elevation in the y direction,  $\Delta X$  = resolution in the X direction (2\*grid cell),  $\Delta Y$  = resolution in the Y direction (2\*grid cell)

In raster, GIS's slope is calculated by passing a  $3\times 3$  kernel over the grid surface; slope for the center cell E is computed from the surrounding eight cells labeled A, B, C, D, F, G, H and I as follows:

A	B	C
D	E	F
G	H	I

Many algorithms exist to compute slope. Differences between approaches are based on methods used to obtain the  $\Delta Z$  value for center cell E from cells A, B, C, D, F, G, H and I. GIS users must recognize the method by which the software used computes slope (and other parameters), because different software may yield different results from the same input data sets (Herrington, 1998). Skidomre and Carter compared methods for computing slope. They found that the method used to calculate slope from grid DEM data provides different results (Carter, 1990; Skidomre, 1989; Ryder, Voyadgis, 1996). The slope algorithm programmed in ArcView GIS software computes slope for the center cell E from the surrounding cells A, B, C, D, F, G and I.

The formulas of the equations 2a and 2b above where  $\left(\frac{\Delta z}{\Delta x}\right)^2$  and  $\left(\frac{\Delta z}{\Delta y}\right)^2$  are computed as follows: (Burrough and McDonnell, 1998; Horn, 1981).

$$\left(\frac{\Delta z}{\Delta x}\right)^2 = \left\{ [(A + 2D + G) - (C + 2F + I)] \div (8 * x \text{ grid spacing}) \right\}^2 \quad (2c)$$

$$\left(\frac{\Delta z}{\Delta y}\right)^2 = \left\{ [(A + 2B + C) - (G + 2H + I)] \div (8 * y \text{ grid spacing}) \right\}^2 \quad (2d)$$

$$Slope^\circ = \arctan \sqrt{\left(\frac{\Delta z}{\Delta x}\right)^2 + \left(\frac{\Delta z}{\Delta y}\right)^2} \times 57.29578$$

This slope equation was first presented by Horn (1981) who justified weighting of cells in the non-diagonal directions through numerical analysis, stating that this weighted average provides a better slope estimate for certain surfaces (Horn, 1981). Burrough and McDonnell (1998) suggest that this method is more suited for rough surfaces.

Other GIS packages use an algorithm called the Rook's Case, where only cells B, D, F and H are used in the calculation as follows (Eastman, 1992; Zevenbergen and Thorne, 1987).

$$\left(\frac{\Delta z}{\Delta x}\right)^2 = \{[(B-H)/2] / (2 * x \text{ grid spacing})\}^2 \quad (2e)$$

$$\left(\frac{\Delta z}{\Delta y}\right)^2 = \{[(D-F)/2] / (2 * y \text{ grid spacing})\}^2 \quad (2f)$$

This method is best suited for smooth surfaces (Burrough and McDonnell, 1998). Unfortunately, GIS packages do not differentiate between rough and smooth surfaces when applying a slope algorithm. It is important for GIS users to recognize the influence that a particular slope algorithm might have on results and report the method used. Slope computed from a grid DEM is not only affected by the algorithm used to compute the slope, but is also affected by the precision of the elevation values in the DEM (Garbrecht and Martz, 1999; Carter, 1992).

Slope is one of the most fundamental measures of landscape characteristics, and is reported as a driving variable in many ecological studies. It has been found to be related to: soil surface depth, subsoil texture, and internal soil drainage, profile, and erosion of soil (Pearson, 1968; Swanston and Dyrness, 1973; Way, 1973; Verstappen, 1983; Turner, 1936, 1937, 1938), soil group (Zahner, 1958), and depth to least permeable soil horizon (Linnartz, 1961). Slope steepness is included as a major factor in determining the soil erosion rate from a site through the Universal Soil Loss Equation. Slope has been used in equations to estimate the climatic variable solar radiation (Lawrence, 1976). Slope is calculated with the ArcView algorithm listed above based on SRTM and GDEM data sets and classified by the Forest Site Quality Index (FSQI) scores from Wathen Table 2.1 (Wathen, 1977).

Slope values of the Lebanese relief are not the same in both data sets, SRTM own a higher percentage of slope than the GDEM datasets. The middle interval of 3 FSQI score has the same percent of slope. Slopes higher than 60% have a 408 square kilometer of area in the GDEM datasets (Figure 2.4).

**Table 2.1** Percent Slope Ranges of GDEM and SRTM Data Sets and Associated Forest Site Quality Index (FSQI) Scores from Wathen (1977)

GDEM Slope				SRTM Slope			
FSQI score	Interval %	Area km <sup>2</sup>	Area %	FSQI score	Interval %	Area km <sup>2</sup>	Area %
5	0-14	4415.36	43	5	0-14	4581.72	45
4	15-29	3184.87	31	4	15-29	3313.59	32
3	30-44	1554.57	15	3	30-44	1505.85	15
2	45-59	644.93	6	2	45-59	550.50	5
1	> 60	408.26	4	1	> 60	256.78	3

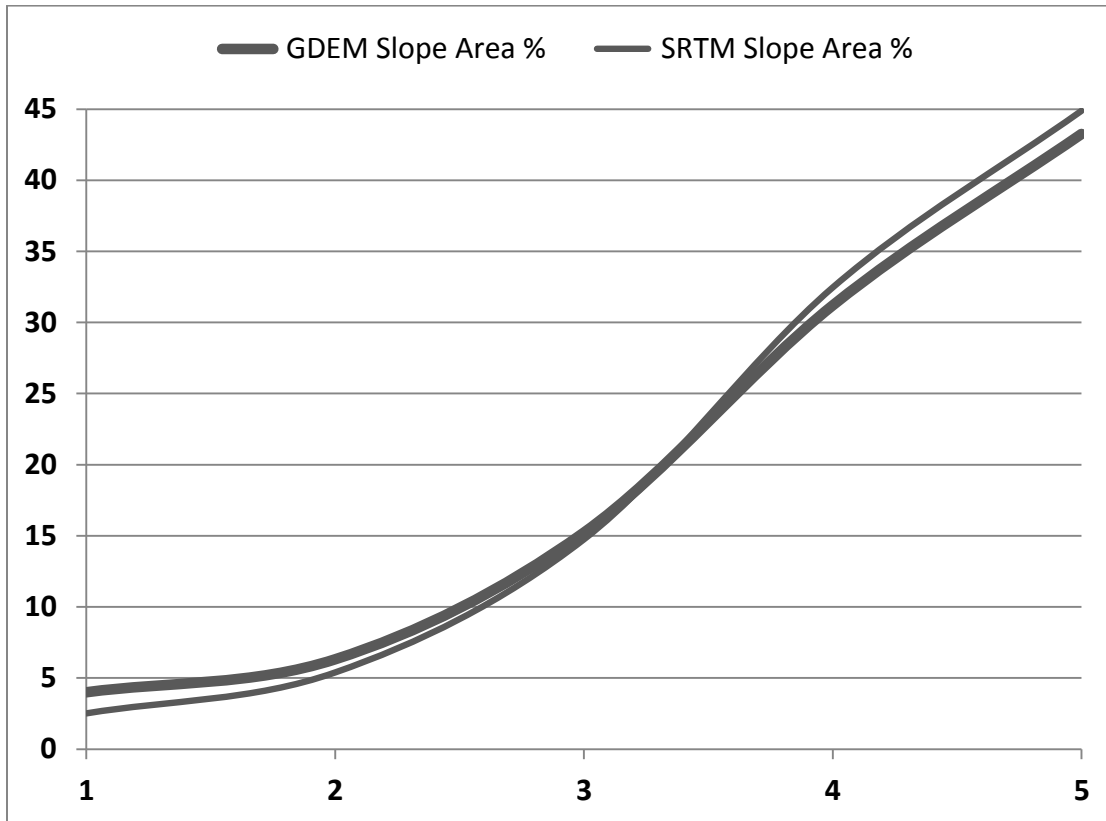


**Figure 2.4** Graph of the Slope Difference between GDEM and SRTM

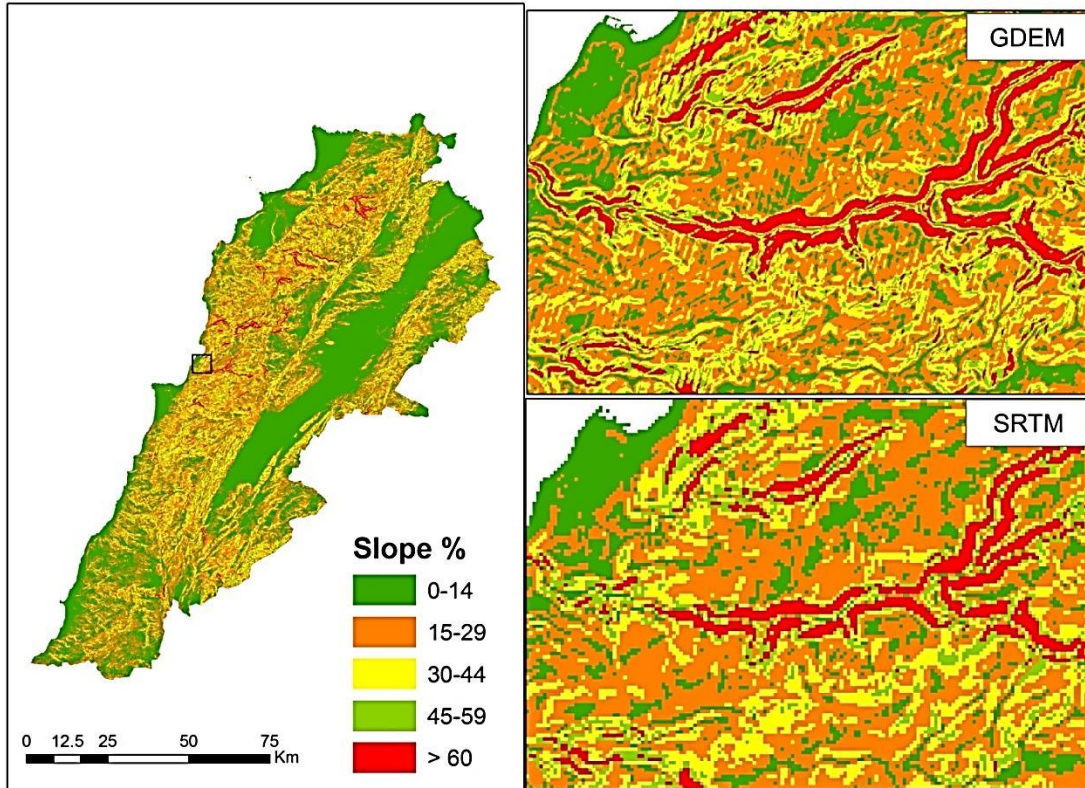


**Figure 2.5 Slope Map of Lebanon from GDEM and SRTM**  
*Slope map of Lebanon from GDEM with diagonal parallel lines or artifacts and SRTM map without artifacts*

## 2.03 Estimation of Slope

A slope estimation method, proposed by Wentworth (1930), is still widely used to estimate the average slope of an area from the contour maps. The average slope value ( $\alpha$ ) can be estimated as follows:

$$\alpha = \tan^{-1} \left( \Delta H \times \frac{\Sigma L}{A} \right)$$

Where  $H$  is the contour interval,  $L$  is the total length of contours in the area and  $A$  is the size of the area. If there is no contour map for such an area, then the slope may be estimated from an aerial photograph. Some of the methods that are available for measurement of slope from aerial photographs have been reviewed by Turner (1997).

## 2.04 Aspect

The first horizontal derivative of elevation is aspect (Evans, 1972). Aspect is the compass direction a slope faces. Similar to slope, aspect can be computed through a variety of mathematical formulae (Chang and Tsai, 1991; Peucker et al., 1979; Green and Sibson, 1978; McCullagh and Ross, 1980; McKenna, 1987; Scarlatos, 1989; Ritter, 1987). Aspect calculation from digital data may also have inaccuracies that are dependent on the scale of the DEM and the relief of the terrain, and will vary from SRTM and GDEM datasets.

Land aspect, the direction a slope “faces” or the compass direction downhill from a point, is a profound land form. This component of topography is a driving force in the development of a forested landscape. In a DEM, aspect identifies the steepest downslope direction from each cell to its neighbors. It can be thought of as slope direction or the compass direction a hill faces. It is measured clockwise in degrees from 0 (north) to 360. The value of each cell in an aspect dataset indicates the direction the cell's slope faces. Flat areas having no downslope direction are given a value of -1.

Aspect in a DEM is calculated using the formulas of derivative below. Changes in the direction of x and y are calculated by:

$$\left( \frac{\partial z}{\partial x} \right) = \frac{[(C + 2F + I) - (A + 2B + c)]}{8}$$
$$\left( \frac{\partial z}{\partial x} \right) = \frac{[(J + 2H + I) - (A + 2B + c)]}{8}$$

Aspect is calculated by the formula (Burrough and McDonnell, 1998; Horn, 1981):

$$\text{Aspect} = 57,29578 \times \arctan 2 \left( \left( \frac{\partial z}{\partial y} \right), - \left( \frac{\partial z}{\partial x} \right) \right)$$

Aspect analyzes the impact of litho-, hydro-, geochemical, aerodynamic flow on the landscape differentiation (through direct and indirect effects on the exogenous processes, soil formation, vegetation, etc. In addition, aspect through the influence of the erosion-denudation activity determines the morphological properties of the earth's surface. On the windward side of mountains, there is often much more rainfall than on the leeward side. This orographic rainfall has been studied and reported by many authors (Swanson, 1979; Howard and Mitchell,

1985; Osmond et al., 1990). Aspect was one characteristic found to play an important role in tree survival, growth potential, growing season, and seedling survival (Shoulders and Tiarks, 1980; Gemborys, 1979; Rehfeldt, 1993; Griffin, 1971; Muick and Bartolome, 1987; Scribner et al., 1991).

**Table 2.2** *The Distribution of Surfaces With Different Aspects in Lebanon (SRTM Data)*

Aspect Surfaces					
Aspect	Orientation degree	SRTM %	GDEM %	SRTM km <sup>2</sup>	GDEM km <sup>2</sup>
N	337.5-22.5	15.3	15.5	1566	1587
NE	22.5-67.5	8.7	9.2	892	942
E	67.5-112.5	8.7	8.8	889	900
SE	112.5-157.5	11.1	11.1	1131	1138
S	157.5-202.5	10.7	11.3	1094	1151
SW	202.5-247.5	10.2	10.6	1042	1086
W	247.5-292.5	14.6	13.8	1492	1408
NW	292.5-337.5	19.8	18.6	2018	1903
Horizontal	-	0.8	0.9	84	94

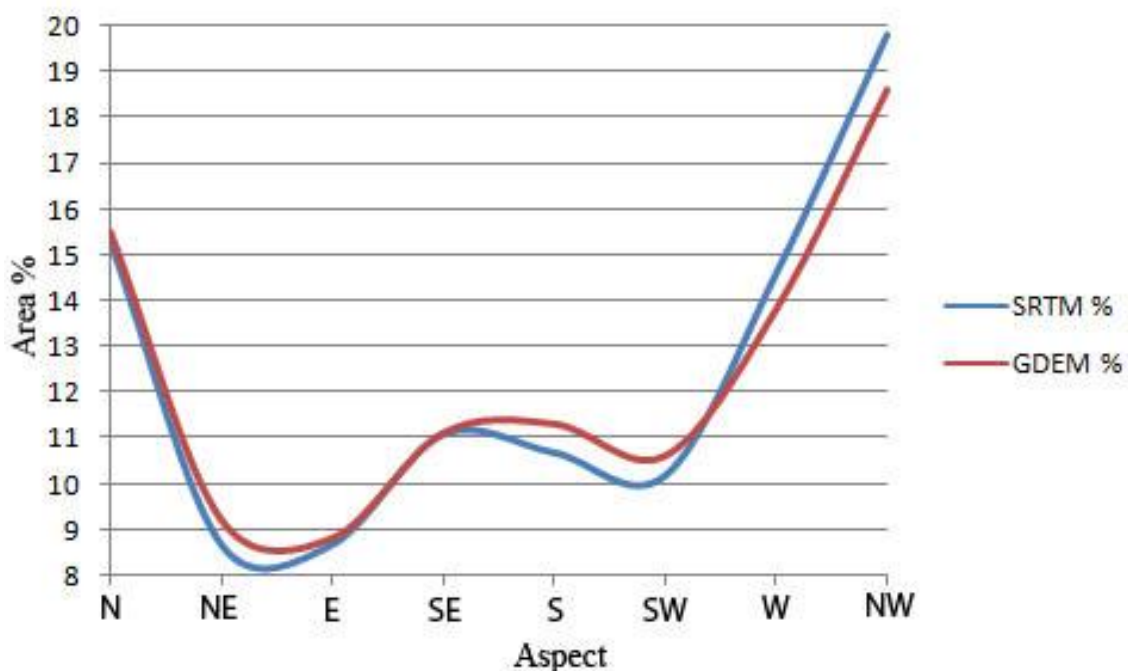


**Figure 2.6** *Aspect Graph of the Difference between SRTM and GDEM*

Figure 2.7 illustrates the distribution of Aspect of different exposures in Lebanon basing to SRTM. Lebanon horizontal surfaces occupy 0.8% of the total area. Slopes facing to the north (the northern, north-west and north-east), constitute almost half of the total area (43.8%). The slope of the opposite orientation (south, south-western, and south-east) has a much more modest area of 32%.

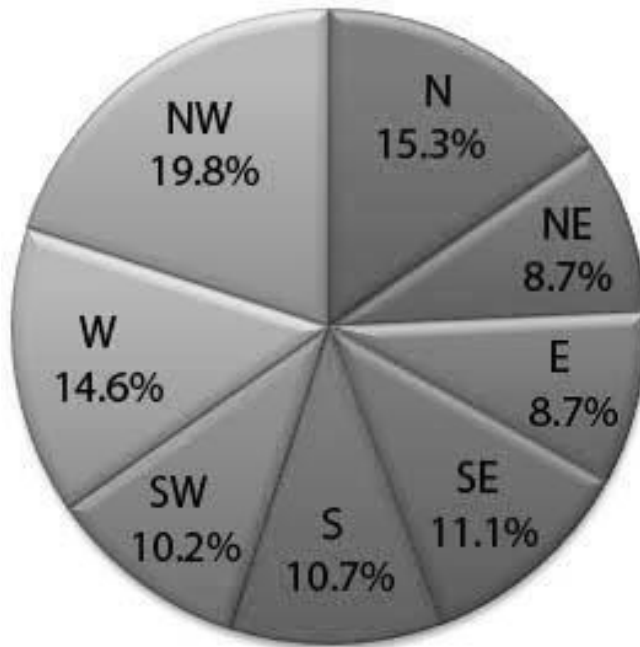


**Figure 2.7 Distribution of Aspect Surfaces in Lebanon Without Displaying Horizontal Surfaces (SRTM Datasets)**

Generally aspect distribution was not surprising because the terrain was very diverse, with slopes facing all directions. At a larger scale, such as along mountain ridges, there may be more direction facing northwest or southeast than other directions. The Mount Lebanon Ridge Mountains run northeast to southwest creating large slopes facing northwest and southeast.

Landscape studies often use generalized or contrasting assessments of the exposition areas of the earth's surface, such as slopes, ridges and sides of the river valleys. This allows the description of the phenomenon of local climate and landscape dissymmetry. To detect such exposition of contrasts, you can resort to classification to get binarization image examples of the el Kaleb river basin (Figure 2.8).

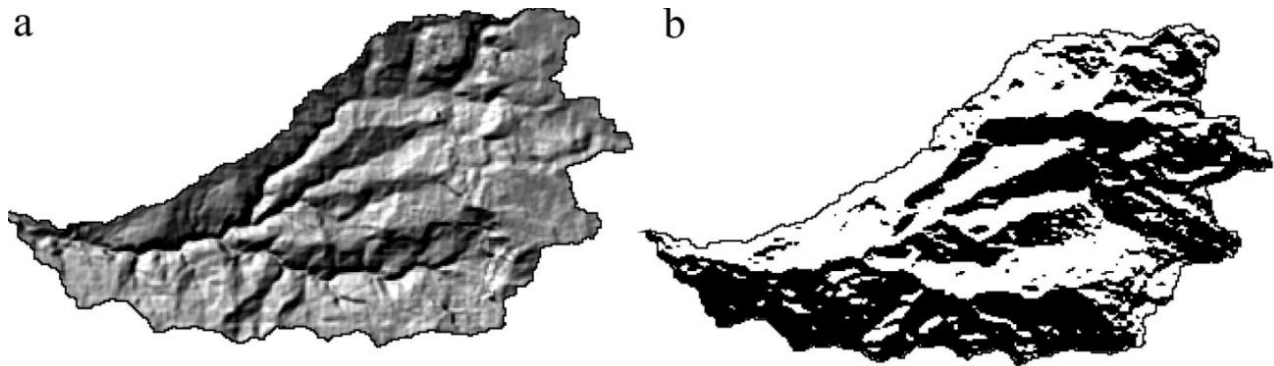


**Figure 2.8** Aspect Dissymmetry on the Example of the El Kalb River Basin:  
 a) Hillshade map, b) Black and white colors are shown with the orientation of the slopes from  $90^\circ$  to  $270^\circ$  (southern exposure) and from  $270^\circ$  to  $90^\circ$  (northern exposure)

The variables elevation, slope, and aspect are 1-dimensional measures, each describing a feature of a site. Several authors have combined and transformed elevation, slope, and aspect to create new variables and mathematical formulae to describe landforms in more than 1-dimension. Mitchell (1995) described a windthrow triangle which rated the risk at a site to wind damage based on topographic exposure (slope and aspect). Gao and Lo (1995) created a linear polynomial regression equation using elevation, slope, aspect, and configuration to model locations with a high potential for landslides. Preliminary evaluation of the model indicated an accuracy of 83%. Peddle and Duguay (1995), similar to a study reported by Stage (1976), combined slope and aspect to create a topoclimatic index.

**Table 2.3** Aspect Classes and Their Ranges and Forest Site Quality Index (FSQI) Scores Assigned by Wathen (1977)

Aspect ranges in degree	FSQI Score
196-260	1
166-195, 261-280	2
146-165, 281-340	3
0-20, 341-360	4
81-145	5
21-80	6

The topoclimate index was used to describe the effects that steep-mountain-faces have on the distribution of snowfall. According to their index and within their area, steep, east-facing slopes received the greatest accumulation of snow, and thus

received the highest topoclimatic index. The aspect classes chosen by Wathen (1977) were used in this study. Each range of aspect was given a score based on its perceived ability to influence tree growth.

After classification of slope and aspect in GIS, we got tow maps with FSQI scores. We calculated them in raster calculation to obtain a forest site quality map of Lebanon (Figure 2.9).

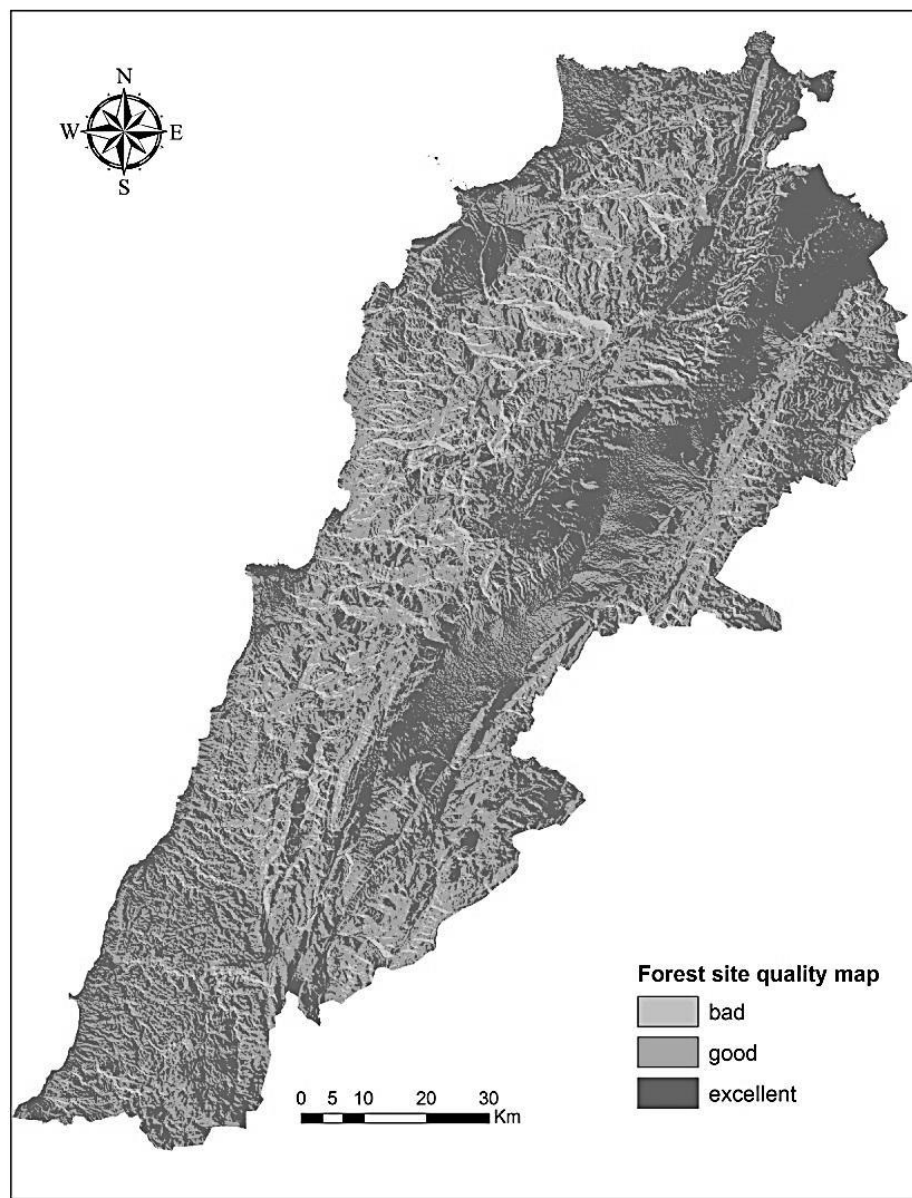


**Figure 2.9** Forest Site Quality Map of Lebanon Extracted from Slope and Aspect

This is a forest site quality map derived from the classified slope and aspect raster showing the best spatial location for the best forest quality on the Lebanese territory. As we can see in Figure 2.9, almost all the ground has a good rate in forest quality except the yellow areas orientated in the interval between 196-260 degrees. Similar to this forest site quality map, using slope and aspect, we can build other derived maps related to other important topics, such as the most suitable place for building or for laying a ski track. Slope and aspect are very important indices influencing our geographical environment.

# **Chapter 3: Morphometric Characterization and Hydrological Assessment**

Digital Elevation Model image is a discretization of the geographic height value, where there will exist, both real natural depressions from the original data (i.e., lakes, depressional wetlands, and karst landforms) as well as artificial sinks. These are possibly caused by incorrect or insufficient data, noise during data acquisition or by an interpolation technique that does not enforce surface drainage. The presence of these sinks will block the water flow. In order to imagine a drainage network, hypothetically, a fluid must flow in some direction. In a depression, all fluid would flow in and none would flow out (Figure 3.1).

Processing Digital Elevation Models (DEMs) for hydrologic modeling generally requires the filling of depressions (sinks) as well as features that inhibit surface flow and cause the inaccurate or incorrect flow direction and flow accumulation. The majority of sinks are spurious artifacts of DEM creation. Yet, some sinks represent real features (i.e., lakes, depressional wetlands, and karst landforms) and should not be filled (Jensen and Domingue, 1988).

## **3.01 Fill Sinks**

Sink filling algorithms in GIS software has the ability to differentiate between two types of depressions: natural-depressions and sinks. When a group of raster cells are at a lower elevation as compared to their surroundings then it is termed a natural-depression. Sinks are the result of a narrow band of raster cells of higher elevation across drainage paths, similar to an obstruction or dam across a stream. These algorithms treat sinks by lowering the selected DEM elevation values to simulate breaching of the obstruction, or dam, across the drainage path. The essential preprocessing step of sink filling has been pointed out by Mark (1984) and several solutions have been proposed since then.

Sinks can occur when neighboring cells of higher elevation surround a cell, or when two cells flow into each other, resulting in a flow loop (Burrough and McDonnell, 1998; ESRI, 1998).

Sink filling algorithms have been proposed (Jenson and Domingue, 1988; Martz and de Jong, 1988; Soille, 1988; Soille and Ansoult, 1990), and it has been shown in that mathematical morphology offers an efficient sink filling procedure even in the presence of natural depressions. The morphological sink filling algorithm is defined as the reconstruction by erosion  $R_\epsilon$  of the input digital elevation model  $f$  using a marker image set to the maximum height  $h_{\max}$  of the

digital elevation model, except along its borders and at the bottom of natural depressions, where it inherits the values of the input digital elevation model:

This procedure is shown in Figure 3.1 (Soille, 2002; Soille et al., 2003).

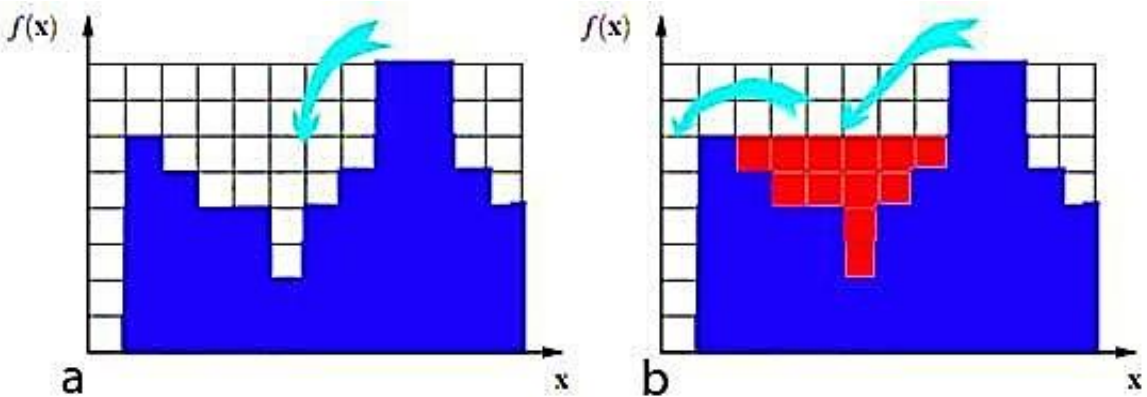


**Figure 3.1** a) Section view of a sink in which the stream cannot flow  
b) Sink filling (designated by raised pixels in red) where stream can flow

$$FILL(f) = R_f^\epsilon(f_m)$$

$$f_m(\mathbf{x}) = \begin{cases} f(\mathbf{x}), & \text{if } \mathbf{x} \text{ lies either on the border of } f \text{ or} \\ & \text{at the bottom of a natural depression,} \\ h_{\max}, & \text{otherwise.} \end{cases}$$

Mark (1984) developed a depression filling procedure in which depression cells are raised to the elevation of the lowest elevation neighbor and are encoded as a flat area. One assumption in this approach is that depressions are the result of underestimation of elevation values. Morris and Heerdegen (1988) found that the procedure of treating sinks as genuine features yielded more realistic flow directions. The approach they used is similar to the procedure of filling sinks. The procedure allows the water to flow in sinks and the water level is raised to the level of the sink's lowest neighbor. Naturally occurring sinks in elevation data with a cell size of 10 meters or larger are rare, except for glacial or karsts areas (Tarboton et al., 1993; Mark, 1988). As the cell size increases (higher resolution), the number of sinks in a data set often increases. We used GIS applications for identifying sink pixels inside the Lebanese boundary, based on SRTM and GDEM data sets and applied the procedure used by J.H. Gritzner (2006) for identifying wet land depressions.

We built a sink mask, where all cell values were coded to 1 using a con statement, which was derived from the difference grid. The Region Group algorithm was then applied to the sink mask to create unique sink regions using this syntax of commands:

Difference Grid = Filled DEM – Original DEM

Sink Mask = Con (Difference >0, 1)

Sink Regions = Region Group (Sink Mask by 8)

As a result, in this phase of study, some 14,157 sink groups of SRTM data and 104,939 sink groups of GDEM data were identified in the territory of Lebanon. Cell counts within sink groups varied from a single cell (8,100 square meters SRTM and 900 square meters GDEM). It is clear from the sink group values of the different datasets, that sink numbers increase with the resolution (pixel size) of the DEM (Figure 3.2).

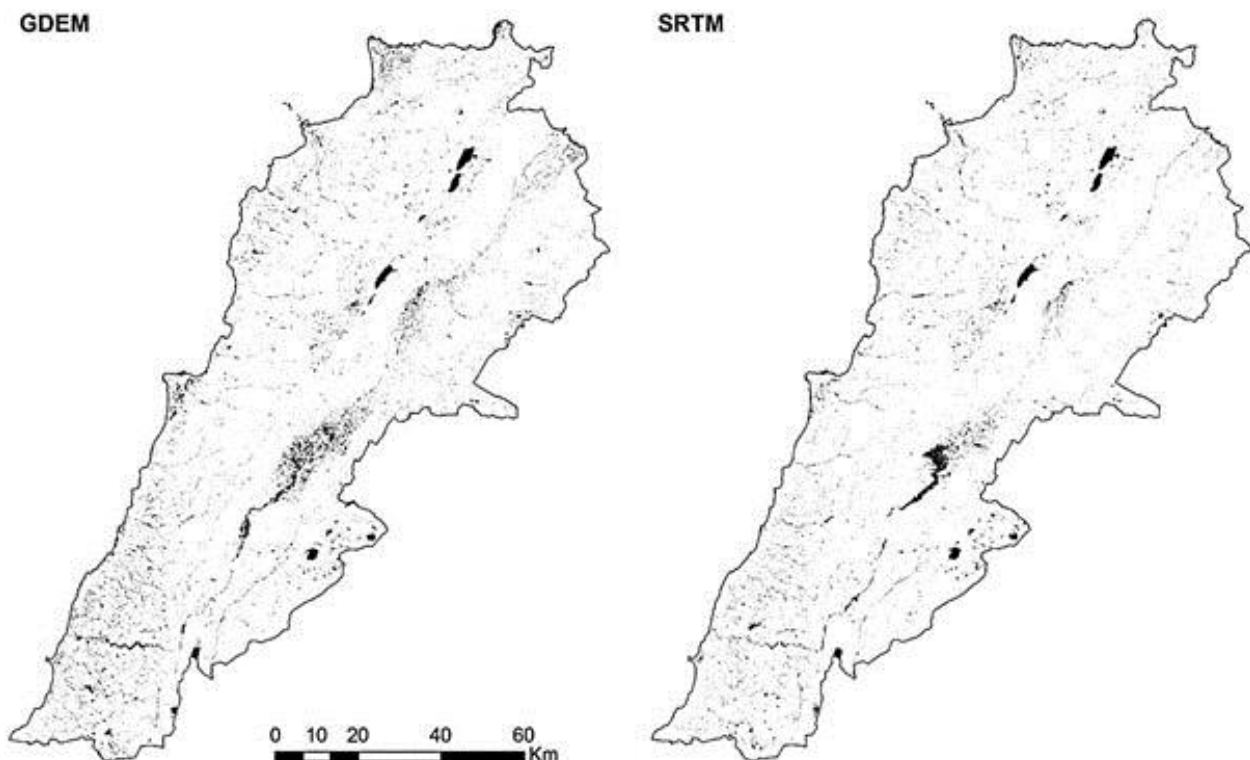


**Figure 3.2** Displays the Region Group Grid of the SRTM and GDEM Data Sets

The resultant DEM after a Fill operation is employed in generating flow direction, flow accumulation, and drainage line grids. Without filling the sinks, no hydrological project could run properly, it will lead to uncontinuous braked stream networks.

## 3.02 Flow Direction

The fundamental principle behind the determination of flow direction is that water will flow from a higher place to a lower place. On a terrain surface, peaks are the maxima and pits are the minima. Ridge lines connect local maxima and valley lines or, thalweg connect local minima. Therefore, water will flow from peaks and ridge lines to valleys and pits. The direction of the flow can also be determined using Digital Elevation Models. The concept of flow direction is very important because it allows for the inference of drainage areas, flow lengths, and the automated delineation of watersheds.

Once the depressions and flat areas are treated, the flow directions are determined for each and all. The flow direction is determined by identifying the neighboring cell which has the highest positive distance weighted drop (Jensen and Domingue, 1988). There are numerous algorithms employed to interpret DEMs for computing flow direction, and are referred to as single or multiple flow path algorithms (Tarboton, 1997; Quinn, 1991, Costa-Cabral and Burges, 1994, Wolock and McCabe, 1995).

1. Single-flow direction: The flow should be received by a single neighboring cell that has the maximum downhill slope to the current cell, as shown in Figure 3.3a.

2. Multiple-flow direction: Multiple flow path methods can distribute flow in all downslope directions, as shown in figure 3.3b (Wolock and McCabe, 1995; Quinn et al., 1991).

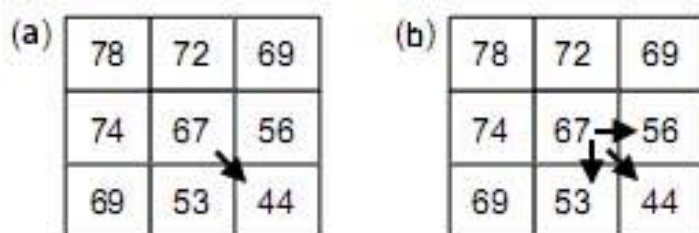


**Figure 3.3 DEM Cells  $3 \times 3$  with Elevation Values**

- a) Single-flow direction
- b) Multiple-flow direction

### 3.02.1 The Single Flow – D8 Algorithm

This algorithm was described by O'Callaghan and Mark (1984). Implementation of this method results in the hydrological flow at a point only

following one of the eight possible directions corresponding to the eight neighboring grid cells (Mark, 1984; O'Callaghan and Mark, 1984; Band, 1986; ESRI, 1991). That is why the approach is called 'single flow' algorithm.

The direction of flow is determined by finding the direction of the steepest descent from each cell (Greenlee, 1987). We first calculate the drop in each 8 neighborhoods as:

$$Drop = \frac{Z^{diff}}{Distance} \times 100 \quad (1)$$

Here  $Z^{diff}$  is the elevation difference between the center cell and its neighbor, and the *Distance* is defined as the distance between 2 cell centers. Note that the distances would be different between two orthogonal cells and two diagonal cells (Figure 3.4).

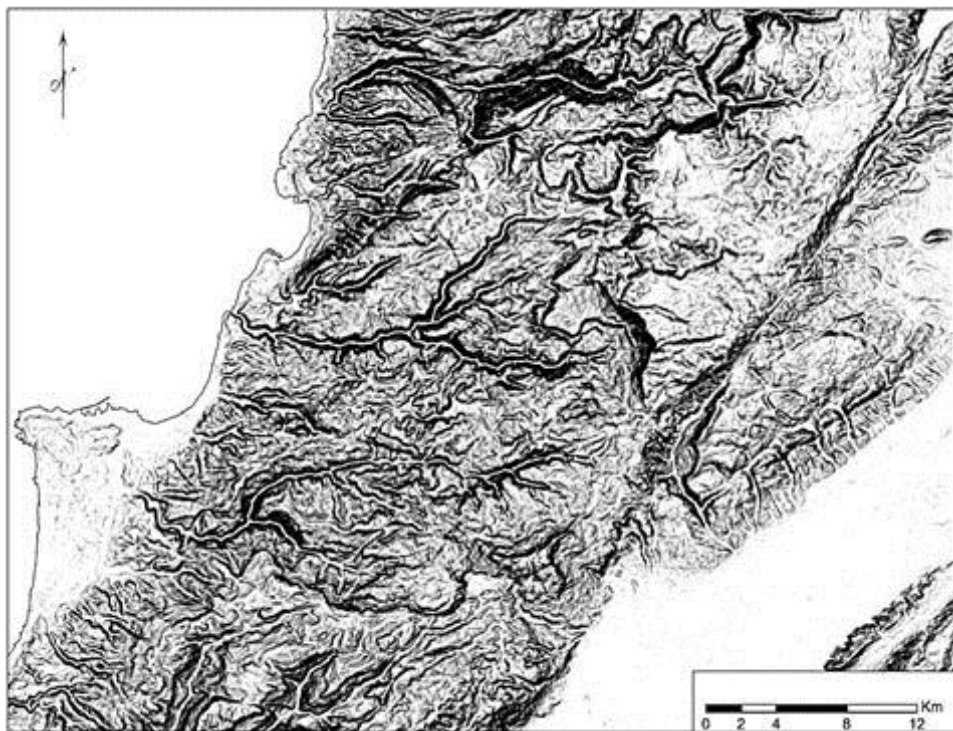


**Figure 3.4 Water Drop Map of Lebanon**

In Figure 3.4, the high values in black are found in valleys such as those of Nahr Ibrahim. The Drop map can be applied in the prediction of electro stations project situations. The next step after calculating water drop is, flow direction encoding as used by ESRI. The direction value starts as 1 from the east, and is multiplied by 2 as it changes clockwise (Figure 3.5).

↖	↑	↗
←	○	→
↙	↓	↘

32	64	128
16	-1	1
8	4	2

**Figure 3.5 An Illustration of the Transformation of Visually Meaningful Flow Direction to GIS Datasets**

In ASTER GDEM data sets, the cell size is 30, the distance between two orthogonal cells is 30 and the distance between two diagonal cells is  $(30 \times 1.414214)$  or 42.43. If the descent to all adjacent cells is the same, the neighborhood is enlarged until a steepest descent is found.

Probably, the most common algorithm is the ‘D8’ algorithm, where the flow direction for every cell within the watershed is determined by considering the surrounding eight neighboring cells.

The single flow path method is integrated with ArcGIS and computes flow direction based on the direction of steepest descent in one of the 8 directions from a center cell of a  $3 \times 3$  window. This method is often referred to as D8. The reader should be able to verify that the flow directions are as those shown in Figure 3.6.

a	1	2	3	4
A	↓	↖	→	↘
B	↗	↓	↘	↓
C	↓	↓	→	↘
D	↓	↖	↘	↓

b	1	2	3	4
A	4	8	1	2
B	2	4	2	4
C	4	4	1	2
D	4	8	2	4

*Figure 3.6 a) Arrows visually indicate the flow directions throughout the  $4 \times 4$  DEM sample; b) GIS matrix of flow directions for  $4 \times 4$  DEM grid, the coding system shown is employed (Zhilin Li et.al, 2004)*

Notice that each cell has only one flow direction. However, some cells, for example cell C4, receive flow from cells B3, B4, and C3.

The arrows indicating flow directions are useful for the human eye to interpret, but unfortunately, the GIS needs some other method to ‘understand’

which way the flow is going in a given cell. The method used to denote these flow directions is arbitrary. The ArcView GIS uses  $\sqrt{2}$  increasing clockwise from due east: 1, 2, 4, 8, 16, 32, 64, and 128. In figure 3.5, we can see the application of a GIS nomenclature for flow directions in a matrix for the  $4\times 4$  DEM. It is worthwhile to briefly comment on some practical difficulties that must often be overcome in determining flow directions from a DEM. The D8 algorithm presented here assumes that flow directions always exist. However, for the quantitative measurement of the flow distribution, this over-simplified assumption must be considered as illogical and would obviously create significant artifacts in the results, as stated by Freeman (1991), Holmgren (1994), Wolock and McCabe (1995), Pilesjö and Zhou (1996). In the present study, the analysis and results are dependent on the D8 method as this is the algorithm employed by ArcGIS (Jenson and Domingue, 1988).

### 3.02.2 The Rho8 Algorithm

In the Rho8 algorithm, presented by Fairfield and Leymarie (1991), water flows from a center cell to one of its eight neighbors, but the choice of the cell is made stochastically. The problem in this method is convergence and divergence where flow is supposed to be parallel due to the randomness of this method. The fact that this stochastic method cannot be reproduced with the same result over the same surface is sometimes also considered unfavorable.

### 3.02.3 Multiple-Direction Algorithms

Multiple-direction algorithms were proposed by Freeman (1991), Quinn et al. (1991), Holmgren (1994), Pilesjö (1994), Pilesjö and Zhou (1996), to solve the problems with the ‘single flow’ algorithms. These algorithms estimate the flow distribution values proportionally to the slope gradient, in each direction. Holmgren (1994) summarizes some of the algorithms as:

$$f_i = \frac{(\tan \beta_i)^x}{\sum_{j=1}^n (\tan \beta_j)^x}, \text{ for all } \beta > 0 \quad (2)$$

Where  $i, j =$  flow directions,  $f_i =$  flow proportion in direction  $i$ ,  $\tan \beta_i =$  slope gradient between the centre cell and the cell in direction  $i$ , and  $x =$  variable exponent.

By changing the exponent ( $x$ ) in Equation (2), two approaches are observed to estimate flow distribution. While  $x = 1$ , flow will be distributed to downhill neighboring cells proportional to the slope gradients, as suggested by Quinn et al. (1991). Holmgren (1994) suggested an  $x$  value between 4 and 6. This gives a result between a very homogeneous flow distribution when  $x = 1$ , and a distinctive flow, which occurs when  $x$  becomes greater than 10. Pilesjö and Zhou (1997) used cone, hemisphere, and inverse hemisphere surfaces to test different  $x$  values. They concluded that an  $x$  value of 1 was optimal, especially on convex surfaces. Freeman (1991) proposed an  $x$  value of 1.1 after testing for flow over a right circular cone. One of the problems with multiple-direction algorithms, independent of the value of the exponent  $x$ , is the diverging flow over planar surfaces where we expect the flow pattern to be parallel.

### **3.02.4 Topographic Form-Based Algorithm**

This algorithm was presented by Pilesjö et al. (1998) and is a ‘multiple flow direction’ approach based on  $3 \times 3$  cell surface analysis. It was assumed that flow diverges over convex surfaces, and converges over concave surfaces. There is no absolute way to determine convexity and concavity – it often implies approximations. One way to approximate, used in the topographic form-based algorithms, is to employ a trend surface based on the elevation values of all nine cells. When the form of the center cell is identified as concave, the flow is distributed fully in the main drainage direction. If the main drainage direction is not equal to the direction of one of the eight neighboring cells, the flow distribution has to be split between two cells. This is done by splitting the drainage vector into two diagonal vectors. When the topographic form of the center cell is identified as convex, the flow is distributed according to Equation 2.

### **3.02.5 The DEMON Algorithm**

The DEMON algorithm was presented by Costa-Cabral and Burges (1994). They used two-dimensional flow tubes in order to trace flow up-stream and down-stream. The direction of flow over each cell is approximated to the aspect value. By connecting (flow) lines, parallel to the aspect values, from the corner points of a cell receiving water, a flow tube can be estimated. Unlike most other flow algorithms, DEMON does not distribute flow directly to diagonal neighbor cells but through a point that has no width. This distribution sometimes causes problems, where all cell surfaces are approximated to first order (planar) surfaces. This often results in ‘gaps’ between individual surfaces, which is unrealistic. Costa-Cabral and

Burges (1994) also write that some problems connected to the method “can be avoided only if a curved rather than a planar surface is fitted to each pixel”.

### 3.02.6 GIS Applied Algorithm

The disadvantages of the single flow algorithms are obvious. Also the limitations of the multidirectional algorithms are problematic. Estimated contributing drainage areas are discontinuous. Another important source of error, both for single and multiple flow algorithms, is the point source assumption. Depending on terrain complexity in relation to cell size, this is more or less pronounced. Only the deterministic eight-node (D8) is introduced because of its simplicity and wide implementation in GIS. However, it has been found from experimental testing and may produce unacceptable errors.

Using ArcGIS D8 algorithm to build a flow direction map with direction coding derived from a water drop map, as seen in Figure 3.6. Each direction code took a different color to be distinguished from the other ones, as also shown in Figure 3.6, where the green color expresses the code number 2 or the South East direction occupying most of the area of the territory especially in the Bekaa valley. We compared two types of flow directions from different DEM precisions (SRTM, GDEM), and it is from the normal that we got two different results caused by pixel size of datasets (Table 3.1).

**Table 3.1** Flow Direction Codes and Pixel Quantity in Each Dataset

Flow Direction Codes	SRTM		GDEM	
	Number of Pixels	Percentage %	Number of Pixels	Percentage %
1	203087	12	1728204	11
2	185438	11	1700890	11
4	234608	13	2223185	14
8	162146	9	1515918	10
16	295909	17	2551705	16
32	262778	15	2305872	15
64	272802	16	2539257	16
128	137817	8	1327048	8

Values of SRTM and GDEM in Table 3.1 are very similar. The biggest area of code 16 expresses the Western direction within 17 % in SRTM and 16 % in

GDEM. Besides the code 128 Northeastern direction, all these values are represented graphically in Figure 3.6, in which the codes 16 and 128 are yellow and dark blue and situated in the mountainous area. The western direction of code number 16 occupies the wide area of Lebanon, and that means most of the streams flow to the western direction. We can conclude from the values in Table 3.1 that, in flow direction processing DEM resolution does not play a big role.

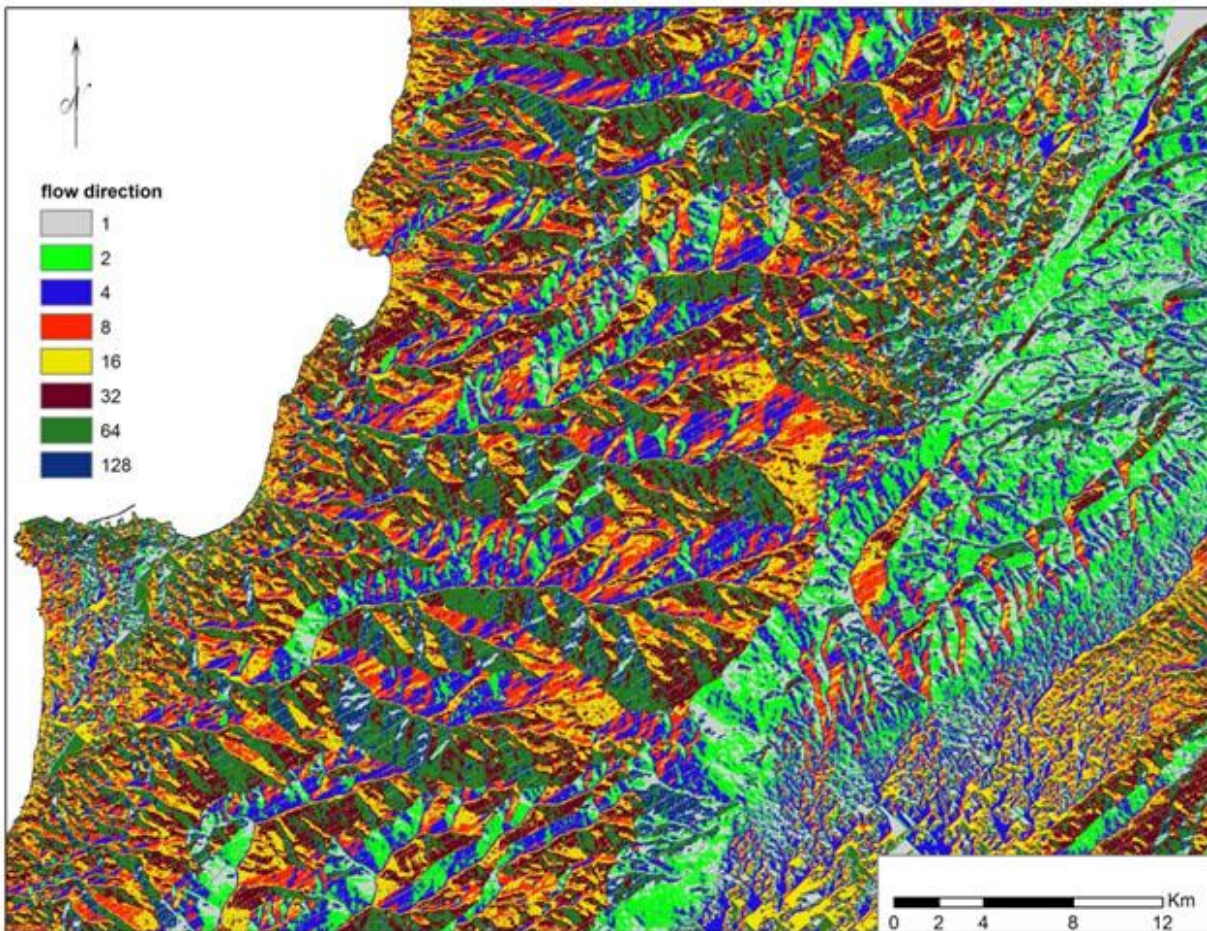


**Figure 3.7 Flow Direction Map of Lebanon with Direction Codes**

### 3.03 Flow Accumulation

Basing to flow directions, we are able to determine flow accumulation. The flow accumulation is synonymous with drainage area. Flow accumulation is very important for hydrologic applications since it determines the size of the region over which water from rainfall, snowfall, etc. can be aggregated. Flow accumulation is also known as basin area, upslope area, and contributing area. Flow accumulation is

computed by accumulating the weight for all cells that flow into each down slope cell (ESRI, 1998; Jenson and Domingue, 1988). The algorithm for computing Flow Accumulation follows two steps:

1. If the cell has no neighboring cells draining to it, a value of ‘1’ is assigned.
2. If the cell receives drainage from any of the eight immediate neighboring cells, it is assigned the value of ‘1’ plus the sum of the flow accumulation draining from each neighboring cell.

	1	2	3	4
A	1	1	1	4
B	5	1	4	5
C	6	1	1	10
D	1	1	15	1

**Figure 3.8** Flow Accumulation for  $4 \times 4$  Grid  
(shaded cells illustrate the beginning of the flow network)

Applying rules 1 and 2 to the  $4 \times 4$  DEM results in the solution shown in Figure 3.7. In rule 1, cells receive a value of ‘1’. In white, cell C4 receives flow from cells B4 and B5, which carry flow accumulations of cells 4 and 5, respectively. Therefore, the flow accumulation for cell C4 is  $4 + 5 + 1 = 10$ .

We should note that the above flow accumulation algorithm is premised on the D8 model of flow directions. If a more complicated flow direction algorithm is used, such as one of those developed by Costa-Cabral and Burges (1994) or Tarboton (1997), then determining flow accumulation is also somewhat more complicated. The main difference in the outcomes from these other algorithms is that the resulting flow accumulations will no longer work out to be in integer counts of cells, but instead flow accumulation will generally be a real quantity. In any case, the physical interpretation remains the same: that flow accumulation corresponds to drainage area.

D8 actually provides a very good estimate of the flow accumulation that is far enough downstream to be in the fully convergent, channelized portion of the landscape. However, for grid cells on hillslopes or near peaks and divides, where

the flow is divergent, values obtained by this method can be off by orders of magnitude (Gruber and Peckham, 2007). Cells with a high flow accumulation value may represent areas of concentrated flow and can be used in the identification of stream channels. Cells with a flow accumulation of 0 are considered topographic highs and can be used to identify ridges. If a cell has a 0 in the flow accumulation matrix, it means that no water from other cells flows to it. Thus, this cell must be a local maxima, corresponding to points at peaks and ridge lines.

Flow accumulation cannot only be used to accumulate contributing area but, also other quantities such as the amount of contributing pixels, accumulated precipitation or, accumulated terrain attributes (elevation) (Gruber and Peckham, 2007). Flow accumulation is a powerful GIS capability because, calculating it as a spatially distributed quantity allows us to determine drainage area, not at just one point, but at any point within the domain of the original DEM field (Figure 3.8).

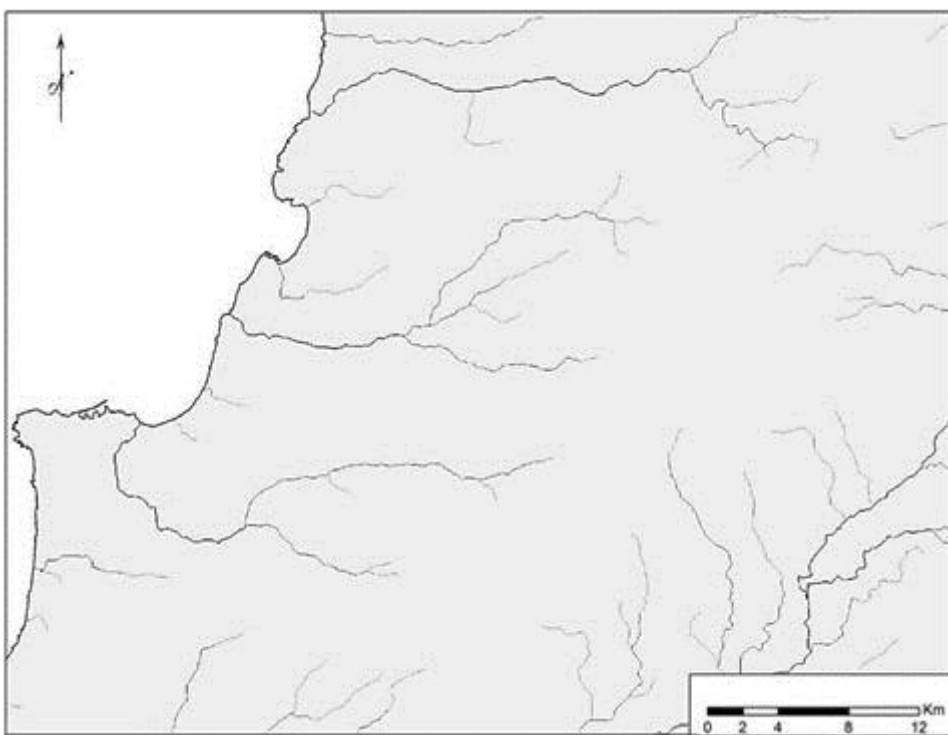


**Figure 3.8** *Flow Accumulation of Lebanon Showing the Flows of the Beirut, El Kalb and Ibrahim Rivers*

Flow accumulation of the Lebanese territory based on GDEM and SRTM gives the same result in both datasets. In Figure 3.8, streams are very bright so we

can distinguish rivers from each other like the El Kalb, Beirut, and Ibrahim, and observe how they flow.

### 3.04 Stream Order

Stream systems are characterized by numerous tributaries that merge downstream, and thus can be represented as networks of segments with a hierarchical structure. Geomorphologists rank the relative importance of stream segments in the network by assigning a numerical order value to each segment, using one of four ordering systems (Strahler, Horton, Shreve, and Scheidegger). In mathematics, the Strahler number or Horton–Strahler number of a mathematical tree is a numerical measure of its branching complexity. These numbers were first developed in hydrology by Robert E. Horton (1945) and Arthur Newell Strahler (1952, 1957). In such an application, they are referred to as the Strahler stream order and are used to define stream size based on a hierarchy of tributaries.

The stream order hierarchy was officially proposed in 1952 by Arthur Newell Strahler, a geoscience professor. A first order stream is the smallest stream and consists of small tributaries. These are the streams that flow into and ‘feed’ larger streams but do not normally have any water flowing into them. In addition, first and second order streams generally form on steep slopes and flow quickly until they slow down and meet the next order waterway. Horton explains: «This system begins with the same ordering scheme as the Strahler system, but the main stream maintains the same order number all the way upstream to a single headwater source. The order of major tributaries is treated in the same way. At each junction where two segments of equal Strahler order meet, the longest or most direct upstream segment is renumbered to the higher order of the main stream or branch». (Horton, 1945)

Shreve also states: «The order or “magnitude” of a stream segment formed at a junction is the sum of the magnitudes of the two tributaries. For example, the confluence of a magnitude 1 and magnitude 3 stream forms a magnitude 4 stream. The magnitude of any stream segment equals the number of its magnitude 1 sources, which means that the Shreve magnitude is more simply related to predicted flood flow than other ordering systems». (Shreve, 1966)

According to Scheidegger, this system defines, for each segment, an ‘associated integer’ that is twice the Shreve magnitude. The Scheidegger stream order is the logarithm to the base 2 of the associated integer.

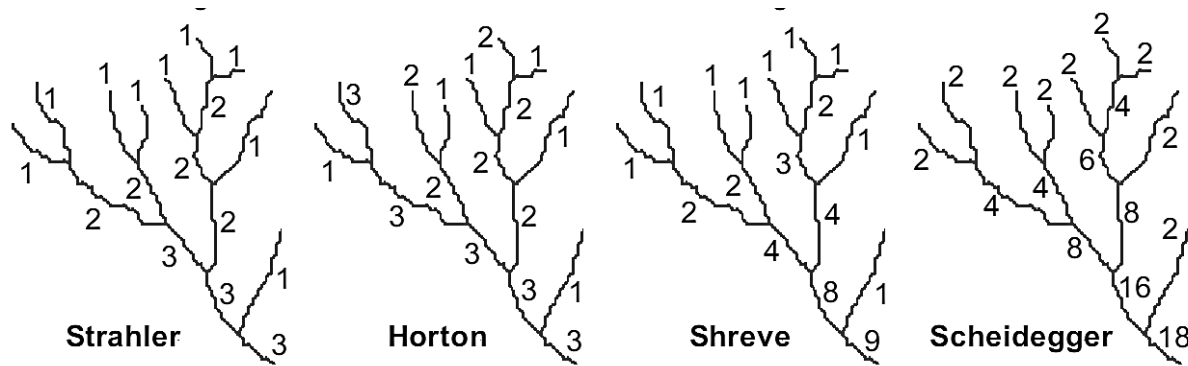


**Figure 3.9 Stream Orders as by Strahler, Horton, Shreve, and Scheidegger**

When studying stream order, it is important to recognize the pattern associated with the movement of streams up the hierarchy of strength. Because the smallest tributaries are classified as first order, they then take a joining of two first order streams to form a second order stream. When two second order streams combine, they form a third order stream, and when two third order streams join, they form a fourth and so on. First through third order streams are also called headwater streams and constitute any waterways in the upper reaches of the watershed. It is estimated that over 80% of waterways are these first through third order. Going up in size and strength, streams that are classified as fourth through sixth order are medium streams while anything larger is considered a river. For example, to compare the relative size of these different streams, the Litani River in Lebanon is an eighth order stream basing to SRTM data sets while a tenth order stream basing to GDEM data sets.

Methods of classifying streams are important to geographers, geologists, hydrologists and other scientists. Classifying stream order allows scientists to more easily study the amount of sediment in an area, and more effectively use waterways as natural resources as well as gives an important component to water management. In our study, stream order has been used in geographic information systems (GIS) to map river networks. The algorithm uses vectors (lines) to represent the various streams. Stream generation is possible after the hydrological correction of the Earth's surface (sink filling). To build a stream order map of the drainage network in GIS, we must follow a few processing steps as shown Figure 3.10.

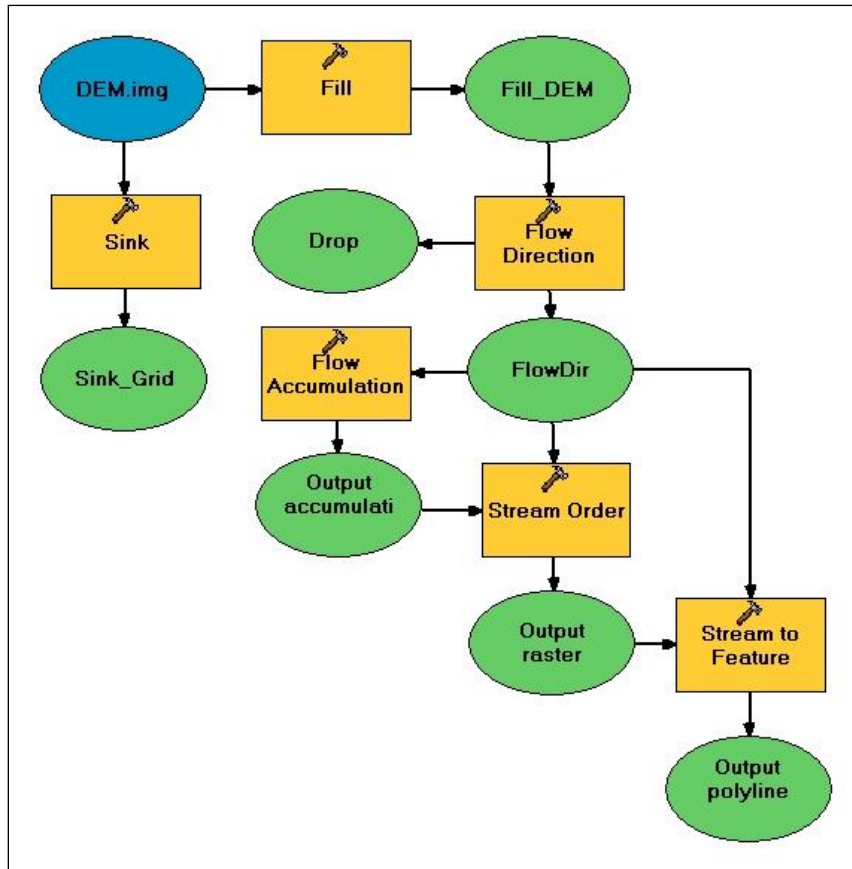


**Figure 3.10 Automated Algorithm for Building a Vector Model of the Drainage Network Elements According to DEM Using ArcGIS Model Builder**

For the generation of stream order network, a computing algorithm was built in Model Builder of ArcGIS following these steps of processing: sink, fill, flow direction, flow accumulation, and stream order. According to the computed algorithm with the SRTM and GDEM data sets of the Lebanese territory, Lebanon selected 8 orders of SRTM streams and 10 of GDEM. The first 3 orders in both data sets are short length straight lines which do not form a natural geographical shape of streams, and are counted as artifacts. The resulting model makes the possibility to perform a number of morphometric calculations and to establish the local empirical relationship between the order of the elements of the drainage network and the number, length, etc. (Horton, 1945; Tarboton et al, 1991; etc.).

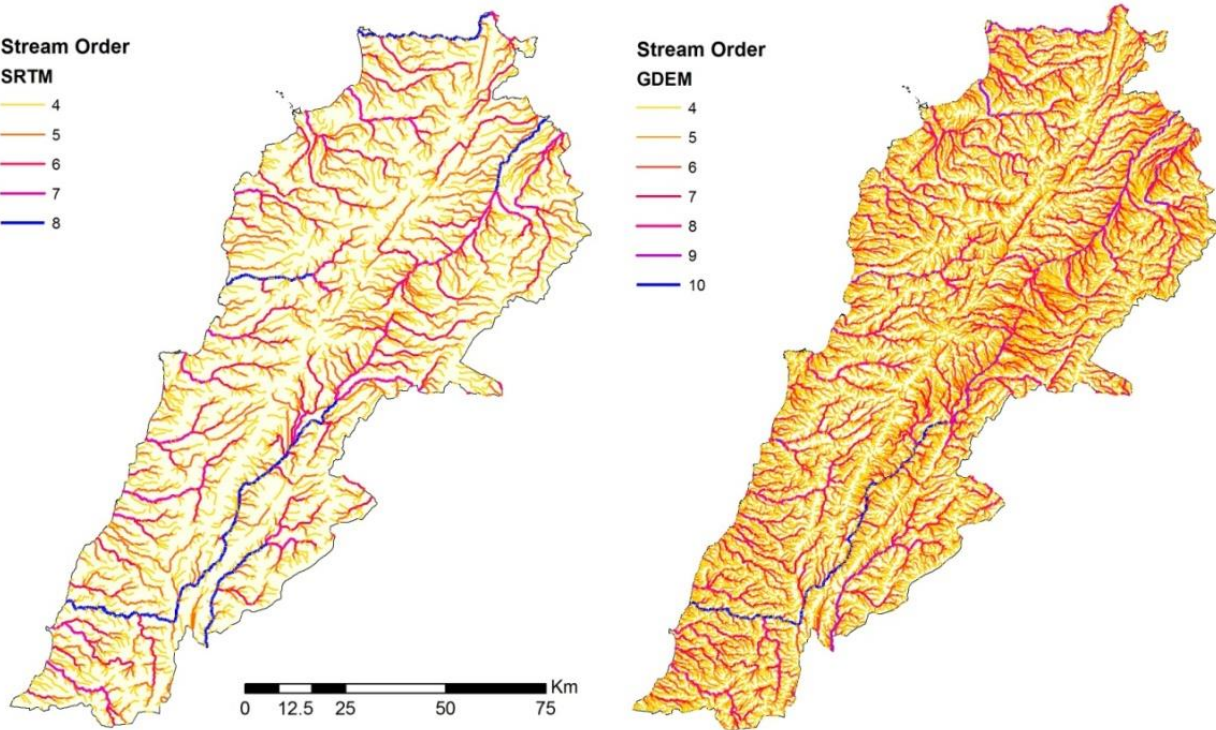


**Figure 3.11 Stream Network Maps of Lebanon Based on SRTM and GDEM**

Information about the drainage network of Lebanon is listed in Table 3.1, according to which the total length of thalwegs 1-8 orders of SRTM data sets is 99.4 thousand km. In this case, the elements of the drainage network 1-order occupied about 69% of the total length, and the total stream length of 1-2 orders occupied more than 86% of the total length. Otherwise the total length of GDEM data sets thalwegs 1-10 orders is 334.9 thousand km because of the high DEM resolution which is three times more than that of the SRTM.

**Table 3.2 SRTM and GDEM Extracted Strahler Stream Orders**

Order	SRTM			GDEM		
	Length ,km	Length ,log	Length ,%	Length /km	Length log	Length %
1	68923	4.8	69.3	229462	5.4	68.5
2	16495	4.2	16.6	67280	4.8	20.1
3	7046	3.8	7.1	19945	4.3	6.0
4	3517	3.5	3.5	8758	3.9	2.6

Order	SRTM			GDEM		
	Length ,km	Length ,log	Length ,%	Length /km	Length log	Length %
5	1931	3.3	1.9	4745	3.7	1.4
6	907	3.0	0.9	2418	3.4	0.7
7	350	2.5	0.4	1393	3.1	0.4
8	256	2.4	0.3	556	2.7	0.2
9	-	-	-	264	2.4	0.1
10	-	-	-	110	2.0	0.03
<b>Total</b>	<b>99425</b>	-	-	<b>334931</b>	-	-

In Table 3.2, we used logarithmic scale to reduce the big difference between first and last order, which helped us in diagram building and analysis.

### 3.05 Watershed Basins

Watersheds are important geomorphologic features, which play an important role in hydrological GIS applications. Watersheds can be regarded as the lines that separate the area where water drains to different locations. The areas that are enclosed by the watersheds are precisely the regions where water drains to the same place, and are conventionally called basins or valleys.

The Watershed process addresses the influence of terrain on surface water hydrology by modeling the movement of water over the land surface. The Watershed process computes the local directions of flow and the gradual accumulation of water moving down slope across the landscape. From these intermediate results, the process then computes the stream network and the boundaries between watersheds. Watersheds can be further subdivided into basins associated with particular branches of the stream network.

A watershed, catchment, or drainage basin is an area from which water, sediments, and dissolved materials flow to a common outlet, as concentrated runoff (Dunne and Leopold. 1978). The boundary between two catchments is referred to as a drainage divide or catchment boundary. In the days before GIS and the availability of DEM data, watershed delineation often required painstaking and time-consuming manual effort on the part of the hydrologist to determine watershed boundaries, hand-draw curves emanating from the watershed outlet, and always travel perpendicular to contour lines of elevation. Today's commonly available GIS-based tools have reduced the efforts of watershed delineation. Until

recently, delineation of drainage networks and catchments has been made from contour lines in topographical maps or from aerial photo-interpretation (Böhme, 1988; Dunne and Leopold, 1978; Klinghammer and Loránd, 1991; Mulders, 1987).

Watershed delineation is one of the most commonly performed activities in hydrologic and environmental analyses. Digital elevation models (DEM) provide good terrain representation from which the watersheds can be derived automatically using GIS technology. The techniques for automated watershed delineation have been implemented in various GIS systems and custom applications (Garbrecht and Martz, 1999). These techniques are independent of the DEM resolution. One of the major categories of approaches to extract watersheds are the ridge detectors, which were first proposed in the early part of the 19th century (Rothe, 1915; Koenderink and van Doorn, 1994). Another theory was proposed by Maxwell, Jordan, and Cayley (Koenderink and van Doorn, 1994; Rieger, 1997). It is based on the observation that, for generic surfaces, there is a unique slope line through every non-critical point of the surface. However, it suffers from some poor implementation choices that lead to inaccurate results and some surprising cases, in which, for example, slope lines can cross each other. A third way to extract watersheds from the image is to use the fact that water will accumulate at the minima of the landscape. This means that each minimum in the image defines a valley or water catchment basin. Watersheds are the boundaries between different basins. This can be implemented by flooding the landscape from the minima (Vincent and Soille, 1991). Since all of the approaches to extract watersheds return the result only with pixel resolution, a pixel accurate watershed extraction algorithm is desirable. This means that either the definition of Maxwell, Jordan, and Cayley must be used, or that of Rothe.

GIS and digital elevation models (DEM) can be used to perform watershed delineation. Watersheds can be delineated quickly and with consistent time response, regardless of the DEM resolution. The most straightforward GIS technique for watershed delineation consists of the below steps (ESRI, 1997; Olivera and Maidment, 1999). The threshold definition (stream definition) is performed after the flow direction and flow accumulation grids are determined. The following process can be implemented:

1. Perform flow direction and flow accumulation computations.
2. Specify a ‘stream’ threshold depending on the desired performance. This operation will identify all the cells in the flow accumulation grid that are greater than the provided threshold. A new grid is formed from those cells. This grid will be an indication of the drainage network.
3. Watersheds grid are defined.

4. Watershed and stream grids are vectorized to produce watershed polygons and stream polylines.

An overview of the process is presented in Figure 3.12.

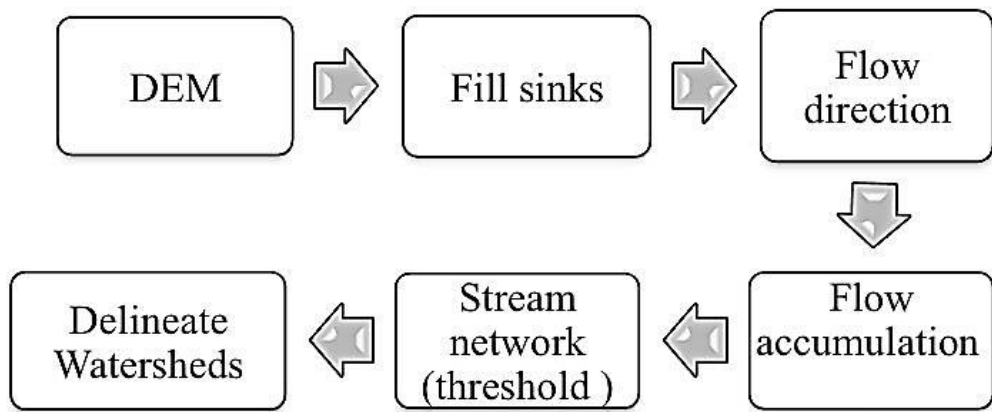


**Figure 3.12 Processing Flow for Initial Arbitrary Subwatershed Delineation**  
(ESRI, 1997)

Figure 3.12 elements are the actual steps used to support the interactive delineation. Delineation of the drainage network of an area from a DEM requires the establishment of a threshold area. Threshold value is referred to as a threshold area that represents the minimum support area required to drain to a point where water can flow in a concentrated manner, and for a channel to form (Rieger, 1993). Different drainage networks are obtained depending on this threshold area. A high threshold area value will create a drainage network with the main streams. According to the objectives of the user's application, different threshold area values can be applied to obtain the best fit drainage network. In this respect, several authors have pointed out that a variable threshold area should be considered for areas with different relief characteristics (Da Ros and Borga, 1997; Gandolfi and Bischetti, 1997). It is important to note that the threshold value in this process does not have any particular geomorphologic meaning through which we are identifying drainage network. As the threshold value is increased, the density of the drainage networks decreases.

The threshold used to delineate the network may vary from one watershed to another since it is dependent on factors such as land use and soil type. Arbitrary methods of threshold value selection without considering factors such as local terrain slope, soil properties, geology, infiltration capacity, surface cover, and climatic conditions can lead to erroneous networks (Garbrecht and Martz, 1993).

In the present research, different drainage networks for different sample catchments of Lebanon, derived from varying the threshold value, were compared with the drainage networks coming from SRTM and GDEM. Cells, having a flow accumulation value of zero (to which no other cells flow), generally correspond to the ridges. A threshold is selected to delineate the drainage network and, all cells, which are greater than the threshold value, are classified as part of the drainage network. This approach is simple and reliable since it depends on accumulated flow to define the flow paths. Arbitrary methods of threshold value selection without considering factors such as local terrain slope, soil properties, geology, infiltration capacity, surface cover and, climatic conditions can lead to erroneous networks (Garbrecht and Martz, 1993).

In our study for delineating watersheds we used the ArcHydro model. ArcHydro is a model developed for building hydrologic information systems to synthesize geospatial and temporal water resource data that supports hydrologic modeling and analysis. The model is developed as an Add-on to ArcGIS software.

As an experiment, the considered threshold area values for SRTM dataset were between 1,000 cells ( $8.1 \text{ km}^2$ ) and 10,000 cells ( $81 \text{ km}^2$ ), and the GDEM dataset were between 10,000 cells ( $81 \text{ km}^2$ ) and 100,000 cells ( $810 \text{ km}^2$ ). ArcHydro surface analysis and terrain processing tools were used to compare the two datasets. Stream networks and watershed delineations for both the 30 m and 90 m DEMs were used as the basis for comparisons.

Very different drainage network representations are produced by using different threshold area values. As an example, Figure 3.13 shows this situation after applying different threshold area values to the flow accumulation grid of Lebanese basins. The idea behind this operation was to obtain different equations to estimate the best fit threshold area, with the only input of easy derived topographical variables.

Very different drainage network representations are produced by using different threshold area values. As an example, Figure 3.13 shows this situation after applying different threshold area values to the flow accumulation grid of Lebanon. This figure also shows the drainage network as derived from DEM, the application of the proposed methodology, to obtain the best fit drainage network for areas with different relief types, producing the results that are summarized in Table 3.3. This table shows the threshold area values that produced the most accurate representation of the drainage networks and their catchments of SRTM and GDEM datasets.

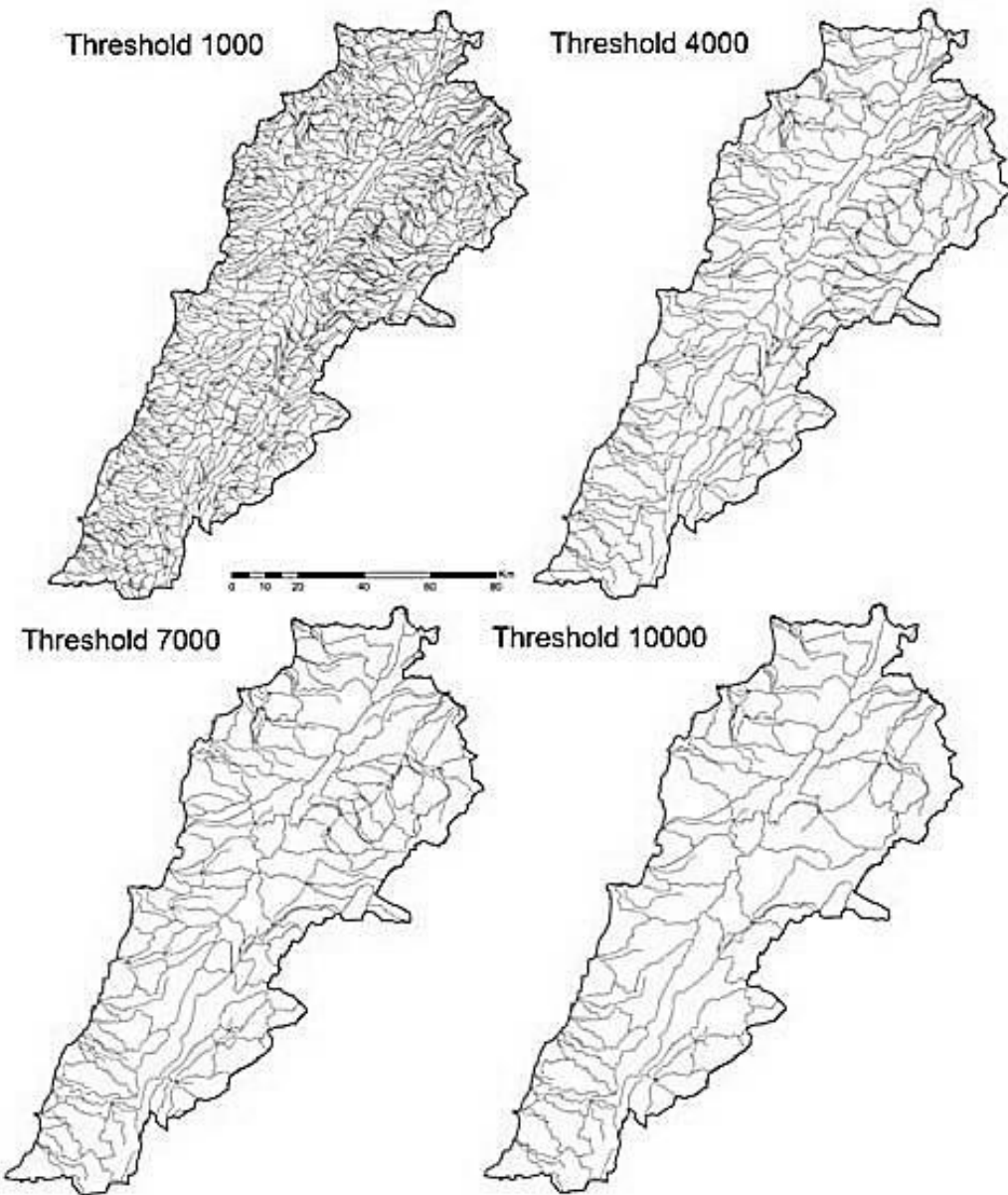


**Figure 3.13 Shows Variety of Maps after Applying Different Threshold Area Values of the Lebanese Territories**

As an experiment, we used different threshold values by using two kinds of dataset, SRTM and GDEM. Values shown in Table 3.3 are not similar to each other because of the difference in DEM resolution between these datasets – 3 arc second for SRTM and one for GDEM. Based on the results achieved, we can say that high DEM resolution needs high threshold values. For example, SRTM threshold values of 10,000 cells ( $81,000 \text{ km}^2$ ) in the Lebanese territory delineate 91 basins; otherwise 10000 cells ( $9000 \text{ km}^2$ ) delineate 859 basins. We have to notice that

between the basins quantity value, we can find artifacts which are counted as basins. These artifacts result from the boundary shape extraction.

**Table 3.3 Shows the Threshold Area Values that Produced the Most Accurate Representation of the Drainage Networks of the Lebanese Territories**

SRTM		GDEM	
Threshold Value	Basins Quantity	Threshold Value	Basins Quantity
1000	929	10000	859
2000	484	20000	491
3000	308	30000	341
4000	238	40000	223
5000	201	50000	187
6000	173	60000	161
7000	150	70000	144
8000	126	80000	128
9000	106	90000	110
10000	91	100000	106

The present research showed that very different drainage network representations can be produced by using different threshold area values. This threshold area is considered the most reliable according to the purposes of the user. The geographic information system and the digital elevation model have reached an advanced step in geomorphologic and hydrological analysis.

During the experiment, it was always necessary to edit the computed drainage network. This necessity arises, among other reasons, due to errors in height that are always found in a DEM. However, the better the chosen threshold value, the less time needed to be spent on editing the drainage network. Typical errors that are found in the computed drainage network include: non-connected arcs to the drainage network; parallel drainage lines in meandering zones; very short drainage lines that are of no significance (Pogorelov and Doumit, 2009). To edit these errors, a vector editing must be implemented. In our case, a vector editing is done for the sub watersheds obtained from the automated delineation to conserve the watershed form drawn by traditional methods.

The first step in watershed delineation correction was digitizing a watershed map of the Lebanese republic from the national office of Al Litani made by FAO. In Lebanon, we have 16 river basins all of which are inside the boundary, except for river Al Kabir watershed which is divided in two parts, half in Lebanon and half in Syria. The second step in the correction of delineated watersheds from SRTM

and GDEM to be suitable with the digitized watershed map was done by merging sub watersheds to form the real basin boundary of each river. Finally, we got three different watershed maps of Lebanon from different sources, topographic maps, SRTM, and GDEM.

The three watershed boundaries were compared visually (Figure 3.14). Regression analyses were then conducted to compare each of the DEM-based watershed boundaries to the manually-delineated boundary. For the regression analyses, the stereographic coordinate system of Lebanon was used to compare the values of  $y$  at the same  $x$  location of a vertical line intersection with basin boundaries, to determine how similar they were. The  $y$  value was chosen because of the longitudinal form of the Lebanese shape. A total of 12 points were utilized in each regression analysis. Then, a t-test was conducted to determine if the differences in the  $y$ -values between GDEM boundary and the manual boundary were significantly different than the differences in  $y$ -values between the SRTM boundary and the manual boundary.

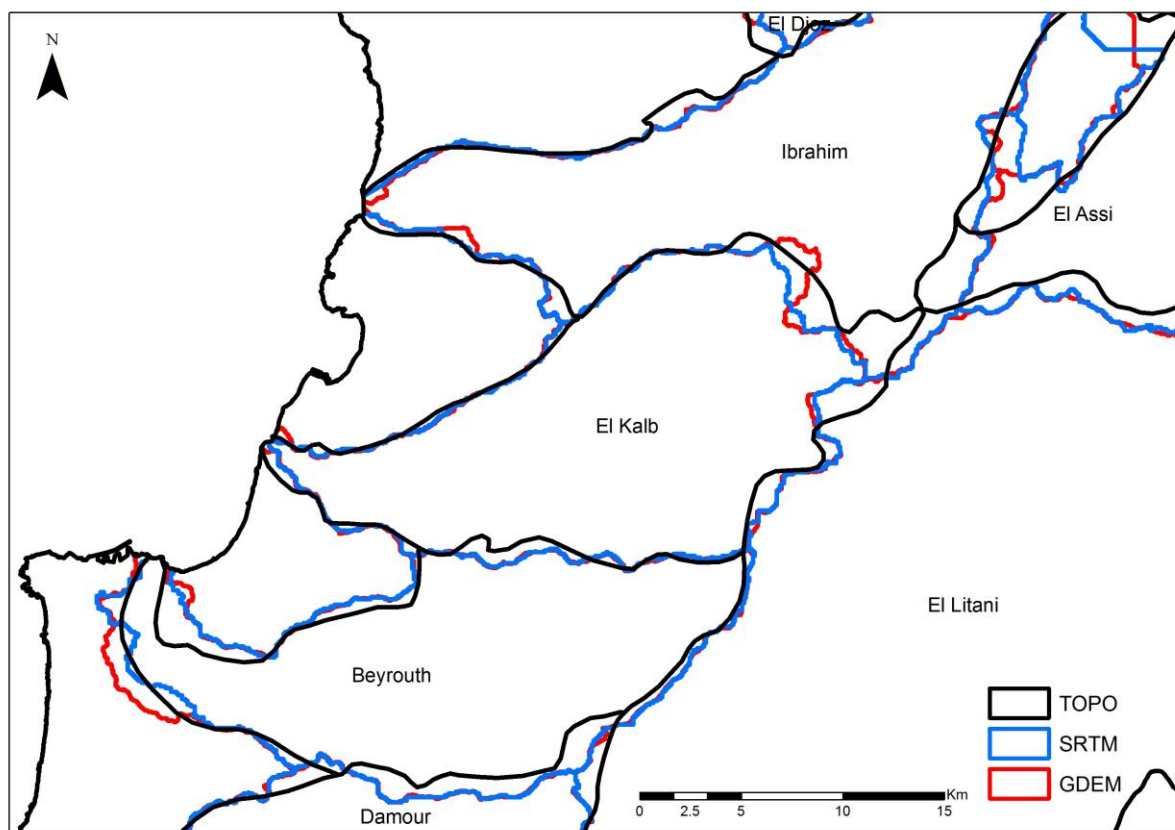


**Figure 3.14** Watershed Boundary Comparisons Based on Topographic Maps and Digital Elevation Models

Visually, there are big differences between the manually-delineated and the DEM-based boundaries (SRTM and GDEM) (figure 3.14) while the DEM-based boundary (SRTM and GDEM) varies from the manually-delineated one (TOPO), in most places. SRTM and GDEM based boundaries are very similar, in most places, with a little difference in the shape. In Figure 3.14, it is very clear that the manually-delineated boundary (TOPO) can only express the form of the watershed without any accuracy. In the North side of El Djoz basin boundary, the biggest difference in y coordinates between the GDEM-based and manual boundaries is 3,580 m while the difference between the SRTM-based and manual boundaries at the same point is 3,580 m. The result is the same because the y of GDEM and SRTM has the same value, which means there is no difference between the DEM based delineations. The regression analyses comparing 12 points along the complete boundaries yielded an R<sup>2</sup> of 0.9986 between the SRTM and manual boundaries TOPO; an R<sup>2</sup> of 0.9987 for the comparison between the GDEM and the manual boundaries; and an R<sup>2</sup> of 1 for the comparison between the GDEM and the SRTM based delineations, with a trend of a straight line, which expresses the similarity of values.

The t-test, comparing the mean distance differences in y for GDEM TOPO, SRTM TOPO, and GDEM SRTM, indicated the statistical values: -173.53 m ( $p=0.6642$ ), -176.008 m ( $p=0.6603$ ) for the GDEM and SRTM, 2.479 m ( $p = 0.001$ ). This came with a high standard error of difference with TOPO data in a range of 389.023 to 389.700 and a low standard error of difference between GDEM-SRTM of 18.834 m. The total area of the watershed delineated manually is 7,955.27 km<sup>2</sup>, while the SRTM-based watershed area is 7,938.96 km<sup>2</sup>, and the ASTER-based watershed area is 7,950.71 km<sup>2</sup>.

We also calculated areas (A), perimeters (P), shape indexes (SI) and fractal dimensions (FD) of each watershed basin for the three types of elevation data (Table 3.4).

**Table 3.4 Areas (A), Perimeters (P), Shape Index (SI), and Fractal Dimension of the Lebanese Watershed Basins Delineated from TOPO M as well as GDEM and SRTM Datasets**

Basin	GDEM				SRTM				TOPO			
	A	P	SI	FD	A	P	SI	FD	A	P	SI	FD
Abou Ali	477	148	1.92	1.19	472	141	1.83	1.19	481	101	1.29	1.49
Arka	136	98	2.36	1.23	133	94	2.29	1.22	127	58	1.46	1.68
Beirut	245	119	2.14	1.21	237	114	2.08	1.21	213	83	1.61	1.65
Damour	316	135	2.14	1.21	308	127	2.05	1.20	316	98	1.56	1.59

Basin	GDEM				SRTM				TOPO			
	A	P	SI	FD	A	P	SI	FD	A	P	SI	FD
<b>El Assi</b>	2017	294	1.85	1.18	2031	292	1.83	1.17	1982	256	1.62	1.46
<b>El Awali</b>	298	167	2.73	1.23	297	157	2.57	1.23	297	116	1.90	1.67
<b>El Bared</b>	265	130	2.25	1.21	263	123	2.14	1.21	279	90	1.52	1.60
<b>El Djoz</b>	193	110	2.24	1.22	194	108	2.18	1.21	203	82	1.62	1.66
<b>El Kalb</b>	259	116	2.02	1.20	254	106	1.88	1.20	268	85	1.47	1.59
<b>El Kebir</b>	329	204	3.18	1.25	336	199	3.06	1.24	290	149	2.46	1.76
<b>El Litani</b>	2112	557	3.42	1.23	2110	538	3.31	1.23	2176	411	2.49	1.57
<b>Hasbani</b>	595	197	2.28	1.21	594	190	2.20	1.20	594	156	1.81	1.58
<b>Ibrahim</b>	327	162	2.53	1.22	332	148	2.29	1.21	312	103	1.64	1.61
<b>Oustouene</b>	171	123	2.65	1.24	164	118	2.60	1.24	179	82	1.73	1.70
<b>Sainiq</b>	109	76	2.06	1.22	109	73	1.99	1.21	139	52	1.24	1.60
<b>Zahrani</b>	103	105	2.91	1.25	102	100	2.78	1.25	98	70	1.99	1.85

If we compare values of El Litani basin we can find that the difference in area between the GDEM and SRTM is 2 km<sup>2</sup>, and between the manual delineated is more than 60 km<sup>2</sup>. The area of the smallest basin Zahrani has a 1 km<sup>2</sup> difference between the GDEM-based and SRTM-based one, and more than 30 km<sup>2</sup> between the manual delineated one. The shape index is a statistic used to quantify the shape of any unit of area. R. J. Chorley and P. Haggett (1969) expressed this statistic as:

$$SI = 1.27^A \times L^2.$$

Where A= area of shape in km<sup>2</sup> and L= the length of the longest axis in km. A value of 1.0 expresses maximum compaction, where the shape is circular. As the shape is elongated, the less compact the slope is, and the lower the value of the index. El Litani basin has the highest shape index value related to its longitudinal form and, contrarily, El Assi basin has the lowest value due to the form of its shape, which is more compact than that of El Litani.

The last index calculated is that of the fractal dimensions. The fractal dimension, D, is a statistical quantity that gives an indication of how a fractal appears to fill space completely, as one zooms down to finer and finer scales (see Chapter 5). Watershed fractal dimension value of GDEM-based and SRTM-based are the same but very different from the manual delineated one. Based on these analyses, it is very clear in all calculated indexes that the watershed delineated from Digital Elevation Models are very similar in shape forms and in statistical values, as well as very different from the manual delineating watershed. We can conclude that watershed boundaries derived from DEM's are more trustworthy and can be good material for hydrographic, geological and topographical research.

# **Chapter 4: Hypsometry**

As is known, hypsometry is the altitudinal distribution area of earth surface. This procedure is a primarily altitude study of diverse geographical phenomena, including relief factors.

## **4.01 Geographical Characteristics and Data Sets**

The Lebanon Mountains are sometimes called Mount Lebanon. Anti-Lebanon was used to designate the eastern range. Geologists believe that the Twin Mountains once formed one range. The Lebanon Mountains are the highest, most rugged, and most imposing of the whole maritime range of mountains and plateaus that start with the Amanus or Nur Mountains in northern Syria and end with the towering massif of Sinai. The mountain range is a clearly defined unit having natural boundaries on all four sides. In the north, Al Kebir River separates it from the Nusayriyah Mountains of Syria. In the south, it is bound by the Al Qasimiyah River, giving it a length of 169 kilometers. Its width varies from about 56.5 kilometers near Tripoli to 9.5 kilometers on the southern end, where Al Qurnat al Sawda reaches more than 3 km of the other peaks that rise east of Beirut (Figure 4.1). The central highland between the Lebanon Mountains and the Anti-Lebanon Mountains is about 177 km in length and 9.6 to 16 km wide and has an average elevation of 762 meters called the Bekaa Valley. Such a distribution of heights in the context above confirms the need for a detailed analysis of the hypsometric area.

The longitudinal profile crossing the ridge of Lebanon shows the elevation distribution and the mountains' amplitude of different geological ages (Figure 4.1). At the transversal profile in blue color of Figure 4.1, the Bekaa valley is very clear between Lebanese and anti-Lebanese ridges.

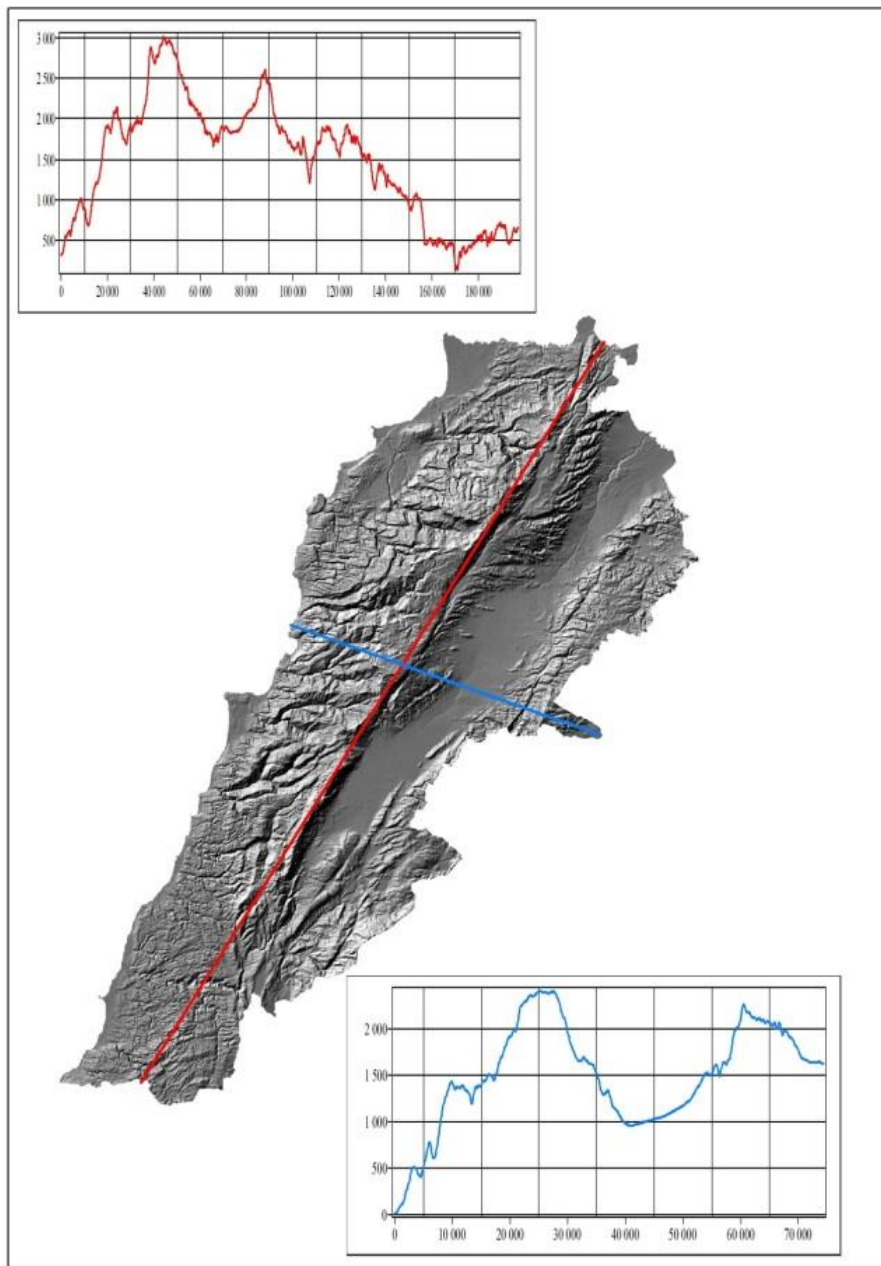


**Figure 4.1** *Longitudinal and Transversal Profiles*

## 4.02 Hypsometry of Lebanon

The possibility of using DEM with hypsometric analysis can reveal the characters of elevation ranges. The evolution of these elevation ranges of different orders may be a consequence of the different factors of relief formation and the

presence of genetically heterogeneous forms of relief. The most common method of elevations structure research is the histogram of areas and hypsographic curve (Pogorelov and Doumit, 2009).

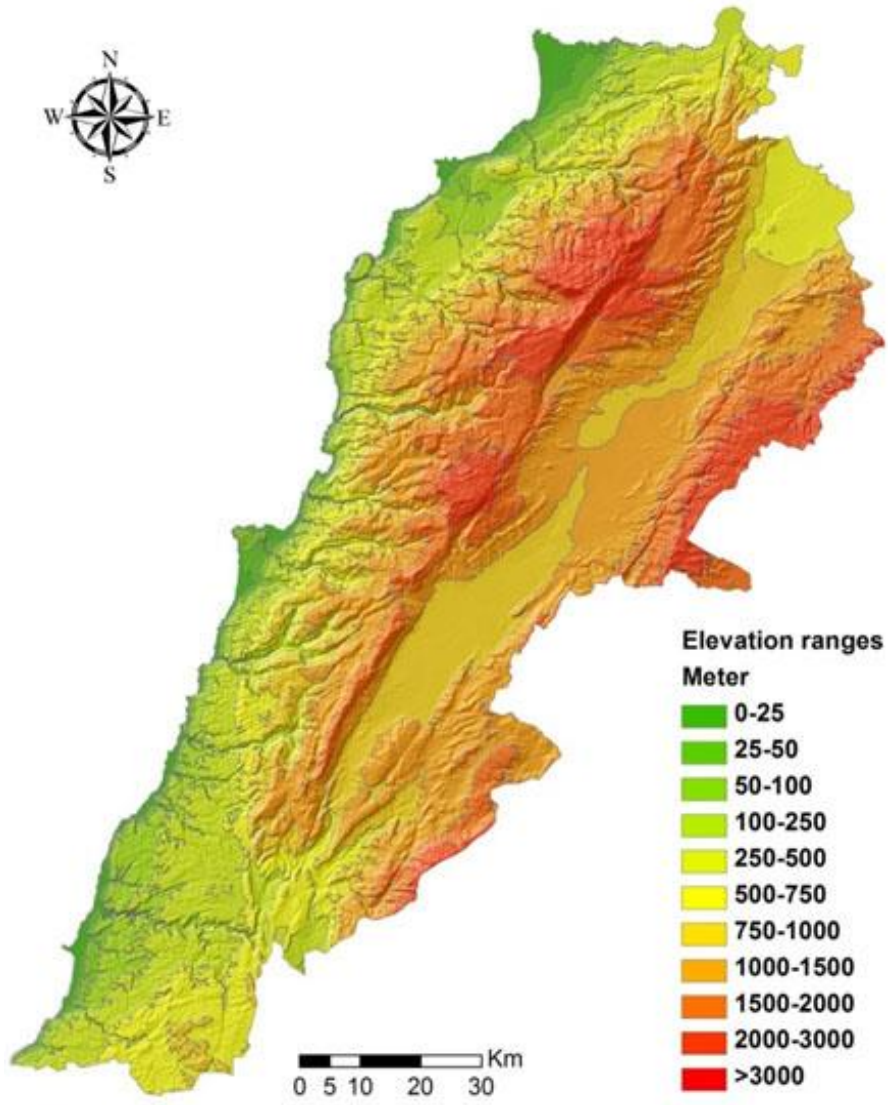


**Figure 4.2 Hypsometric Relief Levels of Lebanon**

The elevation average of the earth's surface in Lebanon is 1,005 m with a fairly large standard deviation of the mean (621 m). Nevertheless, as we can see in Figure 4.2 and Table 4.1, lowlands of Lebanon are located at elevations below 500 m and occupy 24.3 % of the total projection area, 53 % of the total area below 1,000 m and altitudes above 2000 m occupied only 7.3 % of the whole area of the

country. Below is a histogram of the area with high altitude intervals of 1000 - 1500 m occupied the higher area of 2,573 km<sup>2</sup> (Figure 4.2). The relative area of the basin at altitudes above 3000 m are very small – 0.01 %.

**Table 4.1** Areas of the Elevation Ranges in Square Kilometers and Percentage

Elevation Ranges m	Area km <sup>2</sup>	Area%
0-25	197.23	1.94
25-50	127.90	1.26
50-100	201.62	1.98
100-250	631.28	6.20
250-500	1314.26	12.92
500-750	1332.94	13.10
750-1000	1563.52	15.37
1000-1500	2572.98	25.29
1500-2000	1487.87	14.62
2000-3000	744.68	7.32
>3000	1.25	0.01

The use of a logarithmic scale allows us to see non-obvious features of the distribution of areas at high altitudes, where the absence of the monotonic decrease of area with altitude in the altitude range 2500-3000 m on the Lebanon ridge should be noted (Figure 4.3).

It is known that the distribution of elevations in the histograms reveal the patterns of surface structure and terms of relief (Geomorphology, 2005). The observed distribution of elevations, a characteristic of Lebanon, seems to be symmetrical.

Hypsographic curve and histograms are important sources of detecting stratification (speed) of relief. In Figure 4.4, standard shows hypsographic curve of Lebanese terrain, built in the traditional way (Pogorelov and Doumit, 2009). From the nature of elevations, distribution, and the slope of hypsographic curve (see Figures 4.3 and 4.4) we distinguish the high-altitude levels: 0-100 (predominant surface - the accumulative plains), 100-1000 (terraces, gently sloping surfaces of different genesis), 1000-2000 m (erosional-tectonic denudation, relief), 2000-3000 m (ridges, apical level).

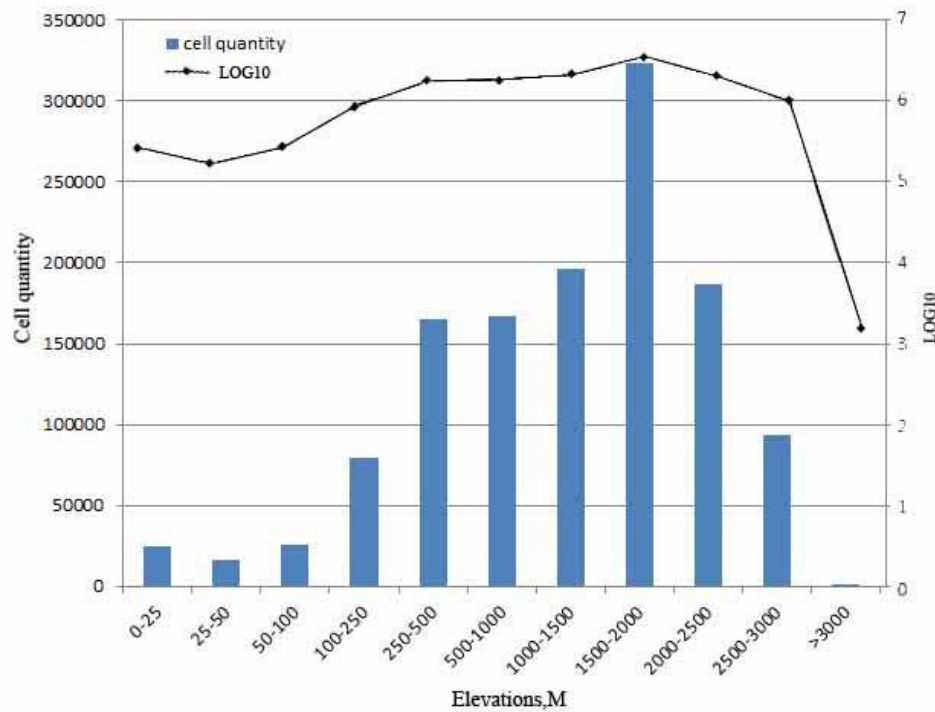


**Figure 4.3 Histogram of Elevations Distribution inside the Lebanese Boundary  
Cell Area – 0.0081 km<sup>2</sup>**

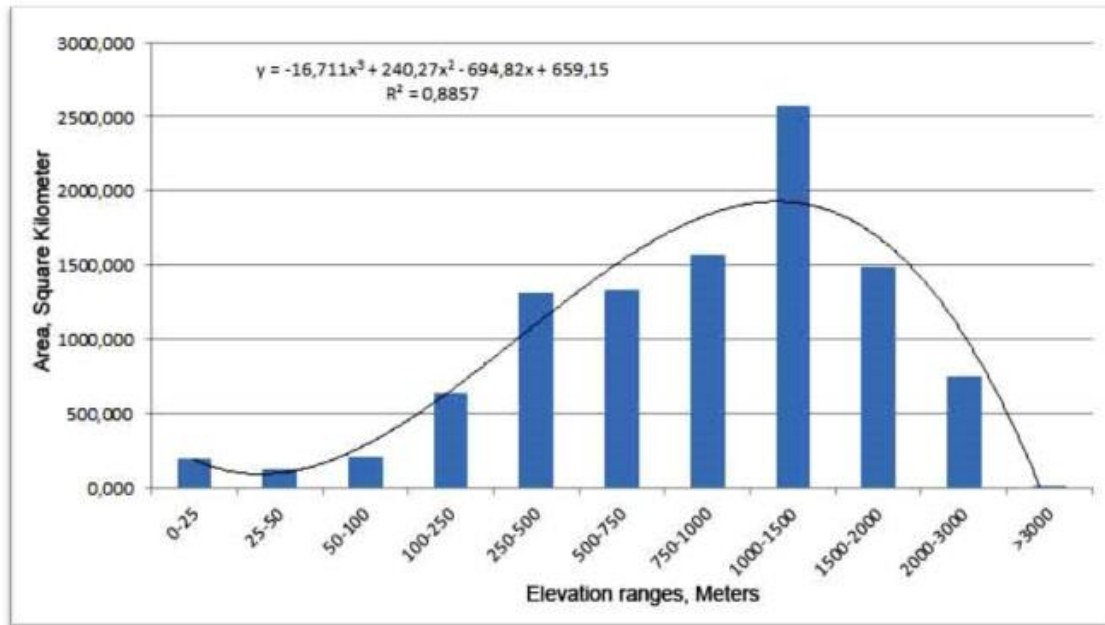


**Figure 4.4 Histogram Showing Distribution of Lebanese Land Area  
at Different Elevations**

## 4.03 The Hypsometric Curve

The hypsometric curve of a watershed was first introduced in 1947 by Langbein, and was further developed by Strahler (1952) to employ proportional heights and areas so as to make each curve comparable and independent of units. The hypsometric curve is typically represented as the distribution of the relative height ( $h/H$ ) with relative area ( $a/A$ ) (Langbein et al., 1947; Strahler, 1952). The percentage hypsometric method used here relates the area enclosed between a given contour and the basal plane of the analyzed area to the height of that contour above the basal plane (Figure 4.5).

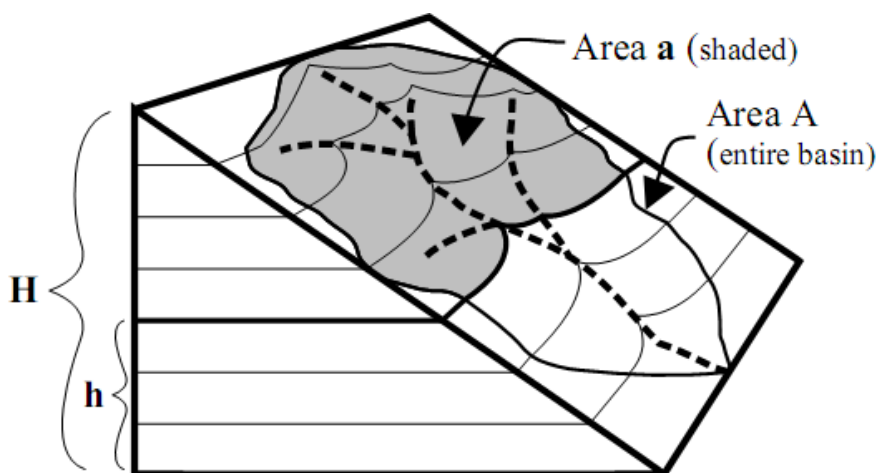


**Figure 4.5** Hypsometric Curve Process of a Watershed Basin

Two ratios are involved and plotted against each other on a diagram: the abscissa represents the ratio of area between a given contour and the basal plane (cumulative area), the ordinate represents the ratio of height of a given contour above the basal plane to the total height of the area (proportion of height). The resulting hypsometric curve permits comparison of areas of different sizes and elevations. Hypsometric curves always originate in the lower left-hand corner and reach the upper right-hand corner. It may, however, take any one of a variety of paths between these points, depending upon the distribution of the landmass from base to top. In theory, hypsometric values range from 0 to 1, low values are interpreted by Strahler to represent old eroded landscapes, and high values as young, less eroded landscapes. The use of hypsometric analysis has been restricted in the past because of the intensive computation required. However, with the advances in computing and GIS technology, hypsometry is worth reinvestigating as a means of objectively quantifying catchment characteristics. Integration of the

hypsometric curve gives the hypsometric integral  $I$ . Pike and Wilson (1971) proved mathematically the elevation-relief ratio  $E$ , which is defined as:

$$E = \frac{(Mean\ elevation - Minimum\ elevation)}{(Maximum\ elevation - Minimum\ elevation)}.$$

$E$  is identical to the hypsometric integral  $I$  but has the advantage that it is much easier to obtain numerically. In this work,  $E$  is therefore used instead of  $I$ .

The dimensionless hypsometric integral map of Lebanon (Figure 4.6) displays a range of value between 0.02 in the plain and 0.8 in the high elevations.

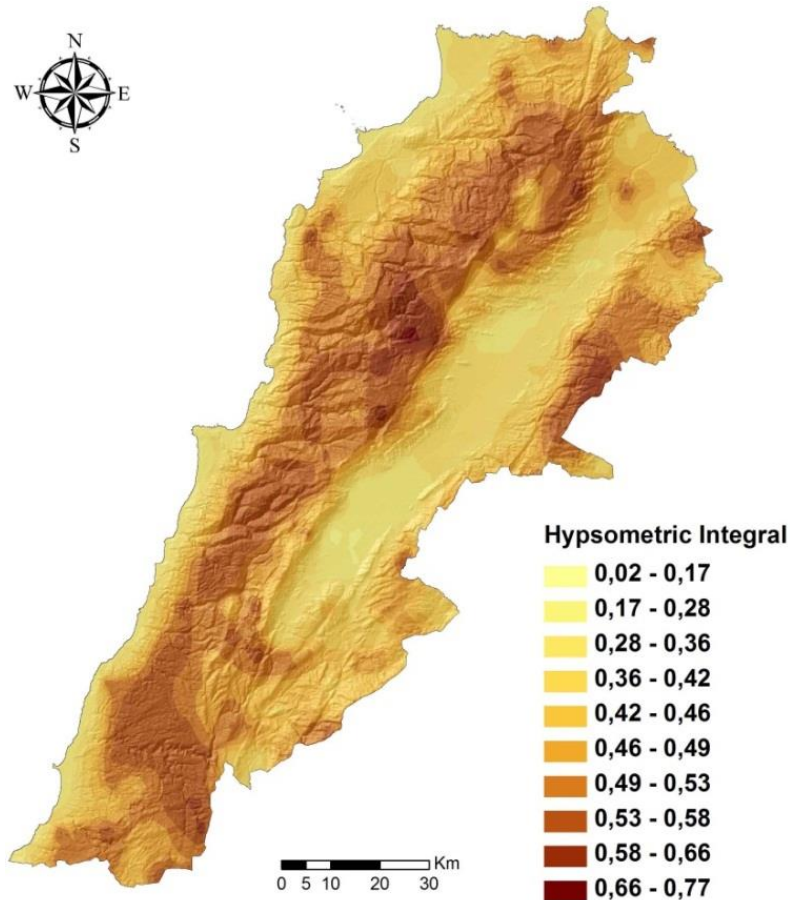


**Figure 4.6 Hypsometric Integer Map of Lebanon Shows the Plain in Yellow and the High Elevations in Brown**

At first, the hypsometric integral was applied to landforms (cirques) by Imamura (1937) and to regions by Péguy (1942). The value approaches to zero

where a few high points rise above a plain, and 1.0 where most surface heights cluster near the maximum. Although this device is useful morphologically and in geomorphology, hydrologic and other applications often require retention of landform dimensions.

Strahler (1952) found that the hypsometric integral is inversely correlated with total relief, slope steepness, drainage density and channel gradients. These parameters would be expected to correlate positively with rates of erosion. One might thus expect that in areas with similar rock type and tectonics, the hypsometric integral would also correlate inversely with erosion.

The hypsometric curve aggregates the three-dimensional basin structure, its shape has been related to the hydrograph peak and travel time (Harlin, 1984; Luo and Harlin, 2003), the regional ground- water base flow (Marani et al., 2001), and the dominant erosion process (Moglen and Bras, 1995; Willgoose and Hancock, 1998; Luo, 2000). Further, the hypsometric curve has been widely used to interpret stages of landscape evolution due to uplift and denudation (e.g., Strahler, 1952; Ohmori, 1993; Willgoose and Hancock, 1998).

Strahler (1952) popularized an integral of the hypsometric curve, which later was proven identical to a simpler measure as well as the approximate reciprocal of elevation skewness (Pike and Wilson, 1971). Péguy (1948) called further for a more conventional statistical approach and proposed the standard deviation of elevation as a measure of relief because of instability of the maximum.

Clarke (1966) critically reviewed hypsometry, clinometry and altimetric analysis, which had often been used in the search for old erosion (planation) surfaces over the prior 40 years. Hypsometric curves and integrals can be interpreted in terms of degree of basin dissection and relative landform age: Convex-up curves with high integrals are typical young terrain (geological age), undissected (disequilibrium stage) landscapes; smooth, s-shaped curves crossing the center of the diagram characterize mature (equilibrium stage) landscapes, and concave-up with low integrals typify old and deeply dissected landscapes (Strahler, 1952). Basing on DEM-SRTM datasets, we built the hypsometric curves of all the Lebanese watershed basins. The hypsometric curves of Lebanese basins are constructed according to the relative height ( $z / Z$ ) and relative area ( $s / S$ ). The shape of the curves appears as a kind of trajectory. In this phase, hypsographic curve of watershed basins are classified into 4 main types: 1) concave (approximated the function  $y = aebx$ ); 2) convex; 3) straight line; 4) the concave-convex (the changing direction of convexity) (Figure 4.7).

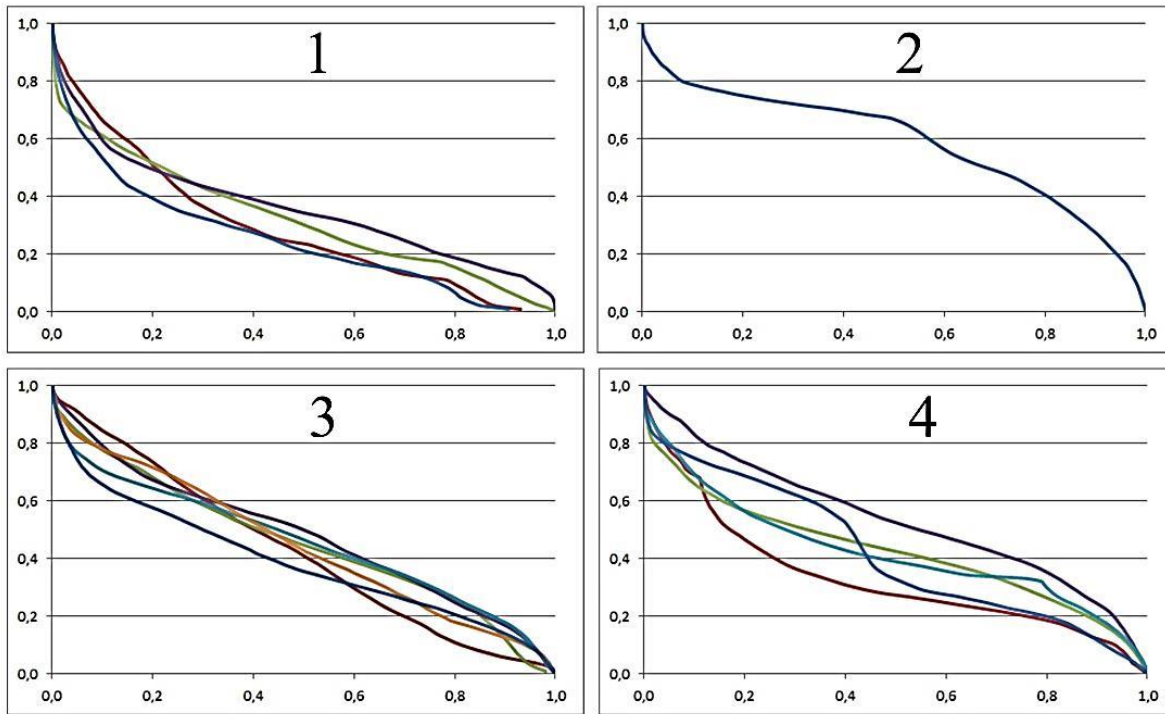


**Figure 4.7** Four Types of Hypsographic Curves of Lebanon Watersheds  
(in the abscise axes the relative areas and in the ordinate axes the relative heights)

Type 1 has a high increase in the relative area with a low one of relative height: a value of 0.5 relative areas for a value of 0.2 relative heights. Watersheds related to type 1 are: El Kebir, El Assi, Hasbani, and Oustouene. Type 2, the convex shape of hypsographic curve, is the Ibrahim River. As mentioned by Strahler, the convex up indicates a young terrain age according to the geological one.

Type 3 shows the characteristic proportional distributions of area and height by a linear function indicating a mature (equilibrium) stage. The shape of the curve clearly indicates the absence of surfaces with the same heights that can be attributed to the influence of the tectonic component of the relief formation. In this type, denudation clearly prevails over the accumulation. Here, there is a value of 0.5 relative areas for a value of 0.5 relative heights. Watersheds related to type 3 are: Abou Ali, Beyrouth, El Awali, El Bared, El Djoz, and Sainiq.

Type 4 group watersheds of Arka, Damour, El Kalb, El Litani, and Zahrani have the same hypsographic curve shape of concave and convex (figure 4.7). At these curves, a point of translation between concave and convex shape is figured especially in the curve of Zahrani reflecting the small proportion of relative area (0.4-0.45) with extreme elevations in the watersheds between (0.38-0.57). A

common feature of all curves is a “shoulder”. This shoulder reflects a landmass distribution where the major volume is at relatively low elevations.

The morphology of a river basin plays a fundamental role in the dynamics of surface and subsurface runoff generation. Substantial modifications of the basin morphologic system can lead to changes in the river basin response to precipitation events. The hypsometric curve is a powerful instrument that encloses the necessary features to represent the form of a watershed and its evolution. It is also able to describe the hydrologic behavior of a river basin through a set of parameters related to the shape of the curve (Di Benedetto et al., 2006).

## Chapter 5: Terrain Structure Lines

In accordance with Chapter 4 regarding terrain structure line analyses, we based our research using SRTM digital elevation model stream orders of all the Lebanese territory, and with the use of GIS tools we divided the stream network inside each watershed basin and studied them separately.

### 5.01 Main Channel and Valley Lengths

The Length of the main channel  $L_c$  is the length of the main channel measured from the outlet of the catchment to a point on the stream nearest to the centroid of the basin. The centroid is found by using a command from Arc Toolbox in ArcMap. Values were found to be very normal, as can be seen in the table. Values showed that El Litani River occupied the longest channel, followed by El Assi and Hasbani Channels.

**Table 5.1 Main Channel and Valley Lengths of Lebanese Watershed Basins**

Basin	$L_c$ , km	$L_v$ , km
<b>Abou Ali</b>	23,69	33,886
<b>Arka</b>	15,93	26,363
<b>Beirut</b>	22,64	29,309
<b>Damour</b>	16,44	31,906
<b>El Assi</b>	34,99	69,189
<b>El Awali</b>	24,04	39,171
<b>El Bared</b>	22,11	29,223
<b>El Djoz</b>	19,84	31,474
<b>El Kalb</b>	19,44	29,58
<b>El Litani</b>	96,75	129,886
<b>Hasbani</b>	30,03	52,725
<b>Ibrahim</b>	22,96	40,727
<b>Oustouene</b>	20,34	29,951
<b>Sainiq</b>	12,54	19,023
<b>Zahrani</b>	17,75	26,629

Valley length  $L_v$  is the distance from the outlet of the basin to the farthest point in the basin. As we can see in Table 5.1a, values of  $L_v$  are very proportional to the values of  $L_c$ , because both of them are changing with the form and the surface of the basin.

## 5.02 Bifurcation Ratio

One quantitative measure of a drainage basin is the bifurcation ratio  $R_b$ . Robert E. Horton was the first to come up with this concept, when he created the law of stream numbers. Once an entire network has been classified, the stream segments are counted by order. The Horton law stated that there is a hierarchy of streams ranked by order. The first order streams are the individual streams starting from the water sources. First order streams merge to form second order streams, and second order streams form third order streams. The ratio is calculated by dividing the number of first order streams by the number of second order streams, then dividing the second order streams by the next highest order, and so on. The average of all these ratios gives the bifurcation ratio.

Horton showed that the bifurcation ratio has low values in flat regions where there is a higher chance of flooding and high values in intensely fragmented areas. It is therefore subordinate to geomorphological factors, which is fully expected, taking into account that the present configuration and morphometric features of the river network reflect the effects of climatic change, orogenic movements, stratigraphic conditions and erosion over a period extending from the geological past. The bifurcation ratio can also show which parts of a drainage basin is more likely to flood, comparatively, by looking at the separate ratios (Horton, 1945). In these analyses of Lebanese river basins, we included only rivers which are inside the territory. Rivers forming a boundary limit between countries are not a part of our analysis.

In this study, we analyzed the geomorphological side and the stream structure influence to the terrain without taking into account the hydrological processes. Based on Table 5.1 and Figure 5.1, the bifurcation ratio values of El Assi river are very similar, specially, from the first to the sixth network orders, which yield to a lowest squared value of the regression equation  $R^2 = 0.0014$ .

Based on our analysis, we can say that in the case of low regression  $R^2$  values, like El Assi, Arka and El Litani, such values express the non-extreme terrain type and a high risk of flooding, contrary to mountainous basins like Abou Ali, Ibrahim and Al Awali which have high values of  $R^2$  and larger risks of erosion.

**Table 5.2 Stream Order Bifurcation Ratio Values of Lebanese Watershed Basins**

Basin	1-2	2-3	3-4	4-5	5-6	6-7	7-8
<b>Abou Ali</b>	4.98	4.98	4.65	4.18	4.25	4.00	-
<b>Arka</b>	4.87	5.48	4.14	3.67	6.00	-	-
<b>Beirut</b>	4.72	4.63	5.11	4.00	4.50	2.00	-
<b>Damour</b>	4.72	4.95	5.97	6.17	2.00	3.00	-
<b>El Assi</b>	4.86	4.91	4.84	4.01	4.22	9.00	2.00
<b>El Awali</b>	4.82	5.41	4.90	4.20	3.33	3.00	-
<b>El Bared</b>	4.00	5.75	5.24	5.29	1.75	4.00	-
<b>El Djoz</b>	4.94	5.16	5.19	4.50	3.00	2.00	-
<b>El Kalb</b>	4.55	5.13	4.89	3.17	6.00	2.00	-
<b>El Litani</b>	4.83	4.96	4.68	4.09	4.16	6.33	3.00
<b>Hasbani</b>	4.60	5.41	3.66	3.56	5.33	3.00	2.00
<b>Ibrahim</b>	4.80	4.83	4.98	3.92	3.25	2.00	2.00
<b>Oustouene</b>	4.79	4.83	5.43	3.29	7.00	-	-
<b>Sainiq</b>	4.88	6.52	4.27	7.50	1.00	-	-
<b>Zahrani</b>	4.69	0.75	1.53	0.57	-	-	-

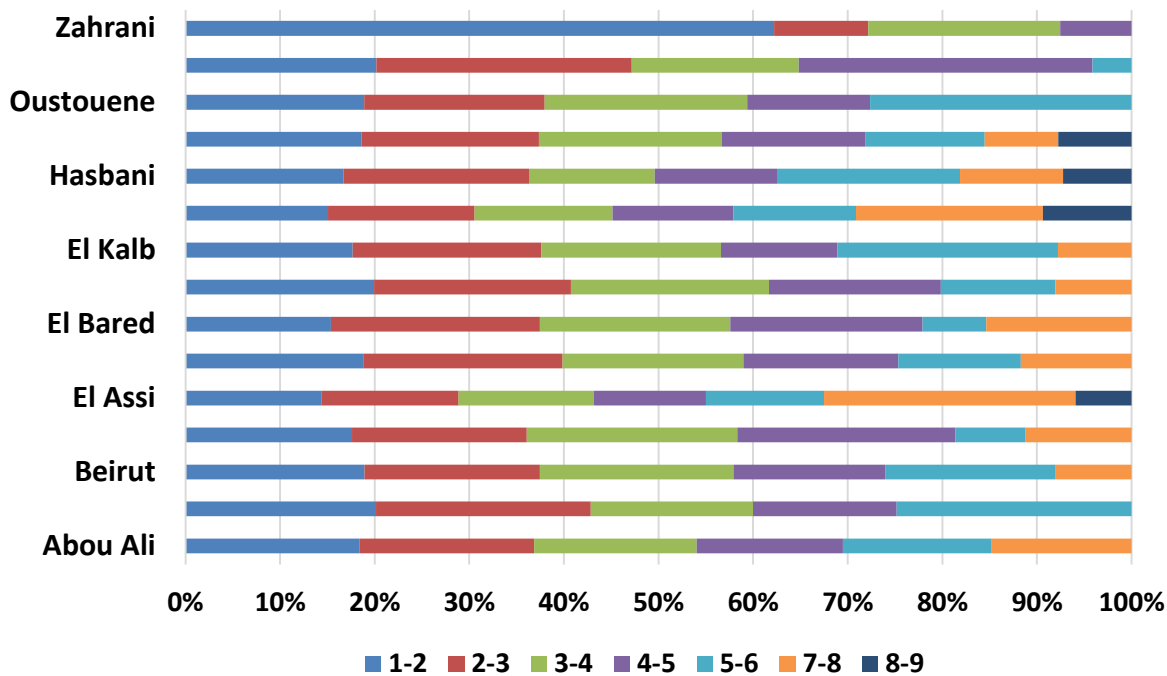


**Figure 5.1 Graphs of Lebanese River Basin Bifurcation Ratios**

Physical quantities of streams depend on the scale (resolution) of the source digital elevation model. By example, the result based to SRTM datasets is very different from that of the GDEM (see Chapter 3).

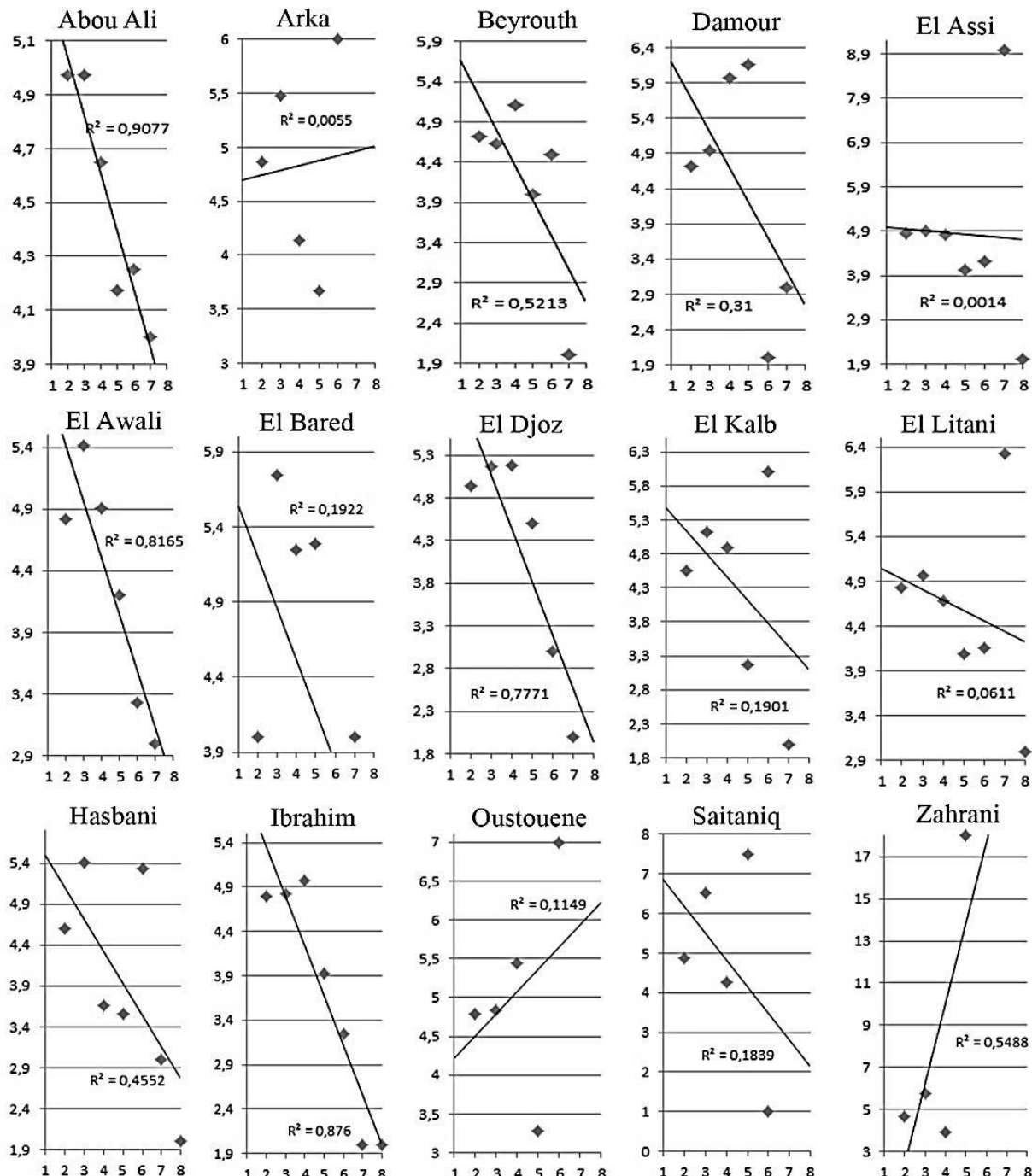


**Figure 5.2 Regression of Numbers of Stream Segments on Orders of Drainage Basins**

## 5.03 Length Ratio

In addition to the latter, Horton proposed a law of stream lengths, in which the average lengths of the streams of successive orders are related by a length ratio RL. Horton's law of stream lengths suggested that a geometric relationship existed between the numbers of stream segments in successive stream orders.

In Table 5.3, we can see that the length ratio RL values of stream orders in most watershed basins are discontinued. Only the Zahrani basin holds a proportion of values which is very close to trend with higher regression value R<sup>2</sup>= 0.94 among all watershed basin values, as also displayed in Figure 5.2 below. Contrarily, the lower R<sup>2</sup> value is found at Abou Ali's basin as 0.003 with a trend line very similar to the horizontal one. Hence, basins with moderate R<sup>2</sup> values range between 0.3 and 0.7 (Figure 5.2).

**Table 5.3 Stream Order Bifurcation Ratio Values of Lebanese Watershed Basins**

<b>Basin</b>	<b>1-2</b>	<b>2-3</b>	<b>3-4</b>	<b>4-5</b>	<b>5-6</b>	<b>6-7</b>	<b>7-8</b>
Abou ali	4.35	2.55	1.85	1.66	1.71	4.60	-
Al assi	3.93	2.25	1.92	1.72	2.49	2.15	3.19
Arka	4.28	2.20	1.89	2.02	1.21	-	-
Beirut	4.32	2.54	2.15	2.64	1.06	1.85	-
Damour	4.39	2.79	2.56	1.25	2.03	2.07	-
El Awali	4.62	2.28	2.22	2.62	1.44	0.78	-
El Bared	4.16	2.70	2.18	1.82	2.27	0.72	-
El Djoz	4.42	2.64	1.69	1.92	1.41	3.16	-
El Kalb	4.08	2.63	2.11	1.96	1.43	2.37	-
El litany	3.99	2.32	2.03	1.84	2.22	2.88	0.52
Hasbani	4.27	2.59	1.86	2.45	1.85	2.70	0.46
Ibrahim	4.10	2.39	2.40	1.84	3.07	1.17	0.57
Oustouene	4.33	2.28	2.29	1.43	1.38	-	-
Sainiq	5.11	2.66	1.51	2,89	0.80	2.70	-
Zahrani	4.64	2.53	1.89	0.85	-	-	-

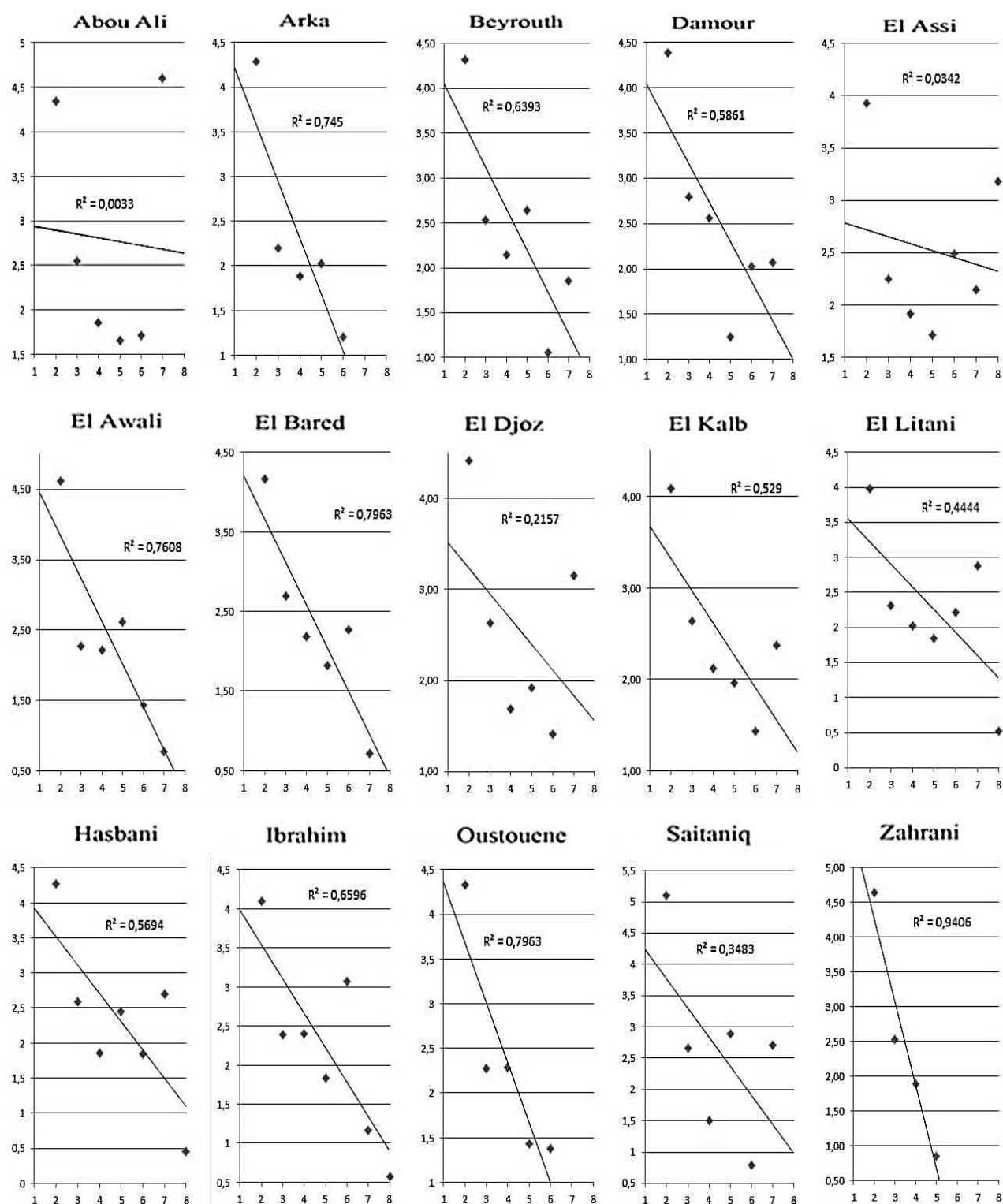


**Figure 5.2 Regression of Lengths of Stream Segments on Orders of Drainage Basins**

## 5.04 Watershed Eccentricity

Watershed eccentricity  $E$  was introduced by Black in 1972 as follows:

$$E = \frac{\sqrt{abs(L_c^2 - W_t^2)}}{W_t}$$

Here  $L_c$ = Length of watershed outlet to the centroid of the basin,  $W_t$ = the width of the watershed at the center of mass and perpendicular to  $L_c$ .

When  $L_c=W_t$  eccentricity becomes zero. The greater the value of  $(W_t - L_c)$  or  $(L_c - W_t)$ , the more the eccentricity, and the lesser the compactness of watershed near the mouth, and the lower the flood peak (Table 5.4).

**Table 5.4** Channel Length, Watershed Width, and Eccentricity of the Lebanese River Basins

Basin	$L_c$ , km	$W_t$ , km	$E$
<b>Abou Ali</b>	23,69	18,48	1,67
<b>Arka</b>	15,93	7,29	0,60
<b>Beirut</b>	22,64	12,57	0,90
<b>Damour</b>	16,44	10,7	1,67
<b>El Assi</b>	34,99	51,76	0,81
<b>El Awali</b>	24,04	8,19	0,39
<b>El Bared</b>	22,11	12,45	0,93
<b>El Djoz</b>	19,84	11,44	1,00
<b>El Kalb</b>	19,44	13,89	4,93
<b>El Litani</b>	96,75	52,39	0,84
<b>Hasbani</b>	30,03	16,56	0,88
<b>Ibrahim</b>	22,96	13,08	0,96
<b>Oustouene</b>	20,34	5,43	0,29
<b>Sainiq</b>	12,54	13,18	0,96
<b>Zahrani</b>	17,75	5,80	0,37

Based on the eccentricity of watershed basins, the most compact is Oustouene's river basin and the least compact is the El Kalb.

## 5.05 Stream Orientation

After analyzing bifurcation and length ratios of each watershed basin, a stream orientation analysis was done excluding first and second order of stream network. Stream orientation is a particularly effective tool in studying and interpreting the tectonic influence on network geometries (Ciccacci et al., 1986; Centamore et al., 1996).

The rose diagrams of Figure 5.3 show the results of azimuthal spatial analysis of all channels excluding the first and the second orders.

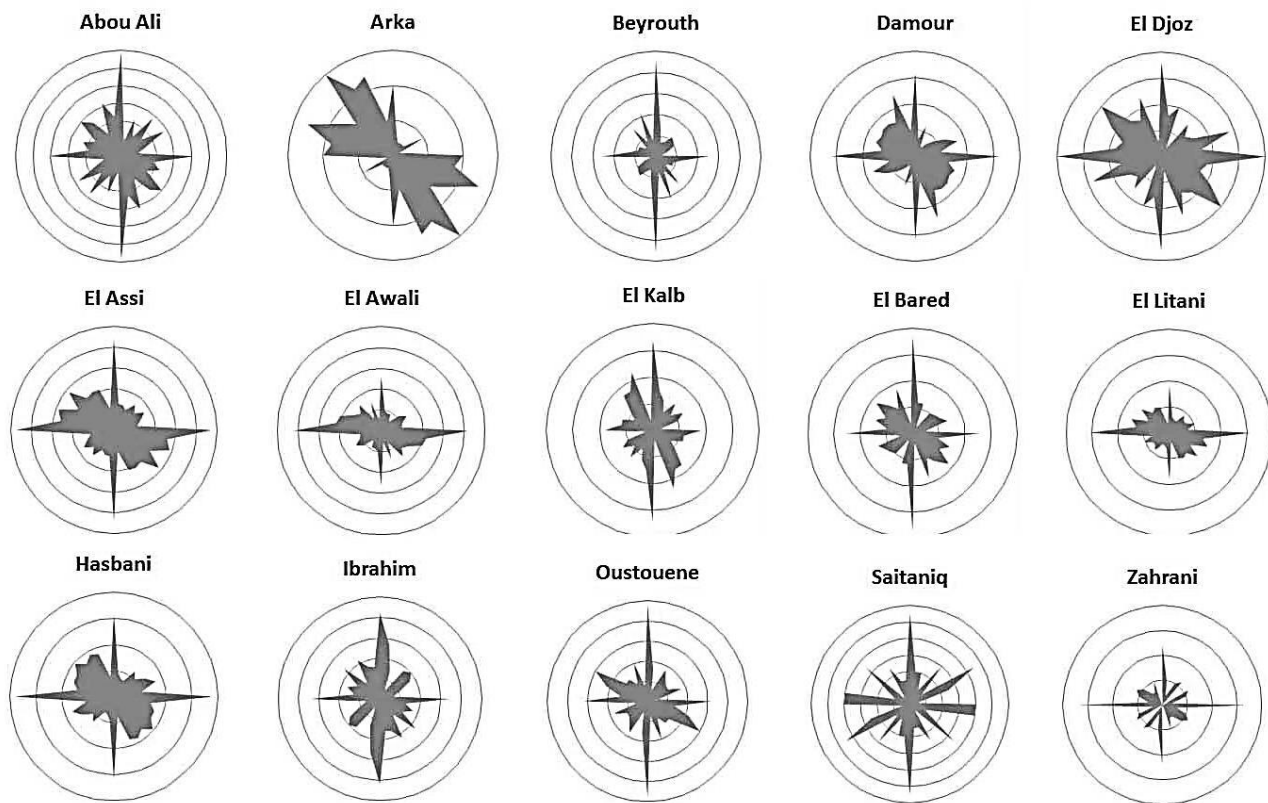


**Figure 5.3** Rose Diagrams of Lebanese Watershed Basin Stream Orientation

In El Litani is the biggest basin in Lebanon, and most of its channels take the North Western and South Eastern directions of the same as El Assi, Arka, and Hasbani. Ibrahim's streams tend to the North and to the South .We can conclude from these diagrams that most channels of Lebanese basins take the North Western direction which makes their outlet flowing into the Mediterranean Sea.

## 5.06 Fractal Dimension

B. Mandelbrot (1967) used the length of the coastline of the United Kingdom in order to illustrate the concept of fractal geometry. He noticed that as the length of the ruler used to measure the coastline was shortened, the length of the coastline increased. Because of the infinite amount of jaggedness that can be displayed by a coastline at infinitely smaller scales, the actual length of coastline can never be accurately determined.

Fractal dimension, introduced and developed by B. Mandelbrot (1982), provides a mathematical description of a wide range of natural forms and phenomena. The essence of any fractal object is its self-similarity (Mandelbrot, 1986). More specifically, fractals can be defined in three contexts – deterministic, self-similar or self-affine.

- Deterministic fractals can usually be defined by some mathematical function applied over a wide range of scales. The result is a (usually geometric) object that contains scaled copies of itself.
- If these copies are identical isotropic scaling and rotation, the fractal is self-similar (Mandelbrot, 1982).
- If the scaling process is itself anisotropic but linear, the fractal is self-affine (Lovejoy and Schertzer, 1995).

Richardson (1961) showed that this is often the self-similar case when measuring cartographic lines. Schertzer and Lovejoy (1995) have shown the self-similar case for measurements such as vegetation cover or albedo from increasingly higher resolution satellite imagery.

B. Mandelbrot (1967, 1977) placed such observations in a fractal framework, by defining a fractional dimension as:

$$D = \frac{\log(\frac{n}{n_0})}{\log(\frac{\lambda}{\lambda_0})}$$

Where  $\lambda$  and  $\lambda_0$  are two different length step sizes, and  $n$  and  $n_0$  are the numbers of these steps that measure the length of a line. Fractal dimensions  $D$  values are: 1 for a line, 2 for a surface, and 3 for a volume. The fractal dimension measures the complexity of the object.

A shape with a higher fractal dimension is more complicated or irregular than one with a lower dimension. For example, a shape with a fractal dimension values ranging from 1 to 3, fills more space than a one-dimensional curve and less

space than a two-dimensional surface. Self-similarity is defined statistically when it cannot be tested through an infinite range of scales. The statistical fractal behavior is then related to a given scale range. When the fractal dimension of a particular pattern changes within consecutive ranges of scale, one generally refers to the notion of multi-fractality.

Fractal dimensions provide a method to compare data collected from discordant measurements. For example, fractal analysis may be used to qualify and evaluate the relationship between variations in topographic relief and subsurface structure (Wilson and Dominic, 1998). Several methods are available for estimating the fractal dimension of surfaces, such as the fractional Brownian model (Mark and Aronson, 1984), triangular prism areas (Clarke, 1986), and box-counting (Falconer, 1990). In this study, the box-counting method was used because it can be applied to various sets of any dimension and patterns with or without self-similarity (Peitgen et al., 1992). According to K. Falconer (1990) who has discussed the mathematical aspect of the box-counting method, which involves covering the data set with boxes of constant size and counting the number of boxes that contain a segment of the data. Box counting begins with one box that covers the entire data set. At this stage, the number of boxes that contain data is equal to one. The box is then divided in fourths, and the numbers of boxes that contain part of the data set are again counted. This procedure of dividing the boxes and counting the number required to cover the data continues until the relationship is clearly defined or until the number of boxes required covering all the data does not increase with decreased box size. The log of the number of boxes required to cover the data is plotted versus the log of the box size, and the fractal dimension is determined from the slope of the best-fit line. This method is used to analyze self-similar data sets such as coastlines, stream networks, and active fault networks.

In our study, by using the box-counting method, we calculated the fractal dimension of all stream orders of the watershed basin as shown in the Table 5.5 below.

As we see in Table 5.5, the higher fractal dimension value is Abou Ali's with 1.44, which expresses the complexity of its stream network and the lower 1.16 value for Beirut river with a simple flow pattern. Based on the average value of fractal dimension, we group rivers in threes:

- Complex pattern: Abou Ali, Damour, El Assi, El Awali, El Djoz, and El Litani.
- Moderate pattern: Arka, El Bared, Hasbani, and Ibrahim.
- Simple pattern: Beirut, El Kalb, Oustouene, Sainiq, and Zahrani.

Fractal dimension values can be used in cartography, specifically in map generalization or scale applications.

**Table 5.5** Fractal Dimension Values of Lebanese River Networks

<b>Basin</b>	<b>Min</b>	<b>Average</b>	<b>Max</b>
<b>Abou Ali</b>	1	1.09	1.44
<b>Arka</b>	1	1.08	1.30
<b>Beirut</b>	1	1.06	1.16
<b>Damour</b>	1	1.09	1.42
<b>El Assi</b>	1	1.09	1.43
<b>El Awali</b>	1	1.09	1.37
<b>El Bared</b>	1	1.08	1.29
<b>El Djoz</b>	1	1.09	1.40
<b>El Kalb</b>	1	1.07	1.28
<b>El Litani</b>	1	1.09	1.39
<b>Hasbani</b>	1	1.08	1.30
<b>Ibrahim</b>	1	1.08	1.30
<b>Oustouene</b>	1	1.07	1.29
<b>Sainiq</b>	1	1.07	1.21
<b>Zahrani</b>	1	1.07	1.25

## Chapter 6: Areal Morphometry

Terrain areal analysis is referring as the quantitative evaluation of earth surface forms characteristics of any landform unit, as morphometry of areal landform unit interpretation and analysis is the exhibitions of an open system of operations. The composition of the areal morphometry system of a drainage basin is expressed quantitatively with drainage density, circularity ratio, elongation ratio, lemniscate ratio, form factor, unity shape factor and areal fractal dimensions of basins. It incorporates quantitative study of their various components which indicates the nature of development of the basin.

Drainage density ( $D$ ) is the total length of the permanent and seasonal streams and rivers divided by a unit size of area ( $A$ ):

$$D = \frac{\sum_1^n L}{A}$$

Where  $L$  is the length and ' $n$ ' is the number of rivers (Horton, 1945). Unfortunately, real drainage density is also difficult to measure from topographic. In our study, we used digital elevation models SRTM.

As a parameter in catchment studies, drainage density can be used in three main ways:

Firstly, it is related to watershed or physiographic characteristics such as relief ratio, rock type and basin shape. Secondly, it is related to input and output of the drainage basin system. Thirdly, drainage density may be useful in relation to studies of past (Schumm, 1965) and future (Strahler, 1964) conditions. K.G. Smith (1950) showed that drainage density was related to topographic texture as quantified by the number of contour crenulations per unit contour length. Numerous researchers have measured values of drainage density from topographic maps and have analyzed variables controlling drainage density and found that it is related to climate, vegetation, bedrock geology, and time. Usually, it has been noticed that increasing drainage density is always responsible for the slope failure (Mimura et al., 2008).

The drainage density of a catchment is the measure of which the catchment is dissected by its drainage networks. Drainage density provides hydrogeomorphologists with a useful measure of landscape dissection and runoff potential. A low value of drainage density indicates a highly permeable landscape,

with small potential for runoff. A high value of drainage density indicates a highly dissected surface.

Drainage density is a critical catchment parameter as it captures the long-term expression of the interaction between climate and catchment properties (topography, soils, vegetation) via the amount of dissectedness in a catchment (Horton, 1932, 1945). Drainage density is a very useful index of basin characteristics and, as M.J. Kirkby and R.J. Chorley (1967) have recently noted, it affects the magnitude of stream flow from a drainage basin. Drainage density is the dynamic manifestation of varying inputs into the drainage basin system and its relation to particular inputs reflects the basin characteristics. It is through drainage density that these characteristics influence the output of water and sediment from the system.

Drainage density is clearly an important geomorphic variable (Gardiner and Gregory, 1982) that has been related to climatic conditions (Gregory, 1976; Chorley, 1957; Chorley and Morgan, 1962; Gardiner, 1983), flood peaks (Carlson, 1963; Gardiner and Gregory, 1982), mean annual discharge, and sediment yields. It has long been used to detect variations of rock type and structure by photogeologists and to document the stage of erosional evolution of drainage systems (Hadley and Schumm, 1961).

When calculating stream network lengths using topographic maps, Spiridonov recommended dividing maps into a grid of 4 square centimeters (Spiridonov, 1975). According to the adopted methodology of calculating stream density, as an experiment, we divided the Lebanese territory into equal squares of  $2 \times 2$  kilometers, with which we determined the overall length of the stream network. The shape of Lebanon constitutes 2,757 squares and characterizes the level of details in drawing isodense (isolines of the same drainage density values).

When mapping the stream density, we followed an experimental way of calculating the value of  $D$ . In the first experiment, we took all the stream orders from 1 till 8 ( $D_{L1-8}$ ). For the second, a generalization was done by excluding first and second order of stream network ( $D_{L3-8}$ ). Using the zonal statistics tools, we could calculate the stream length inside each square of the grid and the statistical values in each watershed basin (see Table 6.1).

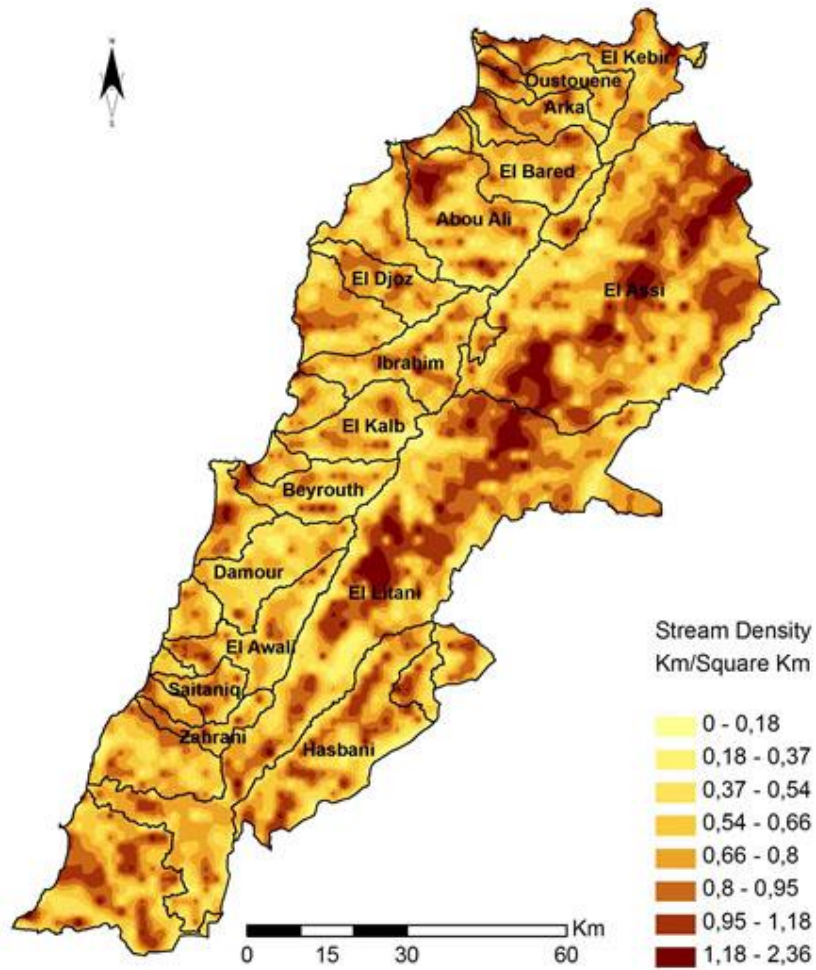


**Figure 6.1 Stream Density Map of Lebanon with Watershed Basins Made from ( $D_{L3-8}$ ) Values**

To build stream density, map values are interpolated using radial bases function (spline with tension) and then classified into 8 intervals using the quantile method. As shown in Figure 6.1, high stream density values are in dark brown and found in Bekaa's valley. This map was interpolated using ( $D_{L3-8}$ ) values. Stream density values of ( $D_{L1-8}$ ) in all watershed basins varied from 0 to 2.24 km/km<sup>2</sup> and a very bright skewness distribution of the Zahrani and El Djoz tending to the right with values of -0.13 ; -0.27 (Table 6.1).

It is very important to highlight in this experiment that the highest values of  $D_{L1-8}$  are found on mountainous areas, because they take into account the first and the second stream order which are excluded in  $D_{L3-8}$ . Values of stream density in  $D_{L3-8}$  are similar to values obtained from topographic maps and are very close to reality.

**Table 6.1a** Stream Density Statistics for  $D_{L3-8}$

Basin	N	Min	Max	Mean	Std.Dev	Skewness	Kurtosis	1 <sup>st</sup> Quartile	Median	3 <sup>rd</sup> Quartile
<b>Abou Ali</b>	118	0	1.72	0.69	0.43	0.28	2.25	0.35	0.64	0.97
<b>Arka</b>	32	0	1.45	0.68	0.39	0.19	2.37	0.45	0.62	0.86
<b>Beirut</b>	58	0	1.60	0.61	0.43	0.26	2.08	0.26	0.60	0.94
<b>Damour</b>	76	0	1.74	0.57	0.34	0.43	3.60	0.35	0.58	0.78
<b>El Assi</b>	503	0	2.24	0.77	0.44	0.41	2.79	0.46	0.75	1.03
<b>El Awali</b>	76	0	1.56	0.62	0.41	0.19	2.09	0.28	0.63	0.90
<b>El Bared</b>	67	0	1.65	0.62	0.38	0.01	2.63	0.37	0.63	0.88
<b>El Djoz</b>	48	0	1.48	0.68	0.39	-0.27	2.28	0.43	0.73	0.93
<b>El Kalb</b>	64	0	1.44	0.60	0.36	0.18	2.48	0.32	0.62	0.82
<b>El Litani</b>	525	0	2.23	0.73	0.44	0.44	3.06	0.43	0.72	1.00
<b>Hasbani</b>	152	0	1.66	0.67	0.42	0.33	2.20	0.34	0.60	0.99
<b>Ibrahim</b>	84	0	1.97	0.65	0.40	0.38	3.00	0.33	0.65	0.91
<b>Oustouene</b>	41	0.08	1.87	0.69	0.40	0.86	3.62	0.44	0.64	0.90
<b>Sainiq</b>	28	0.19	1.65	0.68	0.37	0.65	3.11	0.31	0.74	0.84
<b>Zahrani</b>	23	0	1.51	0.76	0.39	-0.13	2.71	0.52	0.79	0.99

**Table 6.1b** Stream Density Statistics for  $D_{LI-8}$

Basin	N	Min	Max	Mean	Std.Dev	Skewness	Kurtosis	1st Quartile	Median	3rd Quartile
<b>Abou Ali</b>	118	7.90	11.43	9.63	0.77	-0.07	2.45	9.12	9.64	10.24
<b>Arka</b>	32	8.09	10.57	9.41	0.57	-0.17	3.05	9.20	9.39	9.73
<b>Beirut</b>	58	8.07	11.07	9.94	0.72	-0.60	3.11	9.57	10.01	10.40
<b>Damour</b>	76	7.94	11.85	9.96	0.95	0.13	2.29	9.26	9.91	10.67
<b>El Assi</b>	503	6.80	12.48	9.20	0.88	0.25	3.37	8.59	9.19	9.77
<b>El Awali</b>	76	8.04	11.62	9.69	0.76	0.18	2.82	9.22	9.62	10.20

<b>Basin</b>	<b>N</b>	<b>Min</b>	<b>Max</b>	<b>Mean</b>	<b>Std.Dev</b>	<b>Skewness</b>	<b>Kurtosis</b>	<b>1st Quartile</b>	<b>Median</b>	<b>3rd Quartile</b>
<b>El Bared</b>	67	8.58	11.57	9.78	0.66	0.62	3.23	9.32	9.78	10.10
<b>El Djoz</b>	48	7.44	11.18	9.31	0.82	0.23	2.81	8.90	9.16	9.80
<b>El Kalb</b>	64	7.66	11.60	9.52	0.77	0.07	2.79	8.98	9.44	10.05
<b>El Litani</b>	525	2.38	12.51	9.27	1.03	-1.05	9.45	8.78	9.37	9.89
<b>Hasbani</b>	152	8.50	11.58	9.93	0.59	0.20	3.00	9.55	9.90	10.33
<b>Ibrahim</b>	84	7.75	11.19	9.32	0.83	0.24	2.18	8.68	9.12	10.01
<b>Oustouene</b>	41	7.01	11.05	9.05	0.86	-0.49	3.28	8.72	9.19	9.53
<b>Sainiq</b>	28	8.02	10.68	9.44	0.74	-0.13	2.17	9.00	9.34	10.03
<b>Zahrani</b>	23	8.46	11.66	9.49	0.84	0.97	3.52	8.90	9.40	9.77

As we can see in Table 6.1a, statistics of stream density  $D_{L3-8}$  that El Litani and Al Assi river basins occupied the higher stream density value according to their huge surfaces. Arka and El Kalb stream density were very low compared to other basins. The most moderate skewness distribution for  $D_{L3-8}$  was in the El Bared basin. The two extreme values were, tending to the left with the Oustouenes basin, and to the right with El Djoz.

Concerning  $D_{L1-8}$  statistics values in Table 6.1b, high stream density values are found in mountainous basins contrary to  $D_{L3-8}$  values. For example, if we look at standard deviation values we can see that the Damour basin  $D_{L3-8}$  value is 0.34 lower than that of Arka, and 0.39 unlike in  $D_{L1-8}$  the Damour value is higher than Arka (0.95; 0.57), which means that first and second stream orders own a big length in the Damour basin.

From this experiment we can conclude that generalization of stream networks has a big influence on geomorphic values and mapping, for in digital cartography, we have to take into account the fractal dimension values. High drainage density ( $>2.5$ ) indicates impermeable sub-surface materials, sparse vegetation, shallow soils, and high relief areas. The low drainage density is in association with relatively larger areas, permeable sub-surface, and good vegetation cover and low relief. The smaller the area value is, the higher the drainage density, which leads to low infiltration and high run-off. Drainage density is closely associated with the average hillslope length or overland flow length (The distance between the catchment divide to the stream channel). Assuming that  $D$  is constant throughout the catchment, the average hillslope length is computed as follows:

$$L_h = \frac{1}{2}D$$

Horton also introduced the concept of the stream frequency  $F$  or the number of stream segments per unit area:

$$F_s = \frac{N_s}{S}$$

Where  $N$  is the number of Strahler streams.

Melton showed that  $F_s$  is strongly correlated with drainage density (Melton, 1958). He observed that the relationship of  $F_s$  against  $D$  tends to be conserved as a constant in nature through Melton's law:

$$F_s = 0.694 \times D^2.$$

Based on the result of our experiment, average hillslope length  $L_h$  and stream frequency  $F_s$  are calculated using the mean value of  $D_{L3-8}$  (Table 6.2).

**Table 6.2 Hillslope Length  $L_h$  and Stream Frequency  $F_s$  of Lebanese Watershed Basins**

Basin	$L_h$	$F_s$
<b>Abou Ali</b>	0.35	0.33
<b>Arka</b>	0.34	0.32
<b>Beirut</b>	0.30	0.26
<b>Damour</b>	0.29	0.23
<b>El Assi</b>	0.39	0.42
<b>El Awali</b>	0.31	0.27
<b>El Bared</b>	0.31	0.27
<b>El Djoz</b>	0.34	0.32
<b>El Kalb</b>	0.30	0.25
<b>El Litani</b>	0.37	0.37
<b>Hasbani</b>	0.33	0.31
<b>Ibrahim</b>	0.33	0.30
<b>Oustouene</b>	0.34	0.33
<b>Sainiq</b>	0.34	0.32
<b>Zahrani</b>	0.38	0.40

Hillslope length  $L_h$  of the biggest Lebanese watershed basin, El Litani, is lower than the hillslope value of the El Zahrani basin 0.38. These high values in Zahrani basin are related to the high level of erosion of the terrain structure.

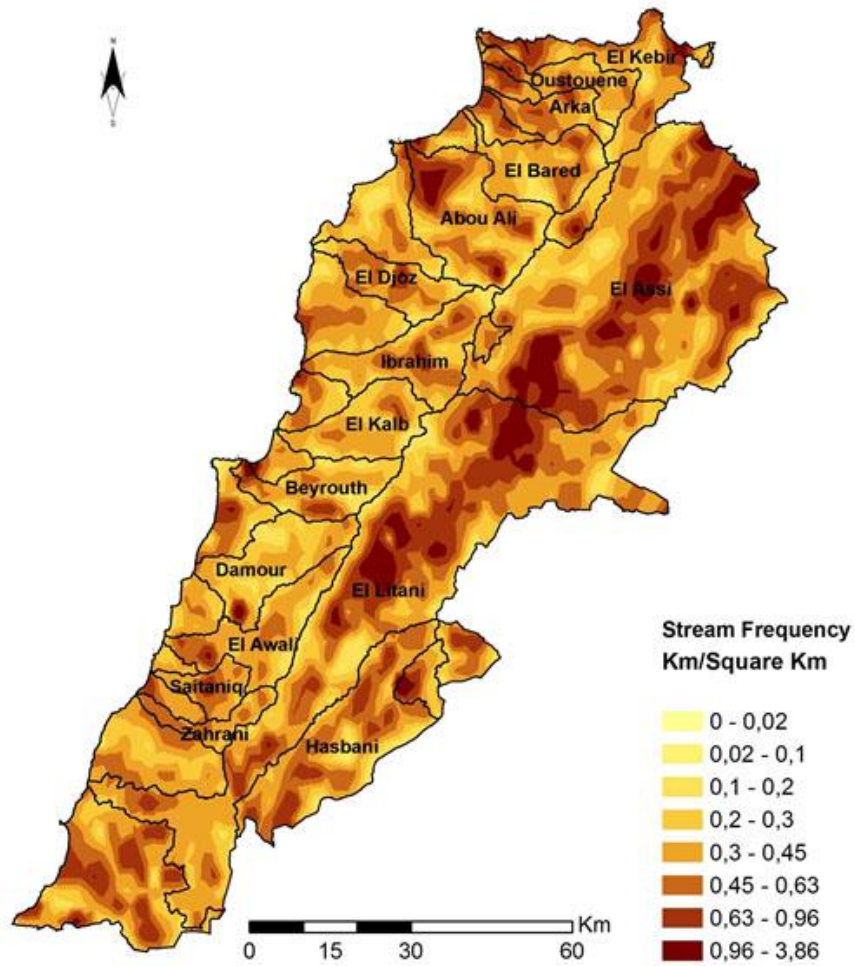


**Figure 6.2 Stream Frequency Map of Lebanon with Watershed Basins  
Made from  $D_{L3-8}$  Values**

Stream frequency of El Assi and Zahrani indicate high amounts of runoff from the watershed due to steep slopes.

## 6.01 Circularity Ratio ( $R_c$ )

Miller (1953) introduced a dimensionless circularity ratio which is defined as the ratio of the basin area to the area of a circle having a circumference equal to the perimeter of the basin (Table 6.3).

$$R_c = \frac{4\pi A}{P^2}$$

Where  $A$  is the basin area and  $P$  is the basin perimeter, for an elongated shape,  $R_c < 1$ .

Miller described the basin of low circularity ratio values, which indicates strongly elongated and highly permeable homogenous geologic materials like El Litani basin with (0.09). The circularity ratio values (0.3) of El Assi basin indicate that the basin is more circular in shape. Based on Stepinski and Coradetti (2004), the normalized circularity function of a basin measures the changes of the basin's elongation with elevation. The normalized circularity function is defined as:

$$R_z = \frac{4\pi A_z}{P_z^2}$$

Using a method similar to how a hypsometric curve is constructed. A horizontal plane at elevation  $h$  cuts through the basin dividing the basin into two parts: one above plane and one below it.

$$z = \frac{h}{H}$$

The circularity function at relative height is based on area  $A_z$  and perimeter  $P_z$ , for an elongated shape  $C < 1$ . The more elongated the shape is, the less the  $R_z$  value. As  $z$  changes from 0 to 1, a series of  $R_z$  values form the circularity function or a circularity curve of the basin (Stepinski and Coradetti, 2004).

## 6.02 Elongation Ratio (EL)

The elongation ratio of a drainage basin is the ratio of the diameter of a circle with the same area to the length of the basin (table 6.3).

$$EL = 2\pi \sqrt{\frac{A}{L}}$$

Where  $EL$  = Elongation ratio,  $A$  = Basin area, and  $L$  = Basin length (Schumm, 1956).

The elongation ratio was proposed to show characteristics of basin shape, and drainage basin evolution. It is a very significant index in the analysis of basin shape, which helps to give an idea about the hydrological character of a drainage

basin. Elongation ratio values of the Lebanese watershed basins run between 12.31 and 34.03 of El Assi basin over a wide variety of climatic and geological types (Table 6.3).

**Table 6.3 Morphometry Parameters of Lebanese Watersheds**

Basin	$L_v$ , km	Area, km <sup>2</sup>	$R_c$	EL	K	F	F.D.	W	U
<b>Abou Ali</b>	33.89	472.49	0.30	23.45	1.91	0.41	1.19	2.76	1.56
<b>Arka</b>	26.36	133.22	0.19	14.12	4.1	0.19	1.22	4.05	2.28
<b>Beirut</b>	29.31	237.19	0.23	17.87	2.84	0.28	1.21	3.37	1.90
<b>Damour</b>	31.91	307.51	0.24	19.5	2.6	0.3	1.2	3.22	1.82
<b>El Assi</b>	69.19	2031.41	0.30	34.03	1.85	0.42	1.17	2.72	1.54
<b>El Awali</b>	39.17	297.33	0.15	17.3	4.05	0.19	1.23	4.03	2.27
<b>El Bared</b>	29.22	263.44	0.22	18.86	2.54	0.31	1.21	3.19	1.80
<b>El Djoz</b>	31.47	194.08	0.21	15.59	4.01	0.2	1.21	4.00	2.26
<b>El Kalb</b>	29.58	254.37	0.28	18.42	2.7	0.29	1.2	3.29	1.85
<b>El Litani</b>	129.89	2109.75	0.09	25.31	6.28	0.13	1.23	5.01	2.83
<b>Hasbani</b>	52.73	594.07	0.21	21.08	3.67	0.21	1.2	3.83	2.16
<b>Ibrahim</b>	40.73	332.25	0.19	17.94	3.92	0.2	1.21	3.96	2.23
<b>Oustouene</b>	29.95	164.48	0.15	14.72	4.28	0.18	1.24	4.14	2.34
<b>Sainiq</b>	19.02	108.68	0.25	15.01	2.61	0.3	1.21	3.23	1.82
<b>Zahrani</b>	26.63	102.39	0.13	12.31	5.44	0.14	1.25	4.66	2.63

### 6.03 Lemniscate Ratio

The shape of the study catchments was expressed on the basis of lemniscate ratio, form factor, and compactness coefficient. Lemniscate ratio was calculated as the ratio of square of maximum length ( $L$ ) of the catchment and four times its area ( $A$ ) (Table 6.3).

$$K = \frac{L^2\pi}{4A}$$

Where  $A$ = Basin area and  $L$  = Basin length.

## 6.04 Form Factor ( $F$ )

Quantitative expression of drainage basin outline form was made by Horton's (1932) dimensionless quantity, which he defined as the ratio of basin area  $A$  to the square of the maximum basin length  $L$ .

$$F = \frac{A}{L^2}$$

Where  $A$ = Basin area and  $L$  = Basin length.

The form factor value of the El Litani basin is 0.13 (Table 6.3) which indicates lower value of form factor, and thus, represents elongation in shape. The elongated basin with low form factor indicates that the basin will have a flatter peak of flow for longer duration. Flood flows of such elongated basins are easier to manage than that of the circular basin. Form factor computed confirms that watershed has moderately high peak flows of shorter duration. Watershed Shape Factor ( $W$ ).

This was defined by Wu et al. (1964), as the ratio of main stream length  $L$  to the diameter  $D$  of an equivalent circle having the same area as the basin.

$$W = \frac{L}{D}$$

As in most parameters, El Litani basin occupied the higher value of shape factor according to its hugeness. Contrastingly, El Assi basin comes second by area among Lebanese watershed basins having the lower watershed shape factor (Table 6.3).

If we compare the watershed shape factor values, we find that they are related with the circularity ratio. This means that when we have a high circularity value, we get a low watershed shape factor value.

## 6.05 Unity Shape Factor ( $U$ )

Smart and Surkan 1967 used the unity shape factor to be defined as the ratio of the basin length  $L$  to the square root of the basin area  $A$ .

$$U = \frac{L}{\sqrt{A}}$$

Same as the form factor, El Assi occupied the lower value and El Litani the higher one (Table 6.3).

## **6.06 Fractal Dimension (FD)**

The fractal dimension measures the complexity of the object. Chapter 5 explains the fractal dimension in details. A shape with a higher fractal dimension is more complicated or irregular than one with a lower dimension. For example, a shape with fractal dimensions of 1.24 like, the Oustouene basin, is more complicated than the fractal dimension of 1.17 of El Assi (Table 6.3).

The quantitative analysis of morphometric parameters is found to be of immense utility in river basin evaluation. The morphometric parameters evaluated using GIS technologies helped us to understand various terrain parameters such as circularity function, elongation ratio, form factor, etc... The geomorphological parameters estimated may be utilized for testing hydrological models to simulate hydrological response of watershed.

# Chapter 7: Terrain Quantitative Analysis (Morphometry)

The measurement and mathematical analysis of the earth's surface and of the shape and dimensions of its landforms, has recently been termed as Quantitative Terrain Analysis. The basin relative and local reliefs are the surface topography constituting earth shape, ruggedness numbers, terrain roughness and fractal dimensions related to the complexity of the terrain surface. These parameters are explaining terrain structure and forms resulting graphs, maps or statistical indices of the Lebanese watersheds basins.

## 7.01 Basin Relief

The term relief is used to describe the vertical dimension or amplitude of topography. I. S. Evans (1972) noted that the majority of relief measures depend upon the extreme values of the distribution of elevations, and he, therefore, proposed that the standard deviation of altitudes would provide a more stable measure of the vertical variability of the terrain. From SRTM digital elevation models we extracted all relief statistics as maximum, minimum, and mean elevations for the Lebanese watershed basins (Table 7.1).

In order to define the spatial position of drainage basins, a series of characteristic points or plans, related to its altitude, must be known. Any point or plane in a basin has a certain altitude from the sea level:

where  $H_{Min}$  – the minimum altitude measured from the sea level to the lowest point of the basin;  $H_{Max}$  – the vertical distance from the sea level to the highest point in the basin;  $H_{Mean}$  – the mean vertical distance of the basin surface above sea level.

Many authors calculated the mean altitudes of peaks and passes using barometer. C. Koritska showed that the relief must be divided into horizontal sections and the mean altitude is obtained by dividing the relief volume by the average area (1854). Russian scientists, Luchisheva (1950) and Chebotarev (1953), calculated the mean altitude from the weighted mean of the sum of partial volumes between contour lines. In Table 7.1, the highest point above the sea level in Abou Ali's watershed basin gave an influence to quartiles statistics and enlarged the interval of values between them. The negative skewness values of Beirut, El Bared, El Kalb, and Ibrahim express a right side tendency of the values. The standard deviation values of terrain elevation express the relief energy.

**Table 7.1 Statistics Relief Values of the Lebanese Watershed Basins**

Basin	$H_{\text{Min}}$ (m)	$H_{\text{Max}}$ (m)	$H_{\text{Mean}}$ (m)	Std.Dev (m)	Skewness	Kurtosis	1 <sup>st</sup> Quartile (m)	Median (m)	3 <sup>rd</sup> Quartile (m)
<b>Abou Ali</b>	0	3072	1306	885	0.24	1.78	476.06	1260.3	2044.7
<b>Arka</b>	0	2100	697	426	1.12	3.77	429.44	576.33	863.97
<b>Beirut</b>	0	2045	932	480	-0.01	2.30	604.67	915.44	1287.3
<b>Damour</b>	0	1888	801	341	0.10	2.77	567.42	804.0	1017.1
<b>El Assi</b>	542	3034	1353	490	0.40	2.36	988.56	1294	1721.1
<b>El Awali</b>	0	1930	926	445	0.03	2.24	571.22	965.33	1233.4
<b>El Bared</b>	0	2873	1316	587	-0.10	2.35	882.72	1338.8	1776.7
<b>El Djoz</b>	0	2316	1039	574	0.11	1.80	515.33	993.78	1565.8
<b>El Kalb</b>	0	2600	1392	564	-0.07	2.46	1021.0	1366.7	1811.7
<b>El Litani</b>	0	2604	1101	484	0.52	3.16	864.22	1014.2	1361.1
<b>Hasbani</b>	162	2794	1109	482	0.69	3.34	723.89	1065.7	1382.6
<b>Ibrahim</b>	0	2681	1573	545	-0.74	2.76	1223.3	1792.4	1970.9
<b>Oustouene</b>	0	1915	482	380	0.95	3.75	216.0	405.06	673.94
<b>Sainiq</b>	0	1398	545	282	0.43	2.62	330.69	499.67	756.19
<b>Zahrani</b>	0	1630	680	398	0.21	1.67	359.67	537.22	1069.4

## 7.02 Local Relief

The local relief is defined as the difference between the highest and lowest elevations occurring within that area (figure 7.1). It is important to note that local relief, in a lot of articles, is termed the «relative relief».

Local relief was introduced by Partsh (1911), who termed it the Relief Energy. Mark (1974) determined local relief for arbitrarily-bounded terrain samples such as squares, circles, or latitude-longitude quadrangles. Trewartha and Smith (1941) stated that the sizes of the rectangle, for which relief readings are made, appear to need adjustment for the degree of coarseness or fineness of the relief pattern. They did not indicate how the appropriate size could be determined. Evans (1972) compared the values of local relief determined over more than one size of area, and he recommended the use of a fairly large sample area.

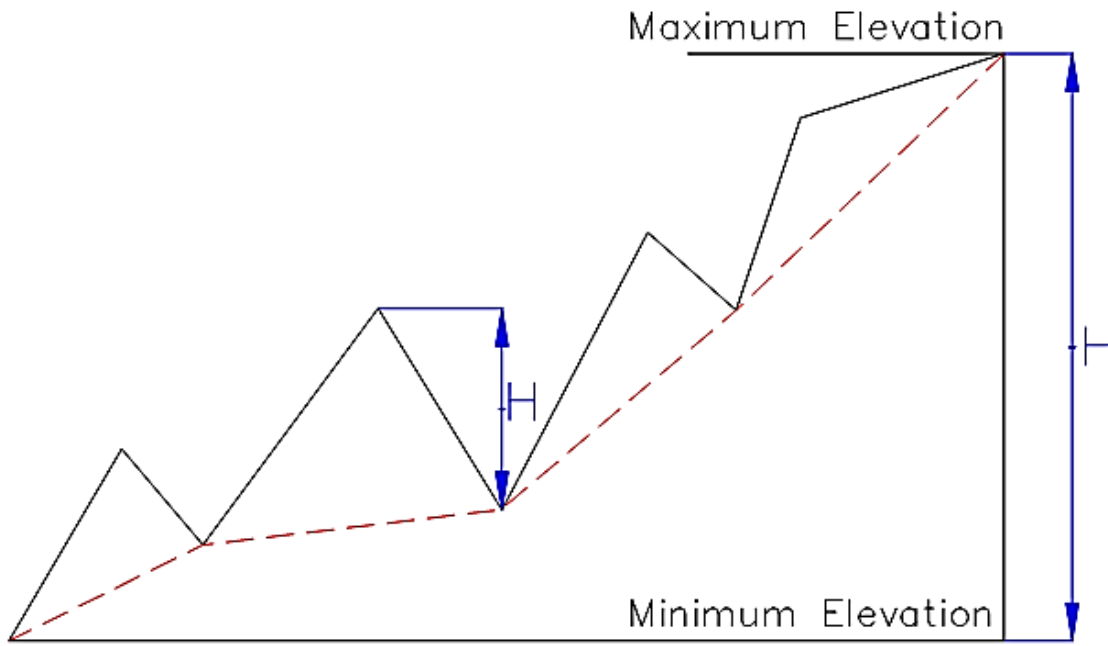


**Figure 7.1 Hypothetical Topographic Profile Illustrating Various Relief Measures  
(Red lines express the local relief)**

In our study we divided the Lebanese shape into a grid of 2 by 2 kilometers, with a calculation of all elevation statistic values (minimum, mean, and maximum). Inside each square of the grid, with the application of the radial basis function, the Local relief map of Lebanon was then made (figure 7.2).

The high local relief values are found in the mountainous area especially in El Yamouneh region, with relief energy which forms the Yamouneh fault. In both computational and geomorphic reasons, local relief represents the best single measure of the vertical dimension. It is obtained from GIS and digital representation of a surface. This parameter is in correlation with intensity of tectonic movements and dynamics of geomorphological processes in analyzed areas. Higher relief indicates greater erosion potential that is why Marković called relief energy (1983).

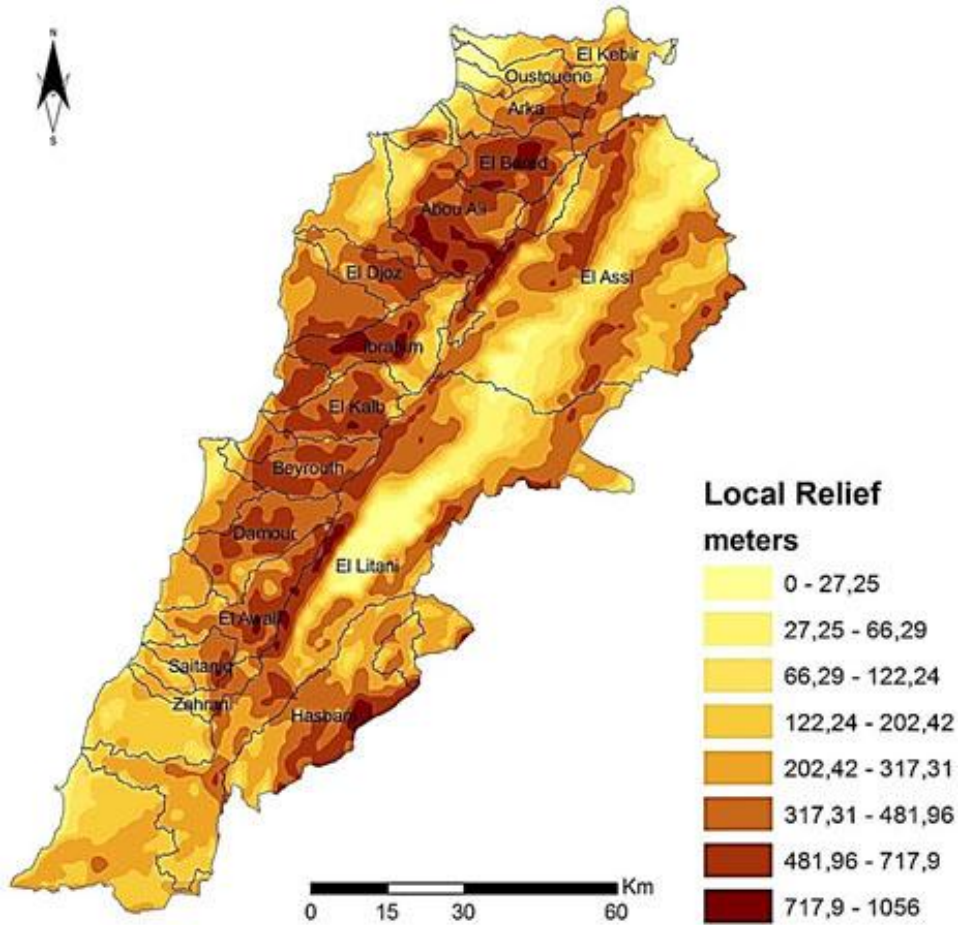


**Figure 7.2 Local Relief Map of Lebanon**

### 7.03 Relative Relief ( $Rh$ )

The basin height  $H$  is given by the difference between the maximum and minimum basin altitudes.

$$H = H_{max} - H_{min}.$$

The basin height determines the potential energy of a basin and the processes taking place at its surface (Schumm, 1956). The relative relief  $Rh$  is the basin height divided by the basin perimeter.

$$Rh = \frac{H}{P}$$

Relative relief expresses the relation between the potential energy of the basin terrain and its perimeter. High  $Rh$  values are related to basins with high local relief and small surfaces and vice versa.

## 7.04 Relief Ratio ( $Rp$ )

The relief ratio is calculated by dividing the basin height by the maximum basin length. From the relative ratio, it is possible to study the downslope value of the watershed basin. Generally, when the basin surface decreases, the value of  $Rp$  increases.

## 7.05 Ruggedness Number ( $Rn$ )

The ruggedness number describes the complexity of the topography and the roughness of the terrain. More rugged terrain exhibits a high complexity. Melton (1958) developed the ruggedness number to describe the ruggedness of land on a drainage basin scale. This is a dimensionless number calculated as:

$$Rn = \frac{H}{\sqrt{A}}$$

Where  $H$  – the relative ratio of the relief , and  $A$  is the basin area.

**Table 7.2 Terrain Parameter Values of Lebanon's Watershed Basins**

Basin	Area, km <sup>2</sup>	L <sub>v</sub> , km	Perimeter, km	H, m	Rh	Rp	Rn
<b>Abou Ali</b>	472.49	33.89	141.2	3072	90.65	21.8	141.3
<b>Arka</b>	133.22	26.36	93.68	2100	79.67	22.4	181.9
<b>Beirut</b>	237.19	29.31	113.51	2045	69.77	18	132.8
<b>Damour</b>	307.51	31.91	127.4	1888	59.17	14.8	107.7
<b>El Assi</b>	2031.41	69.19	291.92	2492	36.02	8.54	55.3
<b>El Awali</b>	297.33	39.17	157.09	1930	49.27	12.3	111.9
<b>El Bared</b>	263.44	29.22	123.07	2873	98.32	23.3	177.0
<b>El Djoz</b>	194.08	31.47	107.53	2316	73.59	21.5	166.2
<b>El Kalb</b>	254.37	29.58	106.11	2600	87.9	24.5	163.0
<b>El Litani</b>	2109.75	129.89	538.44	2604	20.05	4.84	56.7
<b>Hasbani</b>	594.07	52.73	190.01	2632	49.91	13.9	108.0
<b>Ibrahim</b>	332.25	40.73	148.16	2681	65.82	18.1	147.1
<b>Oustouene</b>	164.48	29.95	118.08	1915	63.94	16.2	149.3
<b>Sainiq</b>	108.68	19.02	73.49	1398	73.5	19	134.1
<b>Zahrani</b>	102.39	26.63	99.72	1630	61.21	16.3	161.1

## 7.06 Terrain Roughness

Terrain roughness indicates how undulating and how complex the terrain is.

The simplest way to compute terrain roughness is to calculate the standard deviation of the elevation cells in a DEM inside an analysis window. High value of standard deviation indicates that the terrain is rather irregular around the cell, and low values reflect a smooth terrain. Calculating terrain roughness using standard deviation is not a very precise method. For example, in some places it can assign high values to cells constituting a flat area. To avoid this problem we can use the best fit plane method, and then calculate the standard deviation (Sakude et al., 1998). Hobson (1972) proposed a vector approach to define the following Surface Roughness Factor:

$$SRF = \frac{\sqrt{(\sum_{i=1}^n X_i)^2 + (\sum_{i=1}^n Y_i)^2 + (\sum_{i=1}^n Z_i)^2}}{n}$$

Where  $n$  is the number of cells in the analysis window and  $X_i$ ,  $Y_i$  and  $Z_i$  are the components of the unit vector normal to the land surface at each one of the cells in the analysis window. These can be calculated from slope and aspect, using the following expressions:

$$\begin{aligned} X_i &= \sin(s) \cdot \cos(a) \\ Y_i &= \sin(s) \cdot \sin(a) \\ Z_i &= \cos(s) \end{aligned}$$

Where  $s$  is the slope value and  $a$  is the aspect one.

The surface roughness is the identity of the DEM expressing its quality, and it is used in studies related to wind analysis. Based on Hobson's vector approach, we could calculate the surface roughness factor in each watershed basin of Lebanon (Table 7.3).

**Table 7.3** Surface Roughness Type Percentage Area of Watershed Basins

<b>Basin</b>	<b>Smooth Terrain</b>	<b>Moderate Terrain</b>	<b>Noisy Terrain</b>
	<b>Area %</b>	<b>Area %</b>	<b>Area %</b>
<b>Abou Ali</b>	26	40	34
<b>Arka</b>	68	27	5
<b>Beirut</b>	29	37	33
<b>Damour</b>	31	35	34
<b>El Assi</b>	28	41	31

Basin	Smooth Terrain Area %	Moderate Terrain Area %	Noisy Terrain Area %
<b>El Awali</b>	32	35	33
<b>El Bared</b>	33	35	31
<b>El Djoz</b>	33	36	32
<b>El Kalb</b>	30	38	32
<b>El Litani</b>	80	17	4
<b>Hasbani</b>	33	35	32
<b>Ibrahim</b>	27	40	33
<b>Oustouene</b>	31	37	32
<b>Sainiq</b>	32	35	33
<b>Zahrani</b>	0	50	50

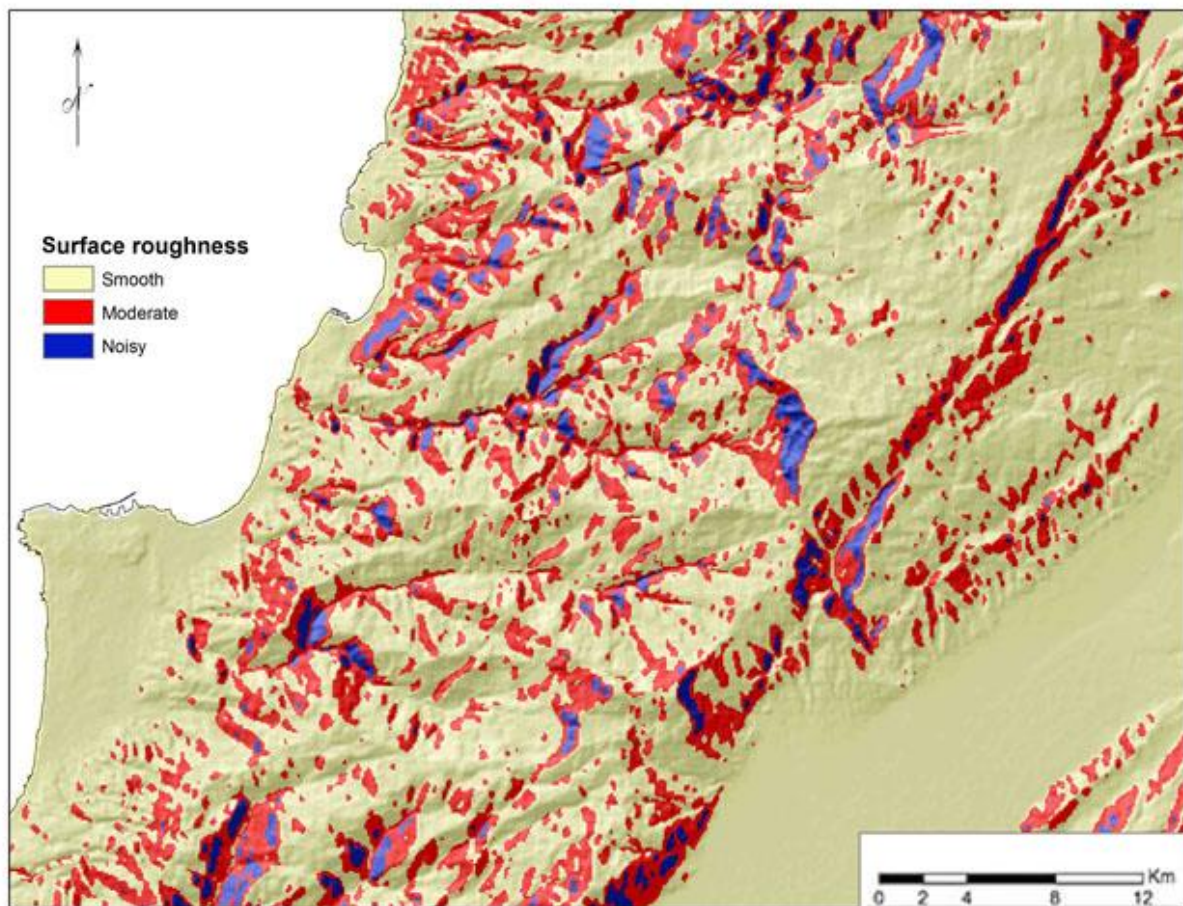


**Figure 7.3 Surface Roughness Showing Smooth, Moderate, and Noisy Terrain**

El Litani basin is the smoothest basin in the Lebanese boundary due to its plane topography. The Zahrani elongated basin of the non-smooth terrain is divided into moderate and noisy. From these results, we can classify Lebanese basins into 3 categories: smooth like Arka and El Litani), non-smooth like Zahrani's basin, and moderate, in which all values are proportional as the majority of Lebanese watershed basins.

## 7.07 Anisotropy

Anisotropy is defined by orientation of the perpendicular axes characterizing the anisotropy and a scaling ratio of the perpendicular axes. These parameters scale distances in the two perpendicular directions that should fit the spatial pattern of the anisotropic phenomenon. Anisotropy Index, which can be defined as the ratio between the minimum and maximum range parameter of spatial dependence, is fitted for various directions.

$$ANI = \frac{R_{min}}{R_{max}}$$

Where  $R_{min}$  is smallest estimated range parameter and the  $R_{max}$  is the highest estimated range parameter in various directions (Bishop and Minasny, 2005).

**Table 7.4 Anisotropy Values of Lebanese Watershed Basins. Lag size – 2000 m**

Basin	Number of lags	Direction Degree	$R_{min}$	$R_{max}$	ANI
<b>Abou Ali</b>	12	27.7	20735.3	23706.5	0.87
<b>Arka</b>	12	54.3	13674	22838.7	0.60
<b>Beirut</b>	12	23.3	21865.6	23706.5	0.92
<b>Damour</b>	12	15.1	18679.4	23359.6	0.80
<b>El Assi</b>	12	41.9	17702.3	23066.8	0.77
<b>El Awali</b>	12	26.9	15682.7	22950.2	0.68
<b>El Bared</b>	12	60.1	13674.5	22884.7	0.60
<b>El Djoz</b>	12	51.3	21672.4	23706.5	0.91
<b>El Kalb</b>	12	7.0	19706.9	23495.8	0.84
<b>El Litani</b>	12	38.6	15668.4	22992.5	0.68
<b>Hasbani</b>	12	32.2	13656	22955.9	0.59
<b>Ibrahim</b>	12	23.6	22205.9	23706.5	0.94
<b>Oustouene</b>	12	78.7	14690.3	22886.9	0.64
<b>Sainiq</b>	12	10.1	12603.6	19790.8	0.64
<b>Zahrani</b>	12	315.1	19560.3	23287	0.84

The proposed method of estimating the parameters of anisotropy is based on the construction of a semi-variogram related to the kriging spatial autocorrelation method (Pogorelov, Doumit, 2009). As the degree of anisotropy index decreases, the kriging variances become relatively worse. Under an incorrectly assumed isotropy, the kriging weights become more unequal as the degree of anisotropy increases. The anisotropy index values of Table 7.4 show that the more isotropic basins, which occupied the high values of ANI, are Ibrahim and Beirut, and the most anisotropic terrain, is for the Arka and El Bared basins.

In this analysis, we took the same lag size and numbers to get a good estimation of values close to one are more isotropic than the others. A simplified version of the ANI is the Anisotropic Coefficient of Variation (ACV), which is defined as the difference of the first derivative in 4 directions.

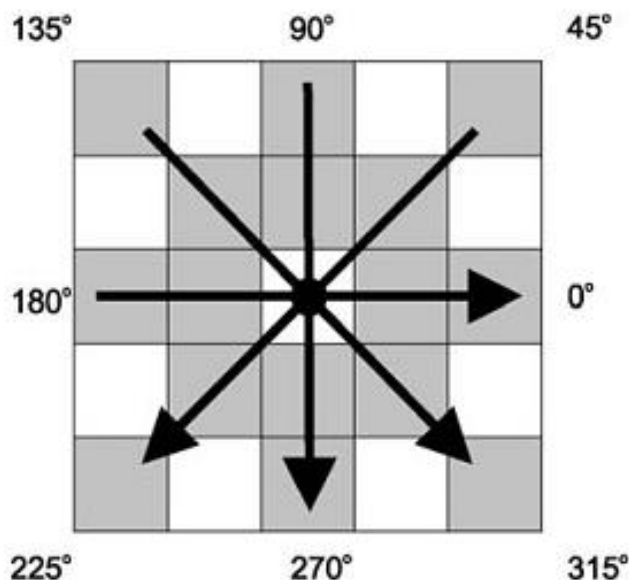


**Figure 7.4 Directions in a  $5 \times 5$  Window Environment**

$$ACV = \log \left[ 1 + \frac{\sqrt{\frac{\sum_{i=1}^8 (\partial z_{NBi} - \partial z_{AVG})^2}{8}}}{\partial z_{AVG}} \right]$$

Where  $\partial z_{AVG}$  is the average value of the first derivative in 4 directions: east/west, north/south, north-east/south-west, and north-west/south-east. The difference

between the average derivatives is then calculated for 8 neighbors ( $2 \times$  in each direction). The ACV of (Figure 7.4) describes the general geometry of the local surface and can be used to distinguish elongated from oval landforms (Olaya, 2009).

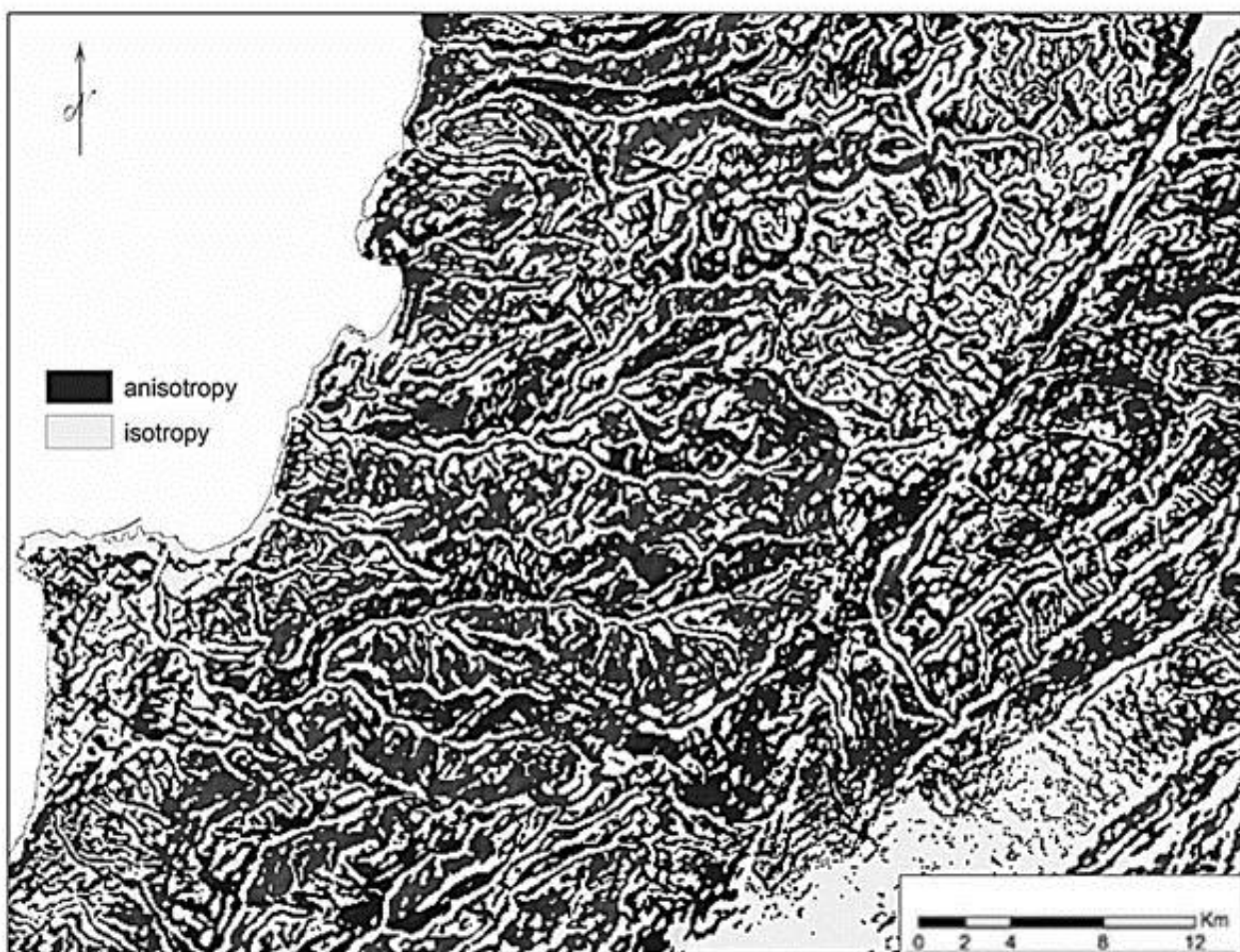


**Figure 7.5** Terrain Isotropy and Anisotropy Map

From Figure 7.5, we conclude that the terrain of streams, river beds, and ridges are isotropy, which means that slope surfaces have an anisotropy elevation values. The anisotropy parameter can be used for interpolation of spatially asymmetric data indicator of terrain complexity, and, therefore, is closely related to terrain roughness.

## 7.08 Fractal Dimensions

Nature is complex. Many important features and patterns of nature are so irregular that classical Euclidean geometry is of hardly any help in describing their form. It was this inability of using classical geometry to describe the real world that led to fractal geometry.

It was introduced and popularized by Mandelbrot (1977, 1982), to describe highly complex forms that are characteristic of natural phenomena, such as coastlines and landscapes. The main attraction of fractal geometry stems from its ability to describe the irregular or fragmented shape of natural features as well as other complex objects that traditional Euclidean geometry fails to analyze. Several authors have demonstrated that the Earth topography exhibits fractal characteristics over a wide range of scales (Huang and Turcotte, 1989; Klinkenberg and Goodchild, 1992). Nature gives so many examples of fractals, and fractal geometry can measure, classify, and represent some properties of objects. If the form is fractal, a linear relationship will exist between precision and length in a log/log plot. The slope of this line is then used to measure fractional dimension. Eastman (1985) developed a single pass technique for measuring the fractional dimension of lines. The procedure considers each slope segment, to provide evidence of an underlying angularity that can be considered as the generating angle of the fractal form. The formula is based on calculated slopes as follows:

$$D = \frac{\log(2)}{\log(2) + \log(\sin(\frac{180 - \text{slope}}{2}))}$$

Using the SRTM of Lebanese territory, we applied Eastman's method to calculate the fractal dimension of the terrain (Figure 7.6). As is known, surface fractal dimension values vary inside the interval between 2 and 3, (Figure 7.6). There are high fractal dimension values in dark colors of complex terrain surfaces, like El Kalb and Ibrahim's stream valleys, and fractal dimension low values of the coastal and El Bekaa plains. Figure 7.6 was made using a fractal dimension module of Idrisi software and then classified in five-class quantile classification.

Evans and McClean (1995) use fractal measures to describe various DEMs, and concluded the approximation of a land surface over a limited range of scales. Estimating the fractal dimension is not a simple problem. Several methods have been developed for this purpose, such as the fractional Brownian model (Mark and Aronson, 1984), triangular prism areas (Clarke, 1986), and box-counting (Falconer,

1990). In our study we used the triangular prism method to calculate the fractal dimension of the Lebanese watershed basins. This method was introduced by Clarke (1986). The triangular prism area method appears to be a reliable and reasonably fast method to compute the fractal dimension of a surface. It makes use of a raster representation of the elevations such as digital elevation model DEM.

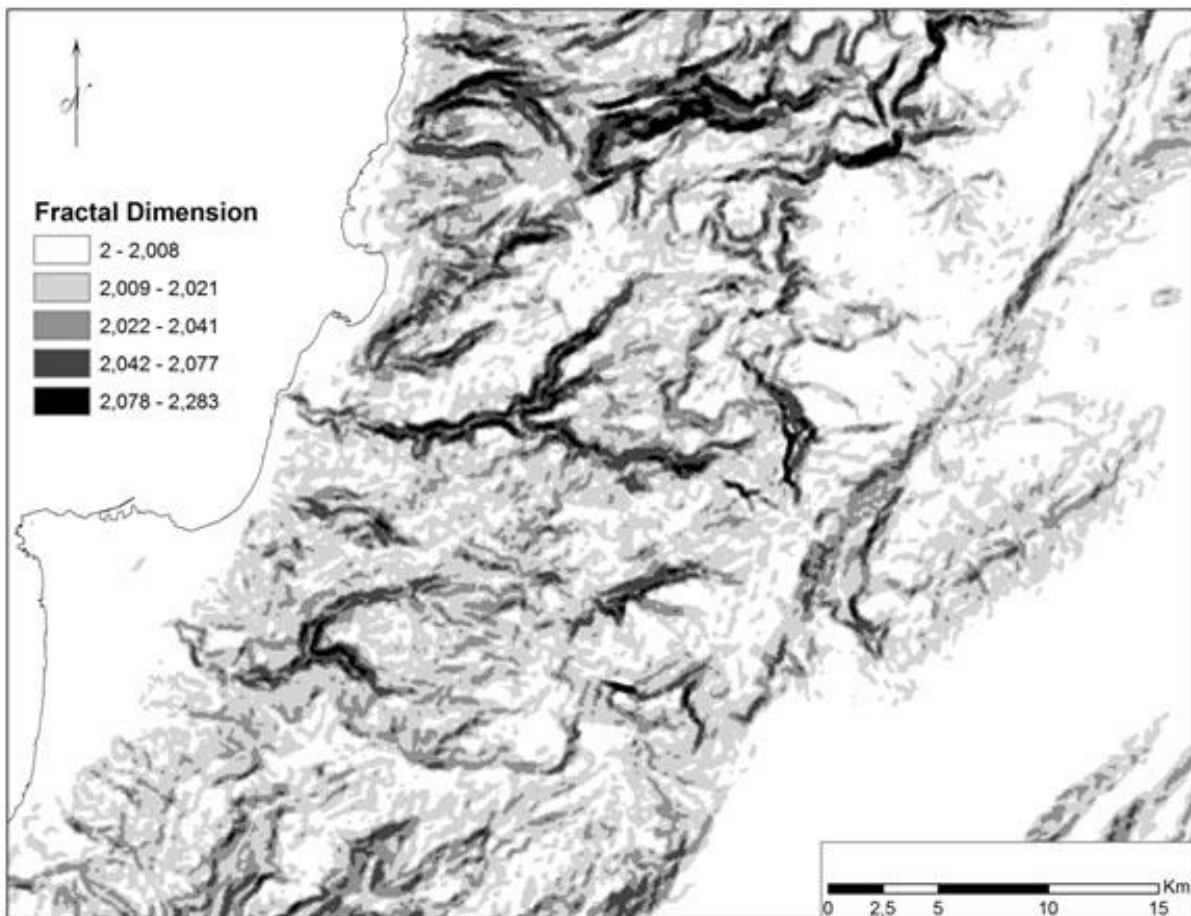


**Figure 7.6** Fractal Dimension Map of Lebanese Territory

Based on this data structure, the method takes elevation values at the corners of squares (*a*, *b*, *c* and *d* in Figure 7.7) and the interpolated center value (*e*) divides the square plan into four triangles, and then computes the top surface areas which result from raising the triangles to their given elevations, forming a prism (*A*, *B*, *C*, *D* in Figure 7.7). By repeating this calculation for increasing square sizes, the relationship between the upper surface of the prisms and the spacing of the squares can be established and used to estimate the fractal dimension. The only input parameter required in this method is the number of step sizes.

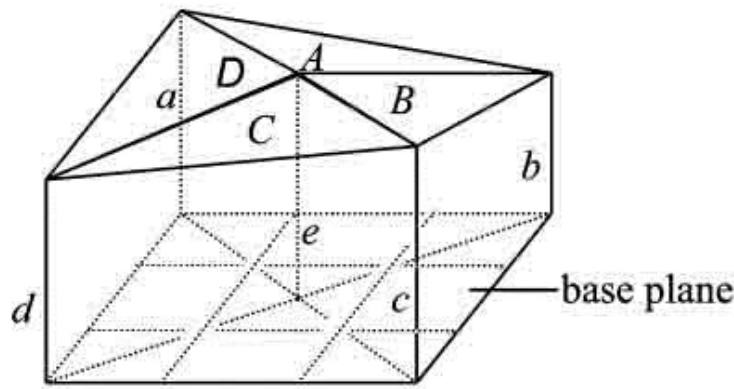


**Figure 7.7 3D View of the Triangular Prism Method (Clarke, 1986)**

**Table 7.4 Watershed Basin Triangular Prism Fractal Dimension Characteristics**

Boxes	Holes	Size (m)	Hole	Edge	Raw area	Corrected area
Abou Ali						
98282	39810	89.3	1.68	1.01	1280040	2179079.53
24492	10067	178.5	1.7	1.02	1232275	2125833.75
6084	2579	357	1.74	1.02	1111594	1973039.32
1521	691	714	1.83	1.02	915152.2	1714876.77
361	175	1428	1.94	1.08	692739.7	1448154.26
81	45	2856	2.25	1.2	441066.6	1190965.88
16	12	5712.1	4	1.52	184460.2	1120676.94
Fractal dimension = 2.09						
Arka						
Boxes	Holes	Size (m)	Hole	Edge	Raw area	Corrected area
33120	16993	89.3	2.05	1.02	272515	573114.19
8280	4361	178.5	2.11	1.02	256905	555830.2
2070	1146	357	2.24	1.02	224226	514396.39
510	307	714	2.51	1.04	167067	436133.64
119	80	1428	3.05	1.11	105223	357445.57
24	17	2856	3.43	1.38	51596.6	244133.85
Fractal dimension = 2.12						
Beirut						
Boxes	Holes	Size (m)	Hole	Edge	Raw area	Corrected area
50179	21074	89.3	1.72	1.02	655371.1	1152511.83
12420	5296	178.5	1.74	1.03	630335.5	1132175.08
3060	1350	357	1.79	1.05	569982.1	1066278.92
765	373	714	1.95	1.05	457715.3	933802.73

Boxes	Holes	Size (m)	Hole	Edge	Raw area	Corrected area
176	94	1428	2.15	1.14	283006.4	690030.36
44	30	2856	3.14	1.14	176422.2	629870.18
10	9	5712.1	10	1.25	18425.28	230239.51

Fractal dimension = 2.17

#### Damour

Boxes	Holes	Size (m)	Hole	Edge	Raw area	Corrected area
88408	50636	89.3	2.34	1.01	870414.3	2065056.36
22016	12756	178.5	2.38	1.02	836095.3	2022835.9
5504	3269	357	2.46	1.02	753424.5	1888069.94
1376	853	714	2.63	1.02	608683.1	1629616.64
336	225	1428	3.03	1.04	396200.7	1249476.79
80	59	2856	3.81	1.09	182239.5	759449.99
20	18	5712.1	10	1.09	48791.97	533745.54

Fractal dimension = 2.17

#### El Awali

Boxes	Holes	Size (m)	Hole	Edge	Raw area	Corrected area
122460	86107	89.3	3.37	1.01	813872.7	2773252.23
30615	21729	178.5	3.45	1.01	778028.8	2711455.81
7566	5442	357	3.56	1.02	684976	2496743.98
1872	1387	714	3.86	1.03	529516.1	2113151.5
456	362	1428	4.85	1.06	338494.4	1742436.04
108	97	2856	9.82	1.12	124463	1368739.73
24	23	5712.1	24	1.26	35874.99	1084938.14

Fractal dimension = 2.12

#### El Bared

Boxes	Holes	Size (m)	Hole	Edge	Raw area	Corrected area
67014	34722	89.3	2.08	1.02	858108.8	1808799.33
16677	8777	178.5	2.11	1.02	824198.2	1775364.58
4104	2213	357	2.17	1.04	738311.2	1661004.94
1026	588	714	2.34	1.04	594916.3	1444590.65
247	151	1428	2.57	1.08	405200.7	1122281.83
54	38	2856	3.38	1.23	242666	1008165.86
12	9	5712.1	4	1.38	168474.3	933244.36

Fractal dimension = 2.09

#### El Djoz

Boxes	Holes	Size (m)	Hole	Edge	Raw area	Corrected area
63296	39577	89.3	2.67	1.02	565932.6	1535526.66
15824	10033	178.5	2.73	1.02	537473	1493248.53
3956	2579	357	2.87	1.02	464409.8	1356552.17

Boxes	Holes	Size (m)	Hole	Edge	Raw area	Corrected area
989	677	714	3.17	1.02	344090.6	1108989.01
231	164	1428	3.45	1.09	221827.6	832319.05
50	39	2856	4.55	1.26	123995.4	708438.12
10	9	5712.1	10	1.57	34332.88	539435.23

Fractal dimension = 2.13

#### El Kalb

Boxes	Holes	Size (m)	Hole	Edge	Raw area	Corrected area
57376	26112	89.3	1.84	1.02	727999.6	1359503.87
14344	6666	178.5	1.87	1.02	701377.8	1333330.4
3564	1711	357	1.92	1.02	631252.1	1243086.24
880	450	714	2.05	1.04	520279.5	1103778.89
220	133	1428	2.53	1.04	333705.1	874777.35
50	33	2856	2.94	1.14	177241.6	594443.51
10	9	5712.1	10	1.43	38706.52	551719.16

Fractal dimension = 2.12

#### El Litani

Boxes	Holes	Size (m)	Hole	Edge	Raw area	Corrected area
1382135	1120925	89.3	5.29	1	3527188	18726908.59
344946	280418	178.5	5.35	1.01	3383767	18181073.53
86086	70335	357	5.47	1.01	3035033	16701774.52
21450	17698	714	5.72	1.01	2456945	14189922.01
5325	4456	1428	6.13	1.02	1863331	11616022.79
1295	1120	2856	7.4	1.05	1187268	9188361.22
306	277	5712.1	10.55	1.11	621050.2	7250968.92
72	70	11424.2	36	1.18	158250	6697630.49

Fractal dimension = 2.12

#### El Assi

Boxes	Holes	Size (m)	Hole	Edge	Raw area	Corrected area
452760	200106	89.3	1.79	1.01	3183881	5739540.69
113190	50466	178.5	1.8	1.01	3065840	5565473.98
28215	12739	357	1.82	1.01	2774751	5103778.34
6970	3189	714	1.84	1.02	2305281	4338939.43
1722	820	1428	1.91	1.03	1831046	3611595.94
420	218	2856	2.08	1.06	1402169	3087418.72
100	58	5712.1	2.38	1.11	1034595	2739097.79
25	18	11424.2	3.57	1.11	572540.7	2273708.68

Fractal dimension = 2.10

#### El Hasbani

Boxes	Holes	Size (m)	Hole	Edge	Raw area	Corrected area
-------	-------	----------	------	------	----------	----------------

Boxes	Holes	Size (m)	Hole	Edge	Raw area	Corrected area
205155	131933	89.3	2.8	1.01	1317910	3725306.19
51062	33045	178.5	2.83	1.01	1267244	3639449.89
12705	8344	357	2.91	1.02	1144937	3396202.16
3120	2094	714	3.04	1.04	941286.2	2966963.91
780	550	1428	3.39	1.04	686597.3	2413527.08
195	152	2856	4.53	1.04	427802.9	2010912.73
42	37	5712.1	8.4	1.2	163932.1	1656731.22

Fractal dimension = 2.10

#### El Ibrahim

Boxes	Holes	Size (m)	Hole	Edge	Raw area	Corrected area
112941	72108	89.3	2.77	1.01	908324.6	2543144.28
28063	18065	178.5	2.81	1.02	868702.7	2483357.62
6930	4523	357	2.88	1.03	775384.9	2301772.99
1716	1160	714	3.09	1.04	604635.4	1942584.78
416	301	1428	3.62	1.07	394916.1	1533586.23
104	88	2856	6.5	1.07	152042.3	1060927.49
24	23	5712.1	24	1.16	45448.85	1268540.1

Fractal dimension = 2.11

#### Oustouene

Boxes	Holes	Size (m)	Hole	Edge	Raw area	Corrected area
56430	36564	89.3	2.84	1.02	285341	824969.61
14025	9198	178.5	2.91	1.02	270500	804662.97
3444	2313	357	3.05	1.04	233083	739795.24
861	614	714	3.49	1.04	167907	610065.36
200	156	1428	4.55	1.12	99324.3	506462.28
50	45	2856	10	1.12	33899.6	380284.59

Fractal dimension = 2.09

#### Sainiq

Boxes	Holes	Size (m)	Hole	Edge	Raw area	Corrected area
29400	16204	89.3	2.23	1.02	291162.2	664227.56
7350	4153	178.5	2.3	1.02	273579.4	644028.29
1820	1063	357	2.4	1.03	228355.5	567570.58
442	277	714	2.68	1.06	148465.9	423240.35
104	70	1428	3.06	1.13	86364.47	298703.57
24	19	2856	4.8	1.22	41201.84	242253.97

Fractal dimension = 2.16

#### Zahrani

Boxes	Holes	Size (m)	Hole	Edge	Raw area	Corrected area
41464	29238	89.3	3.39	1.02	225876.6	782161.91

Boxes	Holes	Size (m)	Hole	Edge	Raw area	Corrected area
10366	7439	178.5	3.54	1.02	210443.1	760960.06
2555	1886	357	3.82	1.04	173718.5	687083.85
612	478	714	4.57	1.08	115810.4	571705.88
144	125	1428	7.58	1.15	48049.18	418217.53
36	35	2856	36	1.15	12063.11	498734.26
Fractal dimension = 2.09						

The triangular prism fractal dimension characteristics tables show in the first column the box quantities in the six rows of calculation, hole quantities, box dimensions, raw areas, and corrected areas. As a result of the triangular prism method, we found that the high values are found in Damour and Beirut basins, and low values in Zahrani, Al Bared, and Abou Ali. These values express the complexity and the exaggeration of the terrain. The proposed method detects different types of structures according to the observation scale, and provides useful information concerning the geological and geomorphologic mapping. Statistical morphometric parameters are increasingly used in geomorphometry, to quantify complexity of terrain. Gloaguen et al. (2007), for example, used fractal dimension derived for DEMs to automatically detect fault lines and similar geomorphological features. Fractals are used to estimate roughness and characterize the morphometry of a terrain.

## Chapter 8: Curvature

A geomorphological landscape could be appreciated in terms of its measurable surface, terrain curvatures computation is very complicated because, in general, the surface has different curvatures in different directions and it was very difficult how to determine them according to the type of processes under study. With the appearance of GIS technology and software, terrain curvature became a very easy parameter to calculate, this chapter describes curvature types and forms.

First derivatives of digital elevation models are slope and aspect, Second derivatives are curvatures, which give a proper assumption about the nature of the land surface.

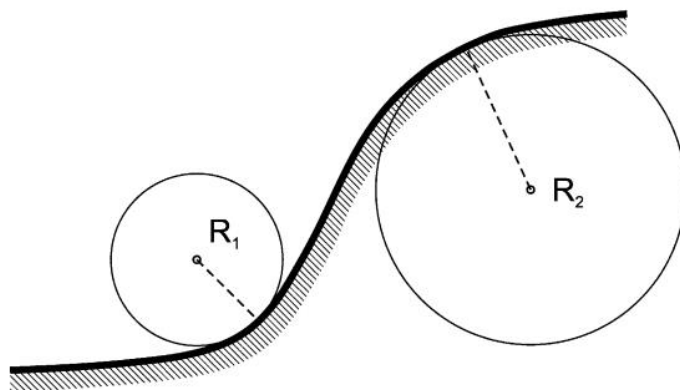


**Figure 8.1 Plan Curvature**

Plan curvature begins with a concave  $R_1$  radius and continues through an inflection point to form a convex circle of a radius  $R_2$ . The curvature of a straight line is  $k = 0$ . The radius of the tangent circle, the curvature radius, is given by  $R = 1/k$ . Curvature radius is measured in meters ( $m$ ) and curvature is measured as  $m^{-1}$ . In practice, prior to geomorphometric analysis, smoothing of DEMs has proved popularity among engineers and scientists because it carries measurement error anyway. The parameter describing the concavity and convexity of the surface is called curvature. The way to introduce curvature onto a smooth surface is to define a plane curve on it. Its curvature is defined as  $1/R$ , where  $R$  is the radius of a circle best fitted to this curve at a given point (Figure 8.1).

Curvature  $1/R$  of a plane curve is the inverse of the radius  $R$  of a circle that is best fitted to this curve at a given point. The curvature  $k$  of a plane curve  $z(x)$  is

given by the below formula as a function  $f(p, q, r, s, t)$  of the first and second partial derivatives of elevation.

$$K = \frac{\frac{d^2 z}{dz^2}}{\left[ 1 + \left( \frac{dy}{dx} \right)^2 \right]^{1.5}}$$

It is agreed in Earth sciences that the sign of curvature is positive for a convex surface shape ( $R_2 > 0$ ), and negative for a concave one ( $R_1 < 0$ ).

Based on Digital Elevation Models, the most popular algorithms for deriving first and second derivatives are those of Evans (1972), Shary (1995), Zevenbergen and Thorne (1987), as well as the modified Evans-Young (Shary et al., 2002) method. When all nine elevations of the  $3 \times 3$  DEM grid have been replaced by their smoothed values, the original Evans-Young algorithm is applied to calculate the derivatives  $p, q, r, s, t$ . This modified Evans-Young algorithm is based on the  $5 \times 5$  rather than  $3 \times 3$  DEM grid.

Burrough and McDonnell (1998) gave preference to the Zevenbergen-Thorne algorithm. Florinsky (1998) compared four algorithms theoretically, and found that the Evans algorithm was the most precise for calculating partial derivatives, compared with the Zevenbergen-Thorne and Shary methods. Recently, Schmidt et al. (2003) compared the Zevenbergen Thorne, Evans-Young and Shary algorithms experimentally, and concluded that the Evans-Young and Shary algorithms provide more precise results for curvatures in contrast to Zevenbergen-Thorne's.

For the extraction of the Lebanese watershed basin curvatures, we used the Zevenbergen-Thorne's method which is based on the idea of representation of a surface by an equation of partial quadratic form (Zevenbergen and Thorne, 1987).

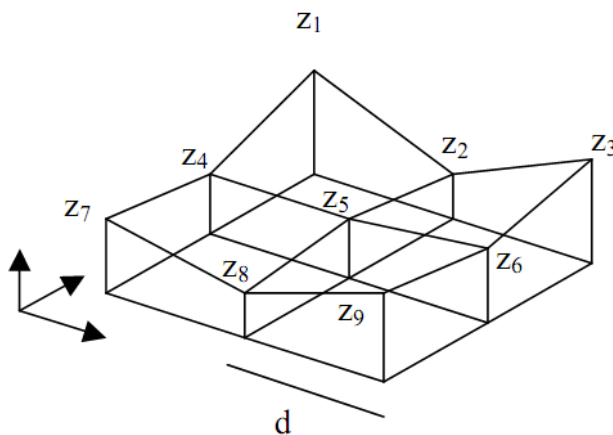


**Figure 8.2**  $3 \times 3$  Matrix of a DEM

$$z = f(x, y) = Ax^2y^2 + Bx^2y + Cxy^2 + Dx^2 + Ey^2 + Fxy + Gx + Hy + I$$

Where:

$$A = \frac{\frac{z_1 + z_3 + z_7 + z_9}{4} - \frac{z_2 + z_4 + z_6 + z_8}{2} + z_5}{d^4}$$

$$B = \frac{\frac{z_1 + z_3 + z_7 + z_9}{4} - \frac{z_2 + z_4 + z_6 + z_8}{2} + z_5}{d^4}$$

$$C = \frac{\frac{(-z_1 + z_3 - z_7 + z_9)}{4} + \frac{z_4 - z_6}{2}}{d^3}$$

$$D = \frac{\frac{z_4 + z_6}{2} - z_5}{d^2}$$

$$E = \frac{\frac{z_2 + z_8}{2} - z_5}{d^2}$$

$$F = \frac{-z_1 + z_3 + z_7 - z_9}{4d^2}$$

$$G = \frac{-z_4 + z_6}{2d}$$

$$H = \frac{z_2 + z_8}{2d}$$

$$I = z_5$$

The Zevenbergen and Thorne module applied to the SRTM datasets of Lebanon shows that 24% of the territory is concave, 49% convex and 27% flat areas. These results can be the proof that Lebanon is a hilly country.

## 8.01 Inflexion Points

The inflection point of a surface curve can be defined as the point separating convex and concave parts of the curve. Thus, point of inflection is given where the curvature of the surface curve changes sign and becomes zero. A simple inflection is where the curve swings from the left of the tangent at the point to its right. Or in the case of simple closed curve, it is where the closed curve changes from convex to concave or from concave to convex. In Figure 8.3 below, the curve on the left has one simple inflection while the curve on the right has six simple inflections (Rutter, 2000).

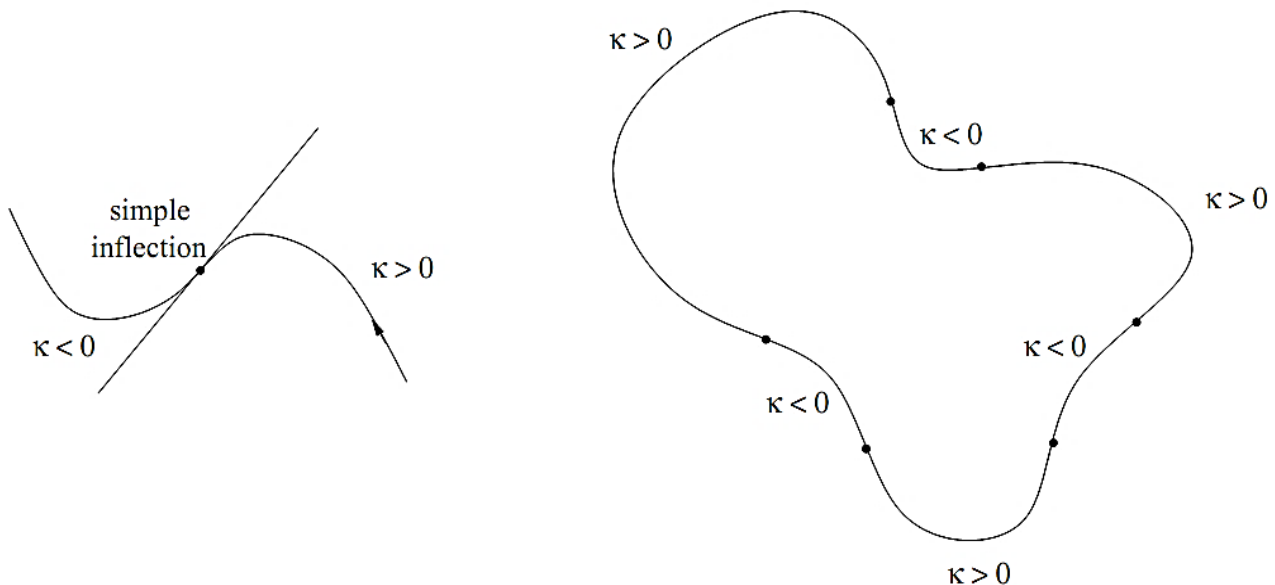


**Figure 8.3** *Inflection Points of a Curve*

Russian scientists, as Philosophov, Florensov, and Stepanov, have carried out a lot of research about the inflection lines. Under the name of morphoisograph, they defined them as the isolines connecting the points of null curvatures (Stepanov, 2006; Pogorelov and Doumit, 2007). The plastic relief method is widely applied in different countries. The essence of this method is that, in addition to the topographic contour line of equal altitude, we use another fundamental isoline – the morphoisograph. To draw a morphoisograph, we used the SRTM digital elevations model applied with GIS technology, resulting in the plastic relief map of Lebanon (Figure 8.4).



**Figure 8.4 Plastic Relief Map of Lebanon  
(Morphoisograph shown in black)**

Plastic relief maps provide an estimate of hazardous and less hazardous areas, and allow us to differentiate the study area as ‘favorable’, ‘less favorable’ and ‘unfavorable’ on the stream structures. This can be used to solve problems relating to construction, agriculture, mining, and environmental assessment. Plastic relief maps identify ways of migration of toxic substances and pollutants in soils, sediments, and groundwater, which allow a short time for the prevention of the consequences of man-made disasters and the reduction of the morbidity of the population. Relief plastic maps allow the defining of areas most prone to erosion, subsidence, landslides, and avalanches (Stepanov, 2006).

## 8.02 Plan and Profile Curvature

The terrain surface can be synthesized by combining terrain form elements, which are defined as relief unit of homogenous plan and profile curvatures. Plan

and profile curvatures are the most sensitive among terrain surface parameters. Plan or horizontal (also called contour) curvature ( $Kh$ ) is the curvature of a hypothetical contour line passing through the cell (a line formed by intersecting a horizontal plane with the terrain). It is given as:

$$Kh = \frac{2(DG^2 + EH^2 + FGH)}{(G^2 + H^2)}$$

Plan curvature is positive for convex-outward surfaces, negative for surfaces that are concave outward, and is undefined for flat areas. Plan curvature influences the convergence or divergence of water during downhill flow. Physically, horizontal curvature describes 1<sup>st</sup> accumulation mechanisms (Shary, 1995).  $Kh$  is negative, where flowlines converge, and  $Kh$  is positive where flowlines diverge. Geomorphologically, convergence areas are known as ‘concave’, while divergence areas are ‘convex’, as first indicated by Aandahl (1948). Terrains with convex plan curvature indicate dispersion of surface waters, and terrains with concave plan curvature indicate contribution-aggregation (concentration) of surface waters. Thus, elevated plan curvature processes deposition (fan, alluvial areas) and reflects the change in aspect angle and influences the divergence or convergence of water flow (Evans, 1980). Plan curvature influences soil moisture, thickness of soil horizons, organic matter, and plant cover distribution. Plan curvature can be used to map accumulation, transit, and dissipation zones of the land surface. Also, plan curvature is an indicator of geological lineaments and ring structures, and can also be used to determine fault morphology. Profile curvature or vertical curvature  $Kv$  is the terrain curvature in the vertical plane parallel to the local slope direction and defined as:

$$Kv = \frac{-2(DH^2 + EG^2 - FGH)}{(G^2 + H^2)}$$

Profile curvature measures the rate of change of slope, and therefore, influences the flow velocity of water draining the surface. It is positive for a convex upward surface and negative for one that is concave upward (Zevenbergen and Thorne, 1987). Physically, profile curvature describes 2<sup>nd</sup> accumulation mechanisms. It has been proven that  $Kv$  is negative on concave profiles, and positive on convex profiles, while zero on straight profiles (Shary, 1995). Therefore, relative acceleration and deceleration areas differ by  $Kv$  sign. Geomorphologically, relative deceleration areas are known as ‘concave’, while relative acceleration areas are ‘convex’, as first indicated by Aandahl (1948).

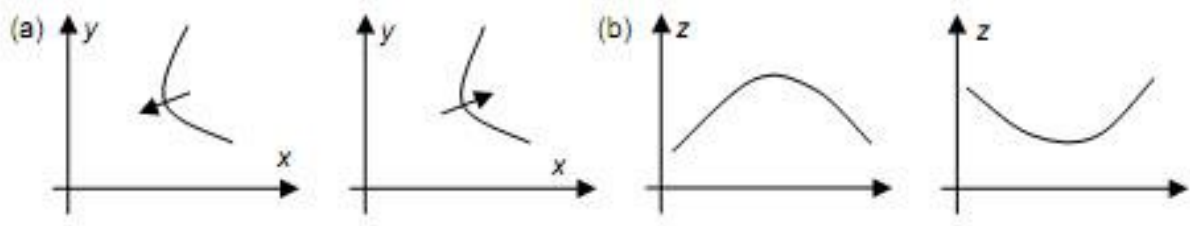


**Figure 8.5 Signs of Curvatures**

a) Positive and negative plan curvature; b) Positive and negative profile curvature

Profile curvature is terrain curvature in the steepest slope direction. This is a very significant topographic element that shows which process tends to be dominant, whether erosion or deposition. On convex terrains, erosion is more likely to prevail, as well as on concave deposition. The profile curvature is important because it reflects the change in slope angle and thus controls the change of velocity of mass flowing down along the slope curve (Evans, 1980). Plan curvature concave areas occupy 47 % of the total area of the Lebanese surfaces, 53 % of the convex areas and 1% of the horizontal surfaces. Profile curvature concave areas occupy 52 %, and convex areas 47 % (Table 8.1).

**Table 8.1 Percentage of Profile and Plan Curvature Area in Each Watershed Basin**

Basin	Plan Curvature			Profile Curvature		
	Concave	Convex	Horizontal	Concave	Convex	Horizontal
Abou Ali	47	53	-	51	49	-
Arka	47	53	-	54	46	-
Beirut	48	52	-	49	51	-
Damour	48	54	-	50	50	-
El Assi	48	52	-	57	43	-
El Awali	48	53	-	50	50	-
El Bared	48	52	-	50	50	-
El Djoz	48	53	-	50	50	-
El Kalb	48	53	-	48	52	-
El Litani	48	53	1	53	47	1
Hasbani	48	53	1	52	47	1
Ibrahim	48	53	-	50	50	-
Oustouene	48	52	-	53	47	-
Sainiq	48	54	-	49	51	-
Zahrani	48	54	-	51	49	-

In Figure 8.5, dark areas are the concave curvature of the land surface, and the light areas are convex. In part B of the figure, representing the profile curvature, the river bed of El Caleb is very clear, dividing the valley into Keserwane and Maten. In cells with concave plan curvature, the flow-lines converge, while they diverge in those with convex plan curvature. In much the same way, material flows experience relative deceleration in cells which have a concave profile curvature, and relative acceleration in those with a convex one (Shary, 1995; Shary et al., 2002). As discussed in previous chapters, it is already known that the geomorphological structures of the Lebanese basins are not similar to each other. They are related to the terrain characteristics variations. Profile and plan curvature analyses show geomorphological structure degrees of variation between the Lebanese river basins.

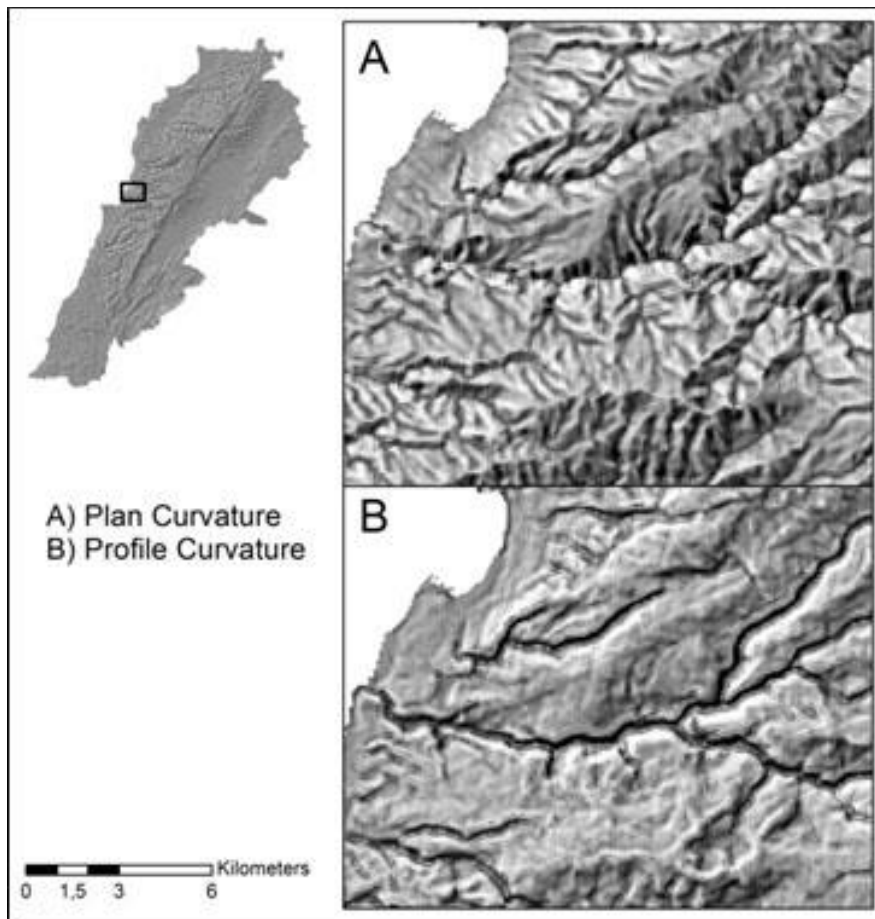


**Figure 8.5 Plan and Profile Curvature of El Caleb River Basin**  
**A) Plan Curvature  $kh$ ; B) Profile Curvature  $kv$**

The convex percentage area of plan curvature is higher than the concave one and proportional in all basins. Horizontal plan curvature areas are found in El Litani basin because of the Qaraoun Lake and some flat areas of Bekaa and Hasbani. In profile curvature percentage, concave is dominant, expressing acceleration in material flow of El Assi, Arka, El litani, Hasbani Oustouene and Zahrani. In other ways, some basins have equilibrium of curvature such as Damour, El Awali, El Bared, El Djoz, and Ibrahim which own a very similar geomorphological structure. Curvatures are not only interesting for hydrologists. For example, wildlife researchers can use curvature values to find out whether some parts of the terrain are protected (concave forms) or exposed (convex forms), as this obviously has an influence on the development of life forms. Curvature values are not similar especially in mountainous terrain. The degree of convexity and concavity differs from one place to another basin with regards to its relief structure (Table 8.1).

We classified concavity and convexity values into extreme, high, and slight. The slightly concave areas in plan curvature occupied the higher percentage (32.1 %) of the Lebanese territory. While slightly convex areas of the profile curvature occupied (30.2 %), flat area (strait areas not horizontal) in both plan and profile curvature values occupied a quarter of the Lebanese surface, due to the small DEM cell size (90 m×90 m).

Based on Table 8.2, the value of the extreme convexity is null. Flat areas are dominating because they take into account the water bodies. We can conclude from Table 8.2, is that the Lebanese terrain is very smooth with moderate curvatures.

**Table 8.2 Area Percentage of Curvature Types of Lebanese Terrain**

<b>Description</b>	<b>Plan Curvature</b>		<b>Profile Curvature</b>	
	<b>Value</b>	<b>Area %</b>	<b>Value</b>	<b>Area %</b>
Extremely convex	-0.018 to -0.008	0.0	-0.018 to -0.008	0.0
Highly convex	-0.008 to -0.004	0.1	-0.008 to -0.004	0.0
Convex	-0.004 to -0.001	7.3	-0.004 to -0.001	9.8
Slightly convex	-0.001 to -0.0001	27.7	-0.001 to -0.0001	30.2
Flat	-0.0001 to 0.0001	24.0	-0.0001 to 0.0001	23.3
Slightly concave	0.0001 to 0.001	32.1	0.0001 to 0.001	27.5
Concave	0.001 to 0.004	8.7	0.001 to 0.004	9.0
Highly concave	0.004 to 0.008	0.0	0.004 to 0.008	0.1
Extremely concave	0.008 to 0.012	0.0	0.008 to 0.012	0.0

## **8.03 Terrain Convergence**

Terrain convergence (divergence) is similar to plan and profile curvature but is more specific in values. It serves for catchment extraction and delineation divisions, as well as specific landform classification (Olaya, V. and Conrad, 2006). The calculation uses the aspects of surrounding cells. It observes to which degree surrounding cells point to the center cell. The result is given as percentages – negative values correspond to convergent, positive to divergent flow conditions (Koethe, Lehmeier, 1996). Terrain convergence values of the Lebanese republic range from -100 maximum concave terrains to 100 maximum concave terrains. In this analysis, zero values are related to terrain with slopes smaller than 1 degree. As a result of convergence, analyses show that the larger area of the Lebanese territory has divergence convex terrain like ridges and peaks. Greater erosion potential has terrains with a curvature index between -25 to -10 and 10 to 30, which cover 33% of the entire country area.

## **8.04 Curvature Classification**

Automated classification of terrain curvature almost always represents an attempt to replicate some previously conceived system of manual classification and mapping based on contour lines of topographic maps. Classifications can be considered to be predictable, while most curvature classifications are based on regional land-surface (Shary et al., 2005).

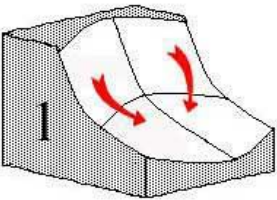
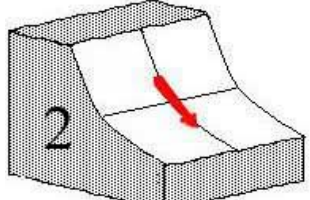
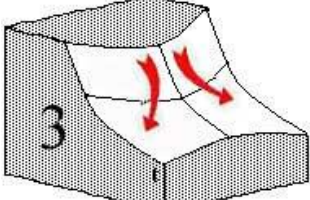
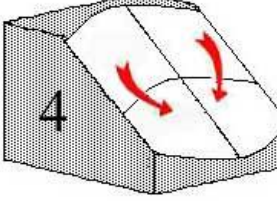
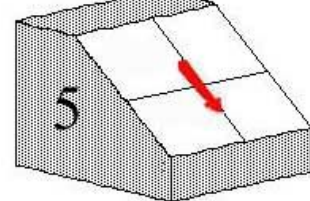
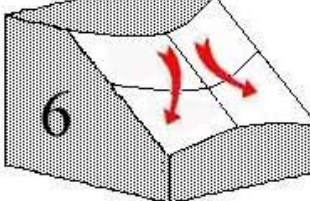
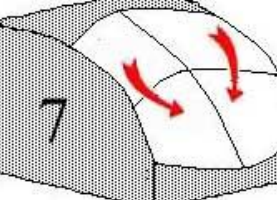
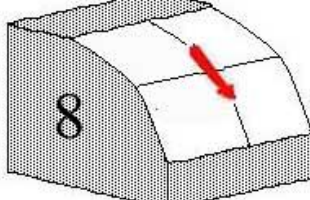
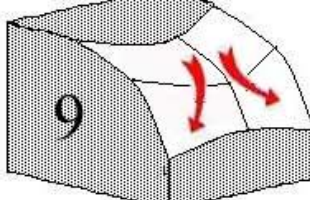
Evans (1980) has empirically found a stable positive correlation between independent local variables and plan and profile curvatures, for about 60 terrains (Evans and Cox, 1999). If we combine the three possibilities of the profile and plan curvature (concave, convex, and plane) we get the following nine possible land forms (Figure 8.6). Ruhe and Walker describe the nine-unit geometry illustrated, displaying the changes in slope curvature with a matrix of nine basic forms (Ruhe and Walker 1968; Dikau, 1989).

These nine curvature forms, shown in Figure 8.6, represent a wide range of hillslope types, traditionally considered in hydrology and geomorphology. Plan curvature and profile curvature straight, like shown in image 5 (Figure 8.6) occupied 70% of the total area of the Lebanese territory, especially in Bekaa, Akkar, and coastal valleys.

Percentage of convex concave (3) and concave convex (7) areas in watershed basins is null or very low in some basins. It is very visible in Table 8.3 that the combination of the curvature (concave and convex) with the straight forms (2, 8, 4, 6) has a proportional percentage of area in all basins. Flow convergence and

deceleration controlled by horizontal ( $kh$ ) and vertical ( $kv$ ) curvatures, correspondingly result in accumulation of soil substances caused by the slowing down or termination of overland and intrasoil transport.

**Figure 8.6 Three Dimensional View of the Nine Different Curvature Forms**

Profile Curvature $kv$	Plan Curvature $kh$		
	Concave $kh < 0$	Straight $kh = 0$	Convex $kh > 0$
Concave $kv < 0$			
Straight $kv = 0$			
Convex $kv > 0$			

**Table 8.3 Percentage Area of Curvature Forms in Watershed Basins**

Basin	Curvature Forms								
	1	2	3	4	5	6	7	8	9
Abou Ali	3	7	0	8	63	7	0	7	4
Arka	2	7	0	8	65	7	0	8	3
Beirut	2	7	0	7	64	8	0	7	3
Damour	3	6	0	12	59	9	0	7	3
El Assi	1	4	0	5	78	5	0	5	2
El Awali	3	7	0	12	54	10	1	8	4

Basin	Curvature Forms								
	1	2	3	4	5	6	7	8	9
El Bared	4	8	1	10	55	9	1	8	5
El Djoz	4	8	1	13	48	10	1	9	6
El Kalb	3	7	1	9	58	9	1	7	5
El Litani	1	4	0	6	77	5	0	4	2
Hasbani	2	5	0	8	71	6	0	6	2
Ibrahim	3	6	1	10	60	8	1	6	4
Oustouene	1	5	0	7	73	6	0	5	2
Sainiq	4	8	0	14	48	13	1	8	5
Zahrani	2	6	0	13	59	9	0	7	3

The intensity of these processes and the spatial distribution of accumulated substances can depend on the spatial distribution of the following landform elements (Table 8.4):

- Elements characterized both by convergence and by deceleration of flow – both by  $kh < 0$  and by  $kv < 0$  (accumulation zones)
- Elements offering both divergence and acceleration of flow: both  $kh > 0$  and  $kv > 0$  (dissipation zones)
- Elements that are free of a concurrent action of flow convergence and deceleration as well as flow divergence and acceleration – that is, values of  $kh$  and  $kv$  have different signs or are zero (transit zones)

**Table 8.4 Curvature Type and Zone**

Plan Curvature	Profile Curvature	Zone
convex	concave	transit
convex	plane	transit
convex	convex	dissipation
plane	concave	transit
plane	plane	transit
plane	convex	transit
concave	concave	accumulation
concave	plane	transit
concave	convex	transit

Dissipation and accumulation occupied only 0.5 % of the Lebanese surface and 99.5 % of the transit zone, from which we can conclude that Lebanese relief is

a migratory terrain. Data on accumulation, transit, and dissipation zones can be used in soil science to predict some soil properties. They can also be used in environmental protection to predict and map migration and accumulation of pollution agents. In addition, this data can be used in geological studies, since fault intersections are associated with accumulation zones, fault segments outside fault intersections relate to transit zones, and areas between faults relate to dissipation zones (Wilson and Gallant, 2000).

## 8.05 Morphometric Features

A lot of software has developed a technique to accurately convert a DEM into a grid where each and every cell has a nominal value representing morphometric feature classifications. The most widely used set of morphometric characteristics, is the subdivision of all points on a surface into one of pits, peaks, channels, ridges, passes, and planes. The names of these features suggest a geomorphological interpretation, but they may be unambiguously described in terms of rates of change of three orthogonal components ( $x$ ,  $y$ , and  $z$ ). Note that the components  $x$  and  $y$  are not necessarily parallel to the axes of the DEM, but are in the direction of maximum and minimum profile convexity. Numerical characterizations are used to quantify generic landform elements (morphometric features) such as point-based features (peaks, pits, and passes), line-based features (channels and ridges) and area-based features (planar) (Evans 1972; Wood, 1996).

Several methods exist for the identification of morphometric features (Evans, 1972; Maxwell, 1870; Peucker and Douglas, 1974; Tang, 1992). A technique developed by Wood (1996) is based on the quadratic approximation of a local window (kernel) and assessment of the second derivative. The second derivative is a function of the rate of change of slope. Wherever the surface is a plane, the second derivative is 0 (Wood, 1996). Due to the scale dependent nature of the phenomena, different kernel sizes result in different classification of each pixel. The standard method of identifying morphometric features is to pass a local (usually 3 by 3) window over the DEM and examine the relationships between a central cell and its neighboring ones (Peucker and Douglas, 1974; Evans, 1979). All cells in a DEM representing terrain can be put into one of these 6 classes (Table 8.5). The general problem was reduced to two sub-problems: smoothing the DEM and classifying the image. There are several techniques for classifying DEMs into morphometric features.

For consistency with the general geomorphometric parameters identified previously, the second derivatives required to identify all six features are extracted

using quadratic approximation of some local window. Profile curvature ( $Kv$ ) is used to characterize the second derivative, as this is the convexity measure that is related to geomorphological processes. Channels have a negative  $Kv$ , ridges a positive  $Kv$ , and planes a  $Kv$  of zero.

Additionally, we can measure the plan curvature ( $Kh$ ) in order to define the three remaining feature types. Pits have a negative  $Kv$  and  $Kh$ , peaks a positive  $Kh$  and  $Kv$ , and passes  $Kh$  and  $Kv$  with opposite signs.

**Table 8.5 Morphometric Features Described By Second Derivatives**

Feature Name	Derivative Expression	Description
Peak	$\frac{\delta^2 z}{\delta x^2} > 0, \frac{\delta^2 z}{\delta y^2} > 0$	A convex surface that is higher in elevation than all surrounding cells
Pit	$\frac{\delta^2 z}{\delta x^2} < 0, \frac{\delta^2 z}{\delta y^2} < 0$	A concave surface that is lower than all surrounding cells
Ridge	$\frac{\delta^2 z}{\delta x^2} > 0, \frac{\delta^2 z}{\delta y^2} = 0$	Contiguous convex lines of cells that occur when the cells are higher than the cells on either side
Channel	$\frac{\delta^2 z}{\delta x^2} < 0, \frac{\delta^2 z}{\delta y^2} = 0$	Contiguous concave lines of cells that occur when the cells are lower than the cells on either side
Pass	$\frac{\delta^2 z}{\delta x^2} > 0, \frac{\delta^2 z}{\delta y^2} < 0$	Intersection of ridge and valley
Plane	$\frac{\delta^2 z}{\delta x^2} = 0, \frac{\delta^2 z}{\delta y^2} = 0$	Surface with no slope no concavity/convexity

Peaks are local maxima on the surface, pits are local minima. An infinite number of slope lines converge at each peak, at their upper ends, and likewise each pit is a point of convergence of the lower ends of many slope lines that drain to it. Passes are the other kind of singularity. The two slope lines leading from the pass through these local maxima continue up to peaks, and are called ridge lines in Cayley/Maxwell terminology (Maxwell, 1870).

They correspond precisely to what we now call drainage divides. Ridge lines are mirrored by course lines. The two slope lines that lead from each, pass down to pits. Concave and convex breaks are surfaces situated between ridges and channels. Maxwell (1870) defined a hill as the region filled by all slope lines that connect to a particular peak, every cell in the network formed by the ridge lines and course lines is a territory (Maxwell, 1870). Warntz (1966) and Pfaltz (1976) rediscovered the Cayley/Maxwell surface theory and proved a number of properties of the graphs and associated networks determined by ridge and course lines.

Mark (1978) showed how these mathematical models could be useful in processing elevation models. This rigorous mathematical model of surface organization has the advantage that it can be applied computationally in straightforward fashion to major topographic data models, such as grids and TINs (Mark, 1979). Topography sometimes bears striking similarity to certain classes of mathematical functions known as fractals (See Chapter 8) (Mandelbrot, 1967, 1975, 1982; Mark and Aronson, 1984; Goodchild and Mark, 1987).

If terrain surfaces were truly fractals with statistical self-similarity, additional local variation in height would always be found with increasing spatial resolution. Here, we have used the techniques developed by Peuker and Douglas, a method classifying terrain surfaces into 7 classes (peak, pit, pass, and ridge, as well as channel, convex, and concave break). All cells were converted into polygons. A clustering algorithm was applied to create boundary polygons (Chaudhry and Mackaness, 2006). The area of the resultant polygon is used as a threshold for elimination of small polygons, since a hill or mountain needs to have a significant area to be identified. Running the basic model, a morphometric feature map of Lebanon was produced (Figure 8.7).

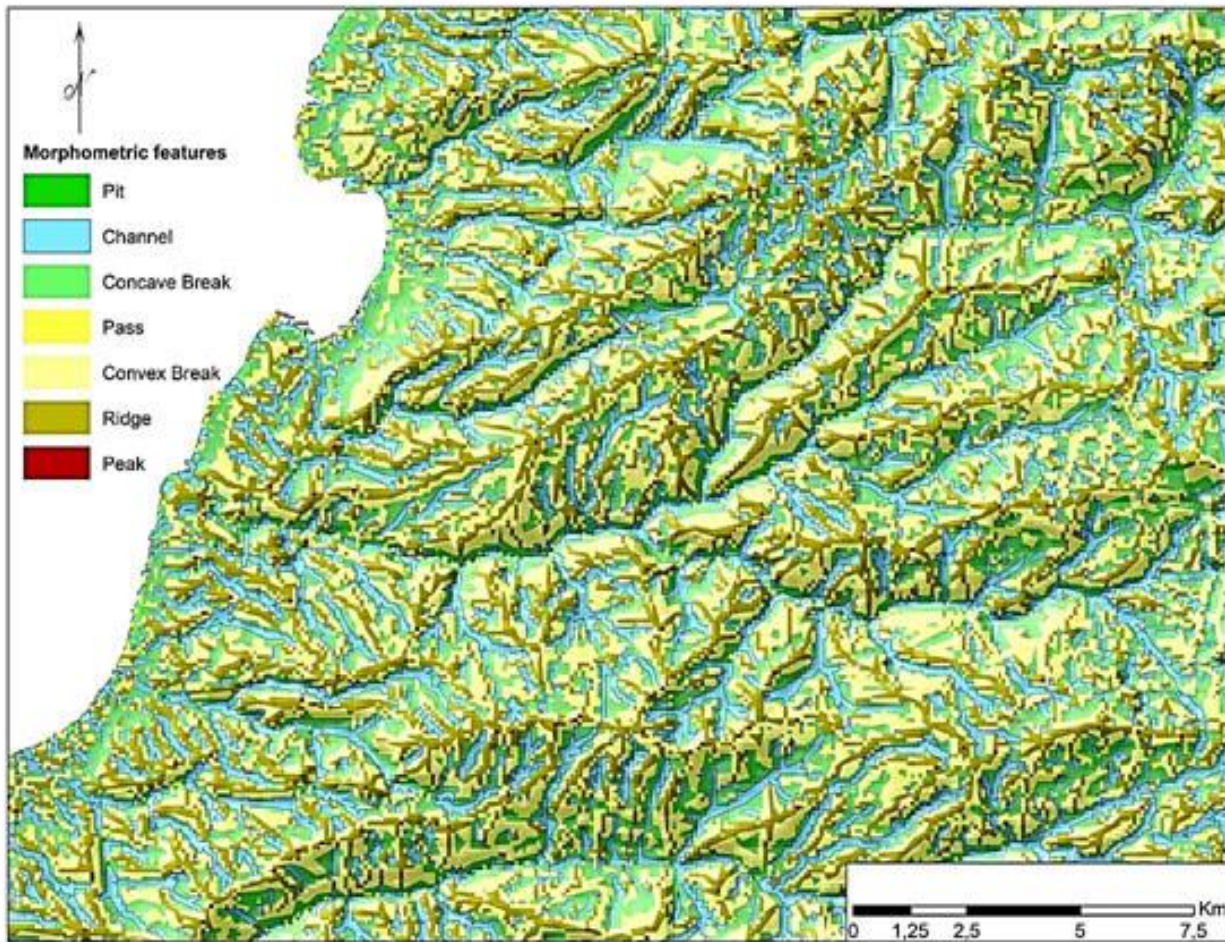


**Figure 8.7 Morphometric Feature Map of Lebanon**

The result shows a very clear distinction between the disparate morphometric features. In all country surfaces, the channel pattern appears similar to drainage network. Plan view, of the classification results draped over the DEM, was used to validate the classification results. In this map, about 42.9 % of the area is concave and convex breaks, 22.1 % are channels and 23 % are ridges. As expected point-based features such as peaks, passes, and pits cover only 12 % of the study area. There are a couple of reasons why that is. Firstly, point based features are comparatively rare. Secondly, due to the rugged terrain, many peaks with steep slopes exceed the slope tolerance value and are classified as ridges. Furthermore, the  $3 \times 3$  window of the DEM with 90 m grid covers a surface of  $270 \times 270$  meters, restricting the detection of small point-based features. The same study applies on a global scale, where morphometric feature percentage of an area was calculated for each watershed basin. Table 8.6 shows the percentage basin feature properties.

Peak and pit areas in all basins are less than one percent. Due to the mountainous terrain of Lebanon, it is not strange to find that channels and ridges occupy half the area and the second half is occupied by concave and convex breaks. El Assi, El Litani, and Oustouwene basins have a high percentage of pass area related to their non-mountainous terrain.

**Table 8.6 Morphometric Features Area Percentage of Lebanese Watershed Basins**

<b>Basin</b>	<b>Pit %</b>	<b>Channel %</b>	<b>Concave break %</b>	<b>Pass %</b>	<b>Convex break %</b>	<b>Ridge %</b>	<b>Peak %</b>
<b>Abou Ali</b>	0.2	21	25	6	25	22	0.2
<b>Arka</b>	0.4	24	24	7	21	23	0.4
<b>Beirut</b>	0.2	19	26	6	28	20	0.2
<b>Damour</b>	0.2	19	26	5	28	20	0.3
<b>El Assi</b>	0.4	22	22	16	18	21	0.4
<b>El Awali</b>	0.3	21	25	6	25	23	0.3
<b>El Bared</b>	0.2	20	27	5	27	21	0.3
<b>El Djoz</b>	0.3	22	24	5	25	23	0.4
<b>El Kalb</b>	0.3	20	24	5	28	22	0.2
<b>El Litani</b>	1.2	21	22	14	19	22	0.7
<b>Hasbani</b>	0.4	20	27	7	24	21	0.3
<b>Ibrahim</b>	0.5	22	24	6	24	23	0.4
<b>Oustouene</b>	0.8	22	21	12	20	24	0.7
<b>Sainiq</b>	0.4	21	23	5	25	24	0.5
<b>Zahrani</b>	0.5	22	23	6	23	25	0.5

Characteristics of land properties are not scale free and vary when measured over different spatial extents or different DEM resolutions. Landform elements are smallest homogeneous divisions of the land surface, at a given scale or resolution. With a multi-scale approach, each location has multiple morphometric features. DEM resolution and window size have a critical influence on the identification of morphometric features depending on terrain characteristics. The scale dependencies in this study are due to spatial extent with window sizes ranging from  $3 \times 3$  cells ( $270 \times 270\text{m}$ ).

# Chapter 9: Terrain Indices

Primary topographic attributes, such as slope, aspect, and curvature, are calculated from the directional derivatives of digital elevation models. They are computed directly by fitting a bivariate interpolation function  $z = f(x,y)$  (Moore et al., 1991; Mitasova et al., 1996; Florinsky, 1998).

Secondary compound attributes such as the compound topographic indices (CTI), stream power, and the LS factor, involve combinations of primary attributes which derive indices that can describe the morphometry, catchment position, and surface attributes of hill slopes and stream channels comprising drainage basins (Moore et al. 1991; Dikau, 1989; Jenson and Domingue, 1988). These attributes may affect soil characteristics, distribution and abundance of soil water, susceptibility of landscapes to erosion by water.

## 9.01 Compound Topographic Index (CTI)

The compound topographic index (CTI) is an index of hydrologic similarity that attempts to approximate the distribution of soil moisture in a watershed. Compound Topographic Index (CTI), also known as Steady State Wetness Index, is an equation adjustable for computing the topographic moisture accumulation. The CTI has been used extensively to describe the effects of topography on the location and size of saturated source areas of runoff generation, and to approximate the distribution of soil moisture in a watershed as follows:

$$CTI = In (A_s / \tan \beta)$$

Where  $A_s$  is the specific catchment area ( $m^2 m^{-1}$ ),  $\beta$  is the slope gradient in degrees (Moore et al., 1991). The formula has been calculated in a Raster Calculator for two raster files: the flow accumulation and the slope, calculated from the DEM (Quinn et al., 1991). Slope is an integral part of the CTI equation. It represents the local hydraulic gradient (Quinn et al., 1991).

The CTI is likely to be sensitive to the method used to calculate slope, and to the other factors that affect slope calculations, such as grid cell resolution, elevation precision, and topographic complexity). Studies that rely on the topographic index as an important parameter should report the methodology used to calculate slope. There are two algorithms generally applied to calculate the index: a single flow path algorithm and a multiple flow path algorithm. The single flow path algorithm assumes that subsurface flow occurs only in the steepest downhill direction, while the multiple flow path algorithms assume that flow at every point occurs in all

downhill directions from any point (Wolock and McCabe, 1995). Calculations of this parameter in our study within ArcMap ESRI are limited to the single directional algorithm, since this is the algorithm applied in calculation of flow direction (Jenson and Domingue, 1988). As a database in our study, we took an SRTM DEM of Lebanon, before calculating the CTI. A reclassification of the slope had been done to deal with the erroneous zero (0). The new slope was given values 0.001 instead of 0 using the Raster Calculator formula (Quinn et al., 1991).

$$[\text{New Slope}] = \text{con} ([\text{slope}] > 0, [\text{slope}], 0.001).$$

It was very important to add the number 1 to the equation too, since while having numbers in both of the files in range from 0 to some number, if one were not to introduce this factor, some strange results would have been observed (for example negative values of wetness index). Such prepared modified slope was calculated, using the formula below.

$$[\text{CTI}] = \text{Log} ([\text{Flow Accumulation}] + 1) / ([\text{Slope}] + 1).$$

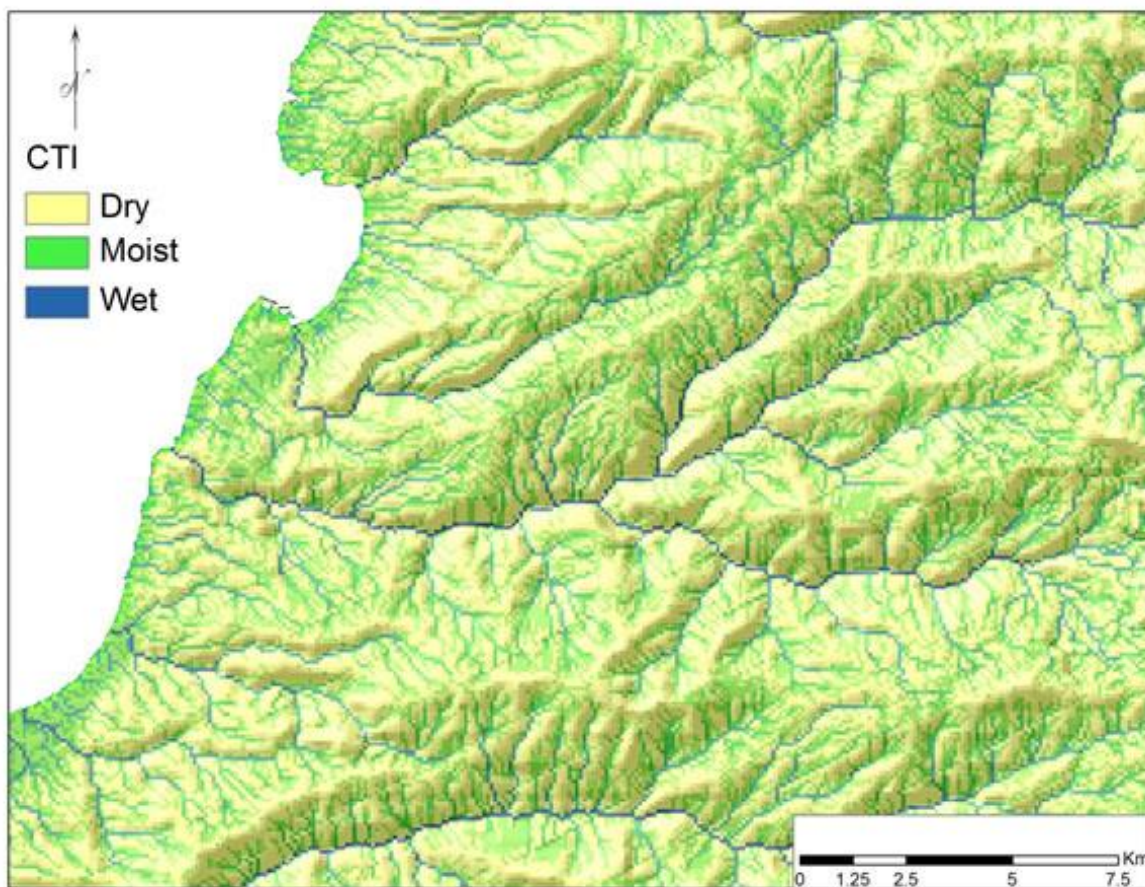


**Figure 9.1** Derived and Classified Compound Topographic Index of Lebanon

Figure 9.1 displays the compound Topographic Index divided into dry, moist, and wet. The ridges, slopes, river valley bottoms, and permanently saturated areas (lakes) were analyzed, and the CTI's index values were distributed. The Index values are as follows:

- Dry areas: 1-2 (bright colored areas on the maps).
- Moist areas: 3-4 (medium dark colored areas on the maps).
- Wet areas: 5 (dark colored water bodies on the maps).

In Figure 9.1 of the CTI of Lebanon, the light color is the dry soil, the medium dark color the moist one, and the fully dark color is the wet soil. As shown in the legend, the color is changing gradually from light to dark, passing by the medium dark that indicates the difference of wetness index from one place to another. For example, the rivers and the lakes have a maximum wetness index; therefore, they appear in the dark color. Based on Herron and Peterson, the high calculated values for CTI should indicate the places with the large contributing areas, like wisely low slopes. These places are susceptible to having high saturated soils. Contrarily, ridges and slopes should point out the dry condition of the soil in the landscape (Herron and Peterson, 2003). Researchers have approved the importance of the CTI analysis in different fields and capabilities. The CTI identify surface saturation zones in landscapes, describe the spatial distribution of soil-water content, characterize hydrologic similarity, characterize the spatial variability of soil properties, predict the degree of soil saturation, delineate wetlands in a coastal plain drainage basin, as was resolved in the Bekaa valley (Burt and Butcher, 1985; Sivapalan et al., 1987; Montgomery and Dietrich, 1995).

Using the CTI module, we studied the percentage area of wet, moist, and dry areas in each of the Lebanese watershed basins, as displayed in the table below (Table 9.1).

**Table 9.1** Wetness Percentage of the Lebanese Watershed Basins

Basin	Percentage of Area		
	Dry %	Moist %	Wet %
Abou Ali	69	24	7
Arka	67	25	8
Beirut	70	24	6
Damour	73	22	5
El Assi	53	36	11
El Awali	73	20	6
El Bared	73	21	6
El Djoz	75	18	7

Basin	Percentage of Area		
	Dry %	Moist %	Wet %
El Kalb	71	23	6
El Litani	53	36	10
Hasbani	65	27	7
Ibrahim	69	23	7
Oustouene	56	35	9
Sainiq	77	17	7
Zahrani	72	21	8

The low percentage of dry area found at El Litani basin and the high percentage of wetness at El Assi's is made from El Bekaa valley, the center of Lebanese agriculture. Besides precipitation, terrain shape and form play a big role in studying soil moisture and wetness. Some studies have shown a strong correlation between the CTI and occurrence of specific soil parameters, such as: horizon depth, silt percentage, organic matter content, phosphorus, and others (Evans J., 2004). The recalled role of topography in soil formations and soil genesis, as a result of differences in relief, is a well-known factor. However, it is not isolated from the other factors. Wet surface may be defined as a top sequence of the soil depicted on the basis of horizontal and vertical water movement in the local landscape drive. In this concept, it is emphasized that even if the soils originate from the same parent material, due to the topographic factor, their parameters may differ significantly from each other (Brown D.J. et al., 2000).

## 9.02 Stream Power

Stream power is an important topographic attribute that measure river environments and influences in sediment transport, erosional capacity, and flood dynamics (Fonstad, 2000). Stream power is the time rate of energy expenditure, and has been used extensively in studies of erosion, sediment transport, and geomorphology as a measure of the erosive power of flowing water (Moore et al., 1991). It is usually computed as:

$$\omega = \rho g q \tan \beta.$$

Where  $\rho g$  is the unit weight of water,  $q$  is the discharge per unit width, and  $\beta$  is the slope gradient (in degrees). The compound topographic index  $A_s \tan \beta$  is, therefore, a measure of stream power, since  $\rho g$  is essentially constant, and  $q$  is often assumed to be proportional to  $A_s$ . Measuring stream power could enhance the analysis of river morphology and could also contribute to determining the impacts of human activity on river environments (Knighton, 1999; Fonstad, 2000). The stream power

map of Lebanon (Figure 9.2) shows potential for channel formation in mountainous regions, and predicts water flow also in low elevation regions. Depicted in a dark color, we see the high values of stream power, and contrasting low values are found at high terrain elevations presented in light colors on the map. Stream power layer draped on the hillshade, as shown in Figure 9.2, can result in the conclusion that the high stream power is in the area of high steepest slope.

We can examine the spatial pattern of fluvial erosion across the entire range and infer the regional exhumation pattern due to geomorphic processes. We use a fluvial erosion index ( $EI$ ) to address the suggestion that spatial patterns of rapid erosion and active crustal upwelling tend to match one another throughout the Lebanese territory.

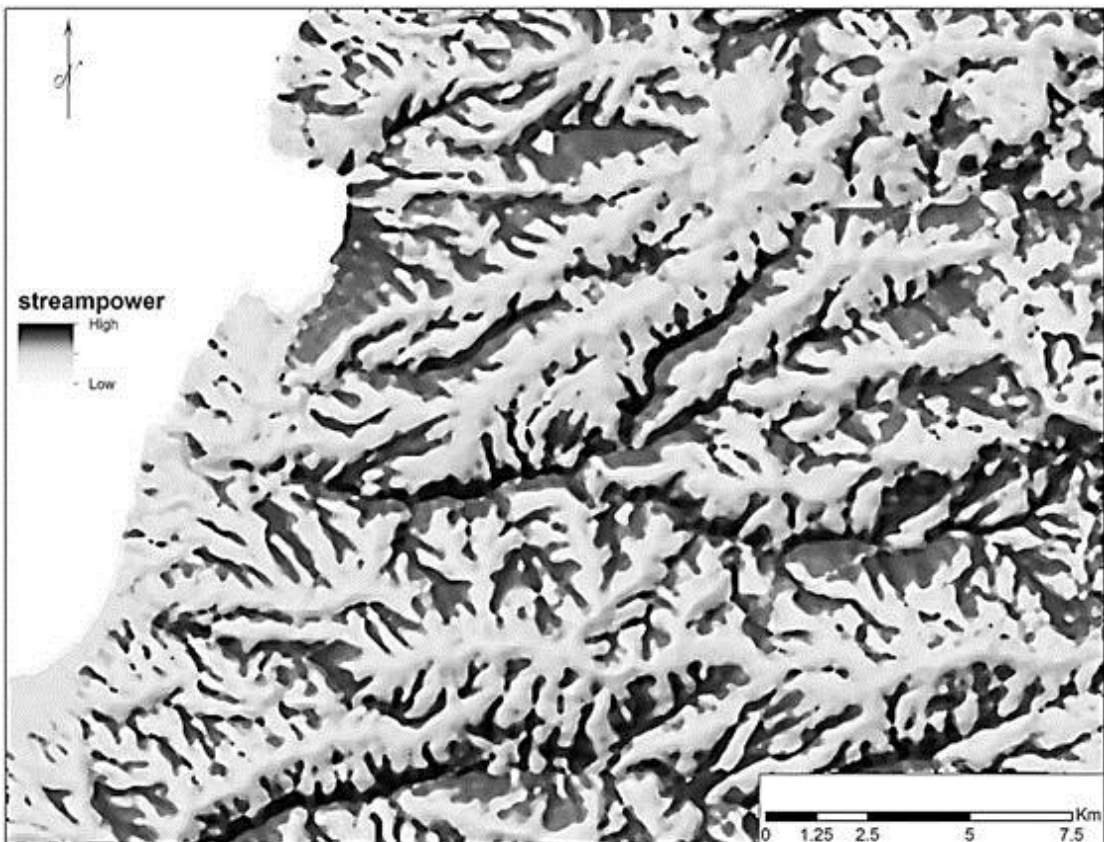


**Figure 9.2 Stream Power Map of Lebanon**

$EI$  model parameters were:  $EI = QS$  (stream power per unit length),  $EI = Q^{\frac{1}{2}}S$  (stream power per unit area), and  $EI = Q^{\frac{1}{3}}S^{\frac{2}{3}}$  (shear stress), where  $Q$  is model discharge and  $S$  is DEM slope (Howard and Kerby, 1983; Whipple and Tucker, 1999). At the scale of this analysis, however, stream power, unit stream power, and

shear stress are generalized abstractions of actual erosion processes. This type of abstraction should serve well as an erosion index in detachment limited regions and allow us to examine the spatial pattern of erosion in Lebanon in a way that is impossible with individual denudation measurements. The *EI* are predictably low in headwater reaches where both the discharge and gradient of the Lebanese terrain are modest, and increase dramatically in the river valleys. In Lebanon, the large discharge fueled by heavy monsoon precipitation combines with the extraordinary gradient of the rivers to produce exceptionally high *EI* values.

The three model results displayed in Figure 9.2, show that the spiked nature of the *EI* reflects large, local changes in slope that are amplified by the very large discharges associated with these rivers systems. The erosion index maps (Figure 9.3) highlight distinct zones of high erosion potential of the major Lebanese rivers. Among Lebanese watershed basins, two zones of high *EI* are apparent; the first is at the Southside of Abou Ali's basin, and the second is downstream of Ibrahim's river.

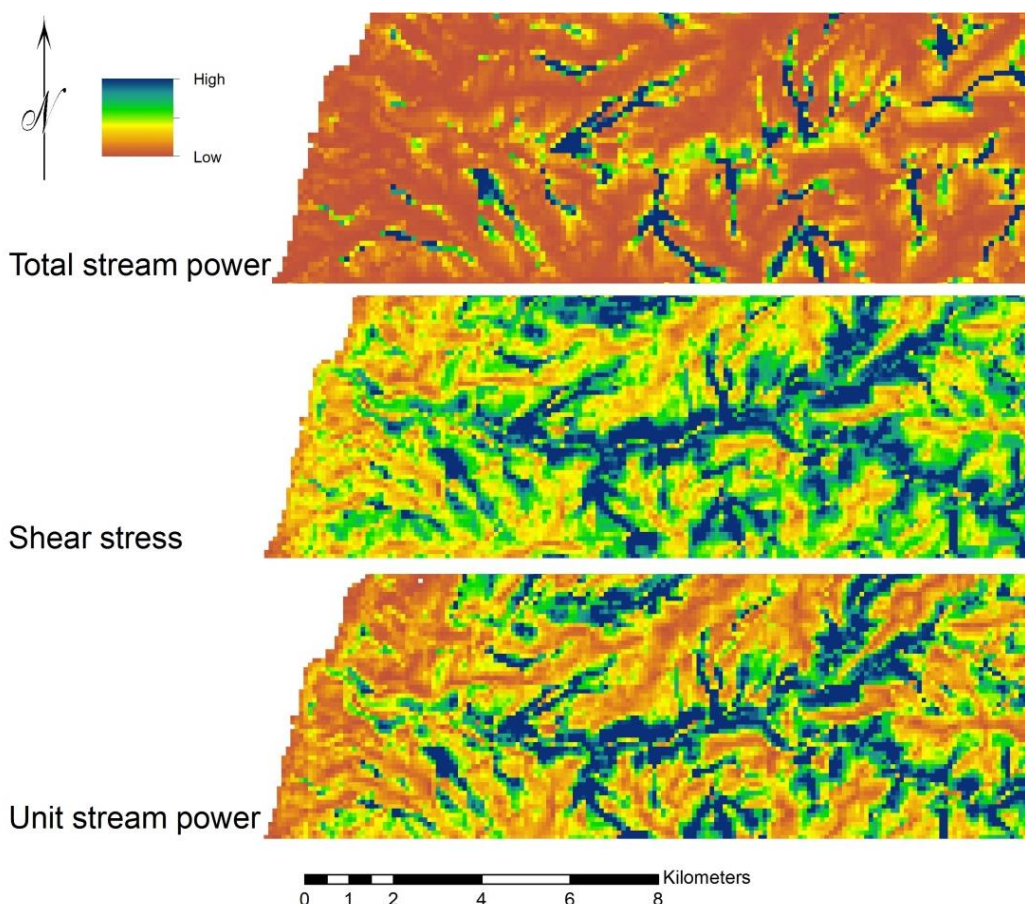


**Figure 9.3** EI Model Parameters of El Kalb River Basin

The most significant zone of elevated erosion potential is the Southside of Abou Ali's basin, where maximum value of  $EI$  estimated is 1.99 (shear stress) to 4.69 (stream power). The difference in the range of  $EI$  values between Abou Ali's basin and Zahrani's basin is 0.77.

One caution in the interpretation of Figure 9.3 is that high  $EI$  values are found only within the river channels, while the adjacent hillslopes have  $EI$  values several orders of magnitude smaller. The smoothing applied to Figure 9.3 exaggerates the areal extent of  $EI$  patterns so that these patterns can be visualized at this small scale. High  $EI$  values predicted by the shear stress model Figure 9.3 appear to be coincident with the transverse anticlines such as Ibrahim, Abou Ali, Beirut, and other rivers (Oberlander, 1985).

This study outlines a simple, practical method for estimating stream power. High-resolution spatial data demonstrates a real and underlying complexity of erosional processes that theoretical models, and point observations, fail to predict. With the emerging availability of high-resolution spatial data, the stream power equation can now find application at a small sub catchment scale. This enables calculation of stream power values at any point in a stream.

### 9.03 LS Factor

$L$  represents the effect of slope length on erosion (slope length factor). Slope length is the distance from the origin of overland flow along its flow path to the location of either concentrated flow or deposition. Slope lengths are best determined by taking measurements directly on site, pacing out flow paths. Obtain  $L$  by measuring perpendicular to the contour from the point of origin of overland flow to where deposition begins or runoff enters a well-defined channel.

$S$  represents the effect of slope steepness on erosion (slope steepness factor). Soil loss increases more rapidly with slope steepness than it does with slope length. The  $L$  and  $S$  factors are commonly combined as  $LS$  and referred to as the Slope Factor (Troeh et al., 1991). In our study, we will focus on generating the  $L$  and  $S$  factors from a DEM, and process an  $LS$  factor map of Lebanon without entering in details of the RUSLE equation calculation.

The effect of topography on erosion is accounted for by the  $LS$  factor, which combines the effects of a slope-length factor  $L$  and a slope-gradient factor  $S$ . As slope length increases, total soil loss and soil loss per unit area increases, due to the progressive accumulation of runoff in the downslope direction. As the slope

gradient increases, the velocity and erosivity increases. The two inputs to the *LS* factor are cumulative slope length and slope-gradient. Generating the *LS* values poses the largest problem in using the RUSLE (Griffin et al., 1988; Moore and Wilson, 1992; Renard et al., 1991), especially when applying it to real landscapes within a GIS (Griffin et al., 1988). The best method of estimating the values of *L* are field measurements, but unfortunately these methods are rarely available or practical. The gradient of a slope profile is defined as the change in elevation per change in horizontal distance, expressed in percent. The gradient of a particular slope can be measured in the field using a rod and a dumpy level or hand level, electronic survey level, or a GPS unit, at the same time that the length is measured. Slope gradients may also be estimated from digital aerial surveys or specific site maps but, again, accuracy decreases as the map scale decreases.

*LS* is the expected ratio of soil loss per unit area and it is calculated by using the below equation:

$$LS = \left( \frac{l}{72.6} \right)^m (65.41 \sin^2 \beta + 4.56 \sin \beta + 0.065).$$

Where *l* is the cumulative slope length in meters,  $\beta$  is the downhill slope angle, *m* is a slope contingent variable, 0.5 if the slope angle is greater than  $2.86^\circ$ , 0.4 on slopes of  $1.72^\circ$  to  $2.86^\circ$ , 0.3 on slopes of  $0.57^\circ$  to  $1.72^\circ$ , 0.2 on slopes less than  $0.57^\circ$  (Wischmeier and Smith, 1978)/

Values of *LS*, higher than 1, are artifacts due to DEM *LS* equation processing. In our case, artifacts in the *LS* factor grid of Lebanon occupied 0.02 % of the whole area. To know how erodible, the particular slope length and steepness of the Lebanese terrain is, a classification of 3 types was necessary: non-erodible, moderate, erodible. This classification was applied to the *LS* factor grid and as a result we got 85 % non-erodible surfaces, 15 % moderate, and 1.5 % erodible. These predictable percentages are very close to reality because of non-extreme relief and plains of Lebanon included in the non-erodible type and occupied half area of the Lebanese territory. As a sample, an *LS* study was conducted for El Kalb watershed basin, with a grid containing 30-m resolution (SRTM). This is represented in the *LS* map of river El Kalb basin (Figure 9.2).

## **9.04 Conclusion of All Indices**

Moore et al. (1991) concluded that the values of these indices are likely to vary from place to place because of differences in soil properties. Moore and Nieber used the stream power index to identify places where soil conservation measures that reduce the erosive effects of concentrated flow, such as grassed waterways, should be installed (Moore and Nieber ,1989).

## Conclusion

Terrain analysis and Geographical Information Systems (GIS) are being increasingly used for many applications in geosciences. Digital elevation data is rapidly becoming available at fine spatial resolution, being useful for a wide variety of purposes. This book has demonstrated the importance of terrain representations in environmental modeling. It serves as an introduction to the potential of digital elevation model as a creative and designing tool for terrain quantitative analysis. The tools and newly developed methods of surface structures extractions were tested out. Readers, especially students, can have a better understanding of the terrain forms and functions. Terrain digital models are a very easy tool to translate the landscape into a mathematical shape, by the integration and the use of Geographical Information System utilities.

Terrain quantitative analysis, or geomorphometry, has undergone a remarkable diversification from its nineteenth-century origins in physical geography. It is now indispensable to much contemporary science and technology. Many factors play a big role in this success, exemplified by the recent work reviewed here. Morphometric methods are scale independent from the Digital Elevation Model (DEM), spatial resolution, and accuracy. Moreover, these methods are effective in both scientific and engineering problem applications. Finally, morphometry captures the shape of discrete landforms, such as drainage basins and terrain curvature forms, as well as the geometry of continuous surfaces – agricultural fields, hill slopes etc. Geomorphometry's rapid growth is paralleling GIS computer technology and digital elevation models resolution, and accuracy will continue evolution to open new inventions. New and better terrain data, such as the high-resolution global DEMs forthcoming from drones and satellite missions, will stimulate fresh applications and increase the number of locations where morphometry can be used. New, advanced software that captures more complex terrain attributes will improve their power in the correlations between topographic form and other geographic phenomena.

The fact that geographers and engineers now have a tool that enriches their experience in terrain analysis and visualization provides a detailed exploratory and analytical method. Researchers should point out methods and assist the development of new tools that will allow a richer experience of analysis.

The main result of this study is a description of the Lebanese terrain morphological structure, the definition and implementation of the morphometric characteristics, as well as the selection and fixation of morphological elements and forms. This book is the first to interpret morphometric calculations using Digital

Elevation Models in GIS environments for the study area. The most significant scientific and methodological achieved results are:

- Hypsometric analysis of the Lebanese terrain in the form of hypsographic curves and statistical parameters.
- According to DEM extraction of the terrain, structural line thalweg's, and ridges with the calculations of bifurcation and length ratios of all watersheds with the fractal dimension of the erosion network.
- Mapping the Lebanese terrain morphological features (slope, aspect, stream density, relief energy, plan and profile curvature and inflection lines).
- Analysis of the terrain morphological structures and characteristics of watershed basins land forms.

The continuous research of the Lebanese terrain analysis with the new technologies will allow us to publish the second edition of this book, bringing modern innovations and new material.

## References

- Aandahl A.R.*, 1948. The characterization of slope positions and their influence on the total nitrogen content of a few virgin soils of Western Iowa. Soil Science Society of America Proceedings, 13, pp. 449-454
- Allder, W.R., Caruso, V.M., Pearsall, R.A., Troup, M.I.*, 1982. An overview of digital elevation model production at the United States Geological Survey. In: Proceedings of Auto-Carto 5. ASPRS-ACSM, pp. 23-32.
- Arrowsmith R.*, 2009. Open Topography.
- Bishop T. F. A., Minasny B.*, 2005. Digital soil-terrain modelling: the predictive potential and uncertainty. Environmental soil-landscape modeling. Geographic information technologies and pedometrics, edited by: Grunwald, S., Taylor&Francis, Boca Raton, Florida, pp.185-213.
- Black P.E.*, 1972. Watershed Hydrology.
- Böhme R.*, 1988. Topographic cartography. In: RW Anson (ed), Basic cartography, pp 1-21. International Cartographic Association and Elsevier, London and New York.
- Brown D.J., et al*, 2000, The Present, Past, and Future of the Catena Concept, Abstract from the University of Wisconsin Web page <http://www.soils.wisc.edu> (Acc. 2005.01.14)
- Brown, D., Bara, T.*, 1994. Recognition and Reduction of Systematic Error in Elevation and Derivative Surfaces from 7.5-Minute DEMs, Photogrammetric Engineering and Remote Sensing, Vol. 60, No. 2, pp. 189-194.
- Burrough P. A., McDonnell R. A.*, 1998. Principles of Geographic Information Systems \_ Spatial Information and Geostatistics, Chapter 8: Spatial Analysis Using Continuous Fields, ISBN 0-19-823365-5
- Burrough P., McDonnell R.*, 1998. Principles of Geographic Information Systems. Oxford University Press, New York, NY, p 333.
- Burrough, P.*, 1986., Principles of Geographical Information Systems for Land Resources Assessment, Oxford University Press, New York, NY, p.194.
- Burt T. P., Butcher D. P.*, 1985. Topographic controls of soil moisture distributions. Journal of Soil Science 36, pp. 469-486.
- Burt T. P., Butcher, D. P.*, 1935a. The role of topography in controlling soil moisture distributions. Journal of Soil Science, 36, pp. 469-486.
- Carlson C.W.*, 1963. Drainage density and stream flow. U.S. Geological Survey,Professional Paper 422-C.
- Carter J.*, 1990. Some Effects of Spatial Resolution in the Calculation of Slope Using the Spatial Derivative. ASPRS-ACSM Annual Convention - Technical Papers, Vol. 1, pp. 43-52.
- Carter J.*, 1992. The Effect of Data Precision On the Calculation of Slope and Aspect Using Gridded DEMs. Cartographica, Vol. 29, No. 1, p. 22-34.

*Cayley A.*, 1859. On contour lines and slope lines. Philosophical Magazine, vol. 18, pp. 264-268.

*Centamore E., Ciccacci S., Del Monte M., Fredi P., Lupia Palmieri E.*, 1996. Morphological and morphometric approach to the study of the structural arrangement of the North-Eastern Abruzzo (Central Italy). Geomorphology, 16, pp.127-137.

*Chandra A.M.*, 2002. Plane Surveying. New Age International, New Delhi.p.652.

*Chang K., Tsai B.*, 1991. The effect of DEM resolution on slope and aspect mapping. Cartography and GIS 18(1), pp. 69-77.

*Chaudhry O., Mackaness W.*, 2006. Creation of Fiat Boundaries in Higher order Phenomenon. In Workshop of the ICA Commission on Map Generalisation and Multiple Representation Vancouver - WA.

*Chebotarev A. I.*, 1964. Dictionary of Hydrology. Gidrometeoizdat,Leningrad (in Russian)

*Chorley R.J., Morgan M.A.*, 1962. Comparison of morphometric features. Unaka Mountains, Tennessee and North Carolina an Dartmoor, England, Geological Society of America Bulletin 73, pp.17-34.

*Chorley, R.J.*,1957. Climate and morphometry. Journal of Geology. 65: pp.628-638.

*Chorley R. J.,MorleyL. S. D.*,1959. A Simplified Approximation for the Hypsometric Integral. J.Geology 67, No. 5, pp. 566-571.

*Chorley R.J., Haggett P.*, 1969. Network Analysis in Geography. London: Arnold.

*Ciccassi S., Fredi P., Lupia Palmieri E., Salvini F.*, 1986. An approach to the quantitative analysis of the relations between drainage pattern and fracture trend. International geomorphology. II, pp. 49-68; Wiley and sons,Chichester.

*Clarke J.*, 1966. Morphometry from maps. In: Dury, G.H. (Ed.), Essays in Geomorphology Heinemann, London, pp. 235–274.

*Clarke K. C.*, 1986. Computation of the fractal dimension of topographic surfaces using the triangular prism surface area method. *Computers & Geosciences*, 12, pp.713-722.

*Costa-Cabral M., Burgess S.*, 1994. Digital Elevation Model Networks (DEMON): A model of flow over hillslopes for computation of contributing and dispersal areas. Water Resources Research, Vol. 30. No. 6, pp.1681-1692.

*Da Ros D., Borga M.*, 1997. Use of digital elevation model data for the derivation of the geomorphological instantaneous unit hydrograph. Hydrological processes, 11, pp. 13-33.

*Desmet P.J.J., Govers G.*, 1996. A GIS procedure for automatically calculating the USLE LS factor on topographically complex landscape units. J. Soil Water Conserv. 51, pp. 427–433.

*Di Benedetto F., Vivoni E. R., Grimaldi S.*, 2006. Use of Hypsometric Analysis for a Classification of Basin Hydrological Response: Surface and Groundwater Partitioning. American Geophysical Union., abstract #H31E-1471.

*Dikau R.*, 1989. The application of a digital relief model to landform analysis in geomorphology. In: Raper J., editor. Three dimensional applications in geographical information system. London: Taylor and Francis, pp.51-77.

*Dowding, S., Kuuskivi, T., and Li, X.*, 2004. Void fill of SRTM elevation data—principles, processes and performance. Proceedings of the conference “ASPRS Images to Decision: Remote Sensing Foundation for GIS Applications”, Kansas City, MO, September 12–16.

*Dunne T., Leopold L B.*, 1978. Water in environmental planning. W.H. Feeman, Co. New York.

*Eastman J.R.*, 1985. Single-Pass Measurement of the Fractional Dimensionality of Digitized Cartographic Lines. paper presented to the Canadian Cartographic Association, Annual Meeting, June 1985.

*Eastman R.*, 1992. IDRISI Technical Reference Version 4.0. Clark University Graduate School of Geography, Worcester, MA.

*Ehlschlaeger, C. R.*, 1998. The Stochastic Simulation Approach: Tools for Representing Spatial Application Uncertainty, Ph.D. Dissertation, University of California, Santa Barbara, 1998.

*El-Sheemy N., Valeo C., Habib A.*, 2005. Digital terrain modelling. Acquisition, manipulation, and applications. Artech House Inc., Boston.

*ESRI*. 1991. Cell-based Modelling with GRID. Redlands, CA: Environmental System Research Institute.

*Evans I.S.*, 1979. An integrated system of terrain analysis and slope mapping. Final report on grant DA-ERO-591-73-G0040, University of Durham, England.

*Evans I.S.*, 1980. An integrated system of terrain analysis and slope mapping. Zeitschrift für Geomorphologie N.F., Suppl.-Bd.36, pp. 274-295.

*Evans I.S., Cox N.J.*, 1999. Relations between land surface properties: altitude, slope and curvature. In: S.Hergarten, H.J.Neugebauer (eds.). Process Modelling and Landform Evolution. Berlin, etc., Springer, pp. 13-45.

*Evans I.S., McClean, C.J.*, 1995. The land surface is not unifractal: variograms, cirque scale and allometry. Zeitschrift für Geomorphologie, Supplementband 101, pp. 127–147.

*Evans I.S.*, 1972. General geomorphometry, derivatives of altitude, and descriptive statistics. In: Chorley, R.J. (Ed.), Spatial Analysis in Geomorphology. Methuen & Co., Ltd., London, Chap. 2, pp.17-90.

*Evans J.*, 2004. Compound Topographic Index script summary description, ESRI Support Center On-line, (<http://arcscripts.esri.com>)

*Fairfield J., Leymarie P.*, 1991. Drainage network from grid digital elevation models, Water Resources Research, 5, pp. 709–717.

*Falconer K.*, 1990. Fractal Geometry Mathematical Foundations and Applications. J. Wiley, Chichester, p. 288.

*Falorni, G., Teles, V., Vivoni, E R., Bras, R.L., and Amarasinghe, K.*, 2005. Analysis and characterization of the vertical accuracy of digital elevation models from the shuttle radar topography mission. *Journal of Geophysical Research*, 110, F02005.

*Farr, T.G.; Kobrick, M.*, 2009. Shuttle Radar Topography Mission Produces a Wealth of Data. *Amer. Remote Sens.*, 1.

*Florinsky I.V.*, 2000. Relationship between topographically expressed zones of flow accumulation and sites of faults intersection: Analysis by means of digital terrain modelling. *Environmental Modelling and Software* 15, pp. 87-100.

*Florinsky I.V.*, 1998. Accuracy of local topographic variables derived from digital elevation models. *International Journal of Geographical Information Science*, 12, pp.47–61.

*Florinsky I.V.*, 1998. Combined analysis of digital terrain models and remotely sensed data in landscape investigations. *Progress in Physical Geography*, 22, pp. 33-60.

*Fonstad Mark A.*, 2000. Spatio-temporal variation in the power of mountain streams. Ph.D. diss., Arizona State University.

*Freeman T.G.*, 1991. Calculating catchment area with divergent flow based on a regular grid, *Computers & Geosciences*, 3, pp. 413–422.

*Gamba, P., Dell'Acqua, F., and Houshmand, B.*, 2002. SRTM data characterization in urban areas. *International Society for Photogrammetry and Remote Sensing Commission III, Symposium 2002*, September 9–13, 2002, Graz, Austria 2004–2008.

*Gandolfi C., Bischetti G B.*, 1997. Influence of the drainage network identification method on geomorphological properties and hydrological response. *Hydrological Processes*, 11, pp. 353-375.

*Gao J., Lo C.P.*, 1995. Micro-scale modeling of terrain susceptibility to land sliding from a DEM: a GIS approach. *Geocarto International* 10(4) pp. 15-30.

*Garbrecht J. Martz L.W.*, 1993. Comment on "A combined algorithm for automated drainage network extraction" by J. Chorowicz, C. Ichoku, S.

*Garbrecht J., Martz L.*, 1999. Digital Elevation Model Issues in Water Resources Modeling, 1999 ESRI International User Conference Proceedings, San Diego CA,<http://www.esri.com/library/userconf/proc99/proceed/papers/pap866/p866.htm>.

*Gardiner V.*, 1983. Drainage networks and palaeohydrology. K.J. Gregory (ed.). *Background to Palaeohydrology*. New York: Wiley& Sons.

*Gardiner V., Gregory K.J.*, 1982. Drainage density in rainfall-runoff modeling in V.P. Singh (ed.) *Rainfall-Runoff Relationships*, Littleton Colo.: Water Resources Publications.

*Gardiner V.*, 1983. Some recent trends in fluvial morphometry. *Natl Geog.* 18, pp. 1-8.

*Gardiner V., Gregory K.J.*, 1982. Drainage density in rainfall-runoff modelling. In *Rainfall-runoff relationship*, V.P. Singh (ed), 449–76. Littleton, Colo.: Water Resources Publications.

*Gemborys S. R.*, 1979. Tree distribution in relation to micro topography: The Bowl, Wonalancet, New Hampshire. Harvard Forest, Harvard University. pp. 5.

- Goodchild M. F., Mark D. M.*, 1987. The fractal nature of geographic phenomena. Annals of the Association of American Geographers, 77, pp. 265-278.
- Green P. J., Sibson R.*, 1978. Computing dirichlet tessellation in the plane. The Computer Journal 21, pp. 168-173.
- Greenlee, D. D.*, 1987. Raster and vector processing for scanned lineword. Photogrammetric Engineering and Remote Sensing, Vol. 53, No. p. 10.
- Gregory K.J.*, 1976. Drainage networks and climate. Geomorphology and climate. E. Derbyshire (ed.), pp. 289-315. Chichester: Wiley.
- Gregory K.J.*, 1976. Dry valleys and the composition of the drainage net. Journal of Hydrology 4, pp.327-340.
- Griffin J. R.*, 1971. Oak regeneration in the upper Carmel Valley, California. Ecology 52, pp. 862-868.
- Griffin M.L., Beasley D.B., Fletcher J.J., Foster G.R.*, 1988. Estimating soil loss on topographically non uniform field and farm units. Journal of Soil and Water Conservation, 43, pp. 326-331.
- Gritzner J.H.*, 2006. Identifying Wetlands Depressions in Bare- Ground LIDAR for Hydrological Modeling. ESRI Users Group Conference.p.13.
- Gruber S., Peckham S.*, 2007. Land-Surface Parameters and Objects in Hydrology. Developments in Soil Science – Volume 33, ch7, pp.171-194.
- Guth, P.*, 2003. Geomorphology of DEMs: Quality assessment and scale effects. Paper No. 175-2. Proceedings of GSA, Seattle Annual Meeting, November 2–5, 2003.
- Gyasi-Agyei, Y., Willgoose, G., and De Troch, F.*, 1995. Effects of Vertical Resolution and Map Scale of Digital Elevation Models on Geomorphological Parameters Used In Hydrology, Hydrological Processes, Vol. 9, pp. 363-382.
- Hadley R.F., Schumm S.A.*, 1961. Sediment sources and drainage-basin characteristics in Upper Cheyenne River basin. U.S. Geological Survey Water Supply Paper 1531-B, pp.137-198.
- Hammer R. D., Young F. J., Wollenhaupt N. C., Barney T. L., Haithcoate T. W.*, 1995. Slope class maps from soil survey and digital elevation models. Soil Sci. Soc. Am. 59, pp. 509-519.
- Harlin J. M.*, 1984. Watershed morphometry and time to hydrograph peak, J. Hydrol., 67, pp. 141-154, doi:10.1016/0022-1694(84)90238-5.
- Helm, A., Braun, A., Eickschen, S., and Schune, T.*, 2002. Calibration of the shuttle radar topography mission X-SAR instrument using a synthetic altimetry data model. Canadian Journal of Remote Sensing, 28(4), pp. 573–580.
- Herrington L.*, 1998. Spatial Modeling: An Introduction to Raster GIS Using Idrisi. State University of New York College of Environmental Science and Forestry, Syracuse, NY, p. 186.
- Herron N., Peterson P.*, 2003. A simplified GIS-based approach to prioritize salinity investment at the property-scale. MODSIM Proceedings, Townsville, Australia
- Hobson R.D.*, 1972. Surface roughness in topography: a quantitative approach. In: Chorley, R.J. (Ed.), Spatial Analysis in Geomorphology. Harper & Row, pp. 221-245.

- Holmgren P.*, 1994. Multiple flow direction algorithms for runoff modelling in grid based elevation models: An empirical evaluation, *Hydrological Processes*, pp. 327–334.
- Horn B.*, 1981. Hill Shading and the Reflectance Map. *Proceedings of the IEEE*, Vol. 69, No. 1, pp. 14-47.
- Horton R. E.*, 1932. Drainage basin characteristics. *Transaction of American Geological Union*, 13, pp. 350-351.
- Horton R. E.*, 1945. Erosional development of streams and their drainage basins: hydro-physical approach to quantitative morphology. *Geological Society of America Bulletin* 56 (3), pp. 275–370.
- Horton R.E.*, 1932. Drainage-basin characteristics. *EOS Transactions of AGU*, 13, pp. 350-361.
- Howard A., Kerby G.*, 1983. Channel changes in badlands. *Geological Society of America Bulletin*, v. 94, pp. 739-752.
- Howard J. A., Mitchell C. W.*, 1985. *Phytogeomorphology*. John Wiley and Sons, Inc., p. 222.
- <http://www.opentopography.org/index.php/blog/detail/comparison of aster gdem to srtm>
- Huang J., Turcotte D. L.*, 1989. Fractal mapping of digitized images: Application to the topography of Arizona and comparisons with synthetic images. *Journal of Geophysical Research*, 94, pp. 7491-7495.
- Hunter, G. and Goodchild, M.*, 1997. Modeling the Uncertainty of Slope and Aspect Estimates Derived From Spatial Databases, *Geographical Analysis*, Vol. 29, No. 1, pp. 35-49.
- Hutchinson, C.F.*, 1982. Techniques for Combining Landsat and Ancillary Data for Digital Classification Improvement. *Photogrammetric Engineering and Remote Sensing*, Vol. 48, No.1, pp. 123-130.
- Imamura G.*, 1937. Past glaciers and the present topography of the Japanese Alps. In: *Science Reports of Tokyo Bunrika Daigaku*, vol. C.7. Tokyo Bunrika Daigaku, p. 61.
- Jarvis, A., Rubiano, J., Nelson, A., Farrow, A., and Mulligan, M.*, 2004. Practical use of SRTM data in the tropics – comparisons with digital elevation models generated from cartographic data. Working Document, Vol. 198. Centro Internacional de Agricultura Tropical (CIAT) p. 32.
- Jenson S.K., Domingue, J.O.*, 1988. Extracting topographic structure from digital elevation model data for geographic information system analysis. *Photogrammetric Engineering and Remote Sensing*. 54, pp. 1593-1600.
- Kellndorfer, J., Walker, W., Pierce, L., Dobson, C., Fites, J. A., Hunsaker, C., et al.*, 2004. Vegetation height estimation from shuttle radar topography mission and national elevation datasets. *Remote Sensing of Environment*, 93, pp. 339-358.
- Kennelly P.*, 2002. GIS Applications to Historical Cartographic Methods to Improve the Understanding and Visualization of Contours. *Journal of Geoscience Education*.50(4), pp. 428-436.

- Kennelly P., Kimerling A. J.*, 2001. Modifications of Tanaka's Illuminated Contour Method. *Cartography and Geographic Information Sciences*. 28, pp. 111-123.
- Kirkby M.J., Chorley R.J.*, 1967. Through flow, overland flow and erosion. *Internat. Assoc. Sci. Hydrol. Bull.*, v. 12, No.3, p. 5-21.
- Klinghammer I., Loránd E.*, 1991. Relief representation. RW Anson and FJ Ormeling (eds), *Basic cartography. Exercise manual*, pp 161-176. International Cartographic Association and Elsevier, London and New York.
- Klinkenberg B., Goodchild M. F.*, 1992. The fractal properties of topography: A comparison of methods. *Earth Surface Processes and Landforms*, 17, pp. 217-234.
- Knighton D.*, 1999. Downstream variation in stream power. *Geomorphology* 29, pp. 293-306.
- Koch, A., and Lohmann, P.*, 2000, Quality assessment and validation of digital surface models derived from the shuttle radar topography mission (SRTM). *Proceedings, IAPRS, Vol. XXXIII*, Amsterdam, 2000.
- Koenderink J. J., Van Doorn A. J.*, 1994. Two-plus-one dimensional differential geometry. *Pattern Recognition Letters*, 15(5), pp. 439–443.
- Koethe R., Lehmeier F.*, 1996. SARA, System zur Automatischen Relief-Analyse. Benutzerhandbuch, 2. Auflage [Geogr. Inst. Univ. Goettingen, unpublished]
- Lactochkin A.N., Lopatin D.V.*, 2005. *Geomorphology: A Textbook for students of high education institutions*. Moscow, Publishing House Academy. p. 528 (in Russian).
- Lam N.S.*, 1983. Spatial interpolation methods: a review. *The American Cartographer* 10, pp.129-149.
- Langbein, W. B.*, 1947. Topographic characteristics of drainage basins. United States Geological Survey, Water Supply Paper 968-C, pp. 125-157.
- Lawrence G. E. Jr.*, 1976. A computer-based insolation mapping algorithm for large areas. M.S. Thesis. VPI and SU, Blacksburg, VA. p. 95.
- Lee, J., Snyder, P., Fisher, P.*, 1992. Modeling the Effect of Data Errors on Feature Extraction From Digital Elevation Models, *Photogrammetric Engineering and Remote Sensing*, Vol. 58, No. 10, pp. 1461-1467.
- Li, Z.*, 1988. On the Measure of Digital Terrain Model Accuracy, *Photogrammetric Record*, Vol. 12, No. 72, pp. 873-877.
- Li, Z., Zhu, Q. and Gold, C.*, 2005. *Digital Terrain Modelling: Principles and Methodology*, Boca Raton: CRC Press.
- Linnartz N. E.*, 1961. Pine site index is related to soil classification in southeastern Louisiana. La. Agr. Exp. Sta., Forest. Note 48. Baton Rouge, LA. p. 2.
- Lovejoy S., Schertzer D.*, 1995. How bright is the coast of Brittany. Wilkinson, G, Kanellopoulos, I. and Mégier, J. (eds) *Fractals in Geosciences and Remote Sensing*. Joint Research Centre, Report EUR 16092 EN. pp. 102-151
- Luchisheva A.A.*, 1950. *Practical Hydrology*, Gidrometeoizdat, Leningrad (In Russian).
- Luo W.*, 2000. Quantifying groundwater-sapping landforms with a hypsometric technique. *J. Geophys. Res.*, 105, pp. 1685-1694, doi:10.1029/1999JE001096.

*Luo, W., Harlin J.M.,* 2003. A theoretical travel time based on watershed hypsometry. *J. Am. Water Resour. Assoc.*, 39, pp.785–792, doi:10.1111/j.1752-1688.2003.tb04405. x.

*Mandelbrot B.,* 1982. The fractal geometry of nature. Freeman, San Francisco, 460 pp.

*Mandelbrot B.B.,* 1967. How long is the coast of Britain? Statistical self-similarity and fractional dimension. *Science* 156, pp. 636-638.

*Mandelbrot B.B.,* 1975. Stochastic models of the Earth's relief, the shape and the fractal dimension of coastlines, and the number-area rule for islands. *Proceedings of the National Academy of Sciences* 72, pp. 3825-3828.

*Mandelbrot B.B.,* 1977. Fractals: Form, Chance and Dimension. San Francisco, CA: W.H. Freeman and Company.

*Mandelbrot B.B.,* 1982. The Fractal Geometry of Nature. New York: W.H. Freeman and Company.

*Mandelbrot B.B.,* 1986. Self-affine fractal sets. Pietronero, L. and Tosatti, E. (eds) *Fractals in Physics*, Holland, pp. 3-28.

*Marani M., Eltahir E. Rinaldo A.,* 2001. Geomorphic controls on regional base flow. *Water Resource. Res.*, 37, pp. 2619 – 2630, doi:10.1029/2000WR000119.

*Mark D.M.,* 1974. A comparison of computer based terrain storage methods with respect to the evaluation of certain geomorphometric measures. Unpub. MA thesis, U. British Columbia (Geog. Dept.), Vancouver, Canada, p 171.

*Mark D. M.,* 1978. Topological properties of geographic surfaces: applications in computer cartography. Harvard Papers on Geographic Information Systems, Laboratory for Computer Graphics and Spatial Analysis, Harvard University, Cambridge, Mass., vol. 5, Mark 1 - Mark 11.

*Mark D.M.,* 1979. Phenomenon-based data-structuring and digital terrain modelling. *Geo-processing*, 1, pp. 27-36.

*Mark D. M.,* 1984. Automatic detection of drainage networks from digital elevation models. *Cartographica* 21(2/3), pp.168-178.

*Mark D.M., Aronson P.B.,* 1984. Scale dependent fractal dimensions of topographic surfaces: An empirical investigation, with applications in geomorphology and computer mapping. *Mathematical Geology*, 16, pp. 671-683.

*Mark D.,* 1988. Network Models in Geomorphology. Modeling in Geomorphological Systems, John Wiley and Sons, New York, NY.

*Mark, D.M., Smith, B.,* 2004. A science of topography: from qualitative ontology to digital representations. In: Bishop, M.P., Shroder, J.F. (Eds.), *Geographic Information Science and Mountain Geomorphology*. Springer–Praxis, Chichester, England, pp. 75–97.

*Marković M.,* 1983. *Applied Geomorphology*. Beograd (in Serbian).

*Martz L., de Jong E.,* 1988. CATCH: a FORTRAN program for measuring catchment area from digital elevation models. *Computers and Geosciences*, 14(5), pp.627-640.

- Maxwell J.C.* 1870. On contour lines and measurements of heights. In London, Edinburgh and Dublin Philosophical Magazine and Journal of Science, 40, pp.421-427.
- McCullagh M.J., Ross C. J.*, 1980. Delaunay triangulation of a random data set for arithmetic mapping. The Cartographic Journal 17, pp.93-99.
- McCullagh M.J.*, 1988. Terrain and surface modelling systems: theory and practice. Photogrammetric Records 12, pp.747-779.
- McKenna D.G.*, 1987. The inward spiral method: an improved TIN generation technique and data structure for land planning applications. Proc. Auto-Carto 8, pp. 670-679.
- Melton M.A.*, 1958. Geometric properties of mature drainage basins and their representation in a E4 phase space. Journal of Geology 66, pp. 35-54.
- Melton M.A.*, 1965. The geomorphic and paleoclimatic significance of alluvial deposits in southern Arizona. Journal of Geology 73, pp.1-38.
- Metzler S.*, 2009. First Look at ASTER GDEM, ISCIENCES, L.L.C., September 24th, <http://geoserver.isciences.com/DataBlog/?p=263>
- Miliaresis, G.*, 2008. Quantification of Terrain Processes. Lecture Notes in Geoinformation and Chartography, 14, pp. 13-28.
- Miliaresis, G.; Kokkas, N.*, 2007. Segmentation and Object Based Classification for the Extraction of Building Class from LIDAR DEMs. Comput. Geosci., 33, pp. 1067-1087.
- Miller V.C.*, 1953. A quantitative geomorphic study of drainage basin characteristics in the Clinch Mountain area, Virginia and Tennessee. Columbia University, Department of Geology, Technical Report, No.3, Contract N6 ONR, pp. 271-300.
- Miller C. and Laflamme R.*, 1958. The digital terrain model – theory and applications, Photogrammetric Engineering, 24 pp. 433-442.
- Mimura T., Hasegawa S., Yamanaka M., Dahal R.K., Nonomura A.*, 2008. Drainage density as a possible index for landslide scale. Symposium on Geohazards and Geo-environment, Shikoku branch of the Japanese Geotechnical Society, vol.8, pp.11-18.
- Mitasova H., Hofierka J., Zlocha M., Iverson L.R.*, 1996. Modeling topographic potential for erosion and deposition using GIS. Int. Journal of Geographical Information Science, 10(5), pp. 629-641.
- Mitchell S.J.*, 1995. The wind throw triangle: a relative wind throw hazard assessment procedure for forest managers. For. Chron. (Ottawa: Canadian Inst. of For.) 71, pp. 446-450.
- Moglen, G.E., Bras R.L.*, 1995. The effect of spatial heterogeneities on geomorphic expression in a model of basin evolution. Water Resour. Res., 31, pp. 2613– 2623, doi:10.1029/95WR02036.
- Monckton, C.*, 1994. Chapter 14: An Investigation into the spatial structure of error in digital elevation data. In: Innovations in GIS Volume 1 Edited by M. Worboys, Taylor and Francis, Bristol, PA, 267 pp.

*Montgomery D.R., Dietrich W. E.,* 1995. Hydrologic processes in a low-gradient source area, Water Resources Research, v.31, no. 1, pp. 1-10.

*Moore I.D., Nieber J.L.,* 1989. Landscape assessment of soil erosion and nonpoint source pollution. In: Minnesota's water resources; a collection of papers to commemorate the 25th anniversary of the founding of the Water Resources Research Center at the University of Minnesota, editors: Brezonik, Patrick L., and James A. Perry, Journal of the Minnesota Academy of Science. 55; 1, Pages 18-25.

*Moore I., Grayson R, and Ladson A.,* 1991. Digital Terrain Modelling: A Review of Hydrological, Geomorphological, and Biological Applications. Hydrological Processes, Vol. 5, pp. 3-30.

*Moore I.D., Burch G.J.,* 1986. Sediment Transport Capacity of Sheet and Rill Flow: Application of Unit Stream Power Theory. Water Resources Research, Vol. 22, No. 8, pp. 1350-1360.

*Moore I.D., Lewis A., Gallant J.C.,* 1993. Terrain attributes: estimation methods and scale effects. In Jakeman, A.J., M.B. Beck and M.J. McAleer, ed. Modelling Change in Environmental Systems. Chichester: John Wiley & Sons Ltd. pp. 189-214.

*Moore I.D., Wilson J.P.,* 1992. Length-slope factors for the revised universal soil loss equation: simplified method of estimation. Journal of Soil and Water Conservation, 47(5), pp. 423-428.

*Morris, D. G., Heerdegen R. G.,* 1988. Automatically derived catchment boundaries and channel networks and their hydrological applications. Geomorphology 1, pp. 131-141.

*Muick P., Bartolome J.W.,* 1987. Factors associated with oak regeneration in California. p. 86-91. in T. R. Plumb and N. H. Pilsbury. (Tech Coords.). Proceedings of the symposium on multiple use management of California's hardwood resources. Pacific Southwest Forest and Range Experiment Station, USDA for. Serv., Berkeley, CA.

*Mulders M.A.,* 1987. Remote sensing in soil science. Elsevier, Amsterdam.

*Muller, J. P.,* 2005. Quantitative assessment of C-band and X-band SRTM datasets over the CEOS-WGCV-TMSG test sites and intercomparison of C-band DEM with the OS® PANORAMA DTM. The Shuttle Radar Topography Mission – Data Validation and Applications, Workshop, June 14–16, 2005, Reston, Virginia.

*NASA/JPL,* 2005. SRTM Topography (SRTM documentation). 8 pp. Available at [ftp://e0srp01u.ecs.nasa.gov/srtm/version2/Documentation/SRTM\\_Topo.pdf](ftp://e0srp01u.ecs.nasa.gov/srtm/version2/Documentation/SRTM_Topo.pdf)

*Niemann, K.O.,* 1991. Landscape drainage modeling to enhance Landsat classification accuracies. geocarto international, No.1. pp. 13-30.

*O'Callaghan J.F., Mark D.M.,* 1984. The extraction of drainage networks from digital elevation data, Computer Vision, Graphics, and Image Processing, (28), pp. 323–344.

*Oberlander T.M.,* 1985. Origin of drainage transverse to structures in orogens. in Morisawa, M., and Hack, J.T., eds., Tectonic geomorphology: New York, Allen & Unwin, pp. 155–182.

*Ohmori H.*, 1993. Changes in the hypsometric curve through mountain building resulting from concurrent tectonics and denudation. *Geomorphology*, 8, pp. 263–277, doi :10.1016/0169-555X (93)90023-U.

*Olaya V.*, 2009. Basic land surface parameters, Geomorphometry concept, software, applications, Developments in soil Sciences-V.33 Elsevier, U.K. pp. 141-169.

*Olaya V., Conrad O.*, 2006. Geomorphometry in SAGA. In: Hengl, T. & Reuter, H.I. (Eds.). *Geomorphometry: Concepts, Software, Applications*.

*Olivera F., Maidment D.R.*, 1999. GIS Tools for HMS Modeling Support. Proceedings of the 19th ESRI Users Conference, San Diego, CA (this issue).

*Osmond C. B., Pitelka, L. F., Hidy. G. M.*, 1990. Plant biology of the Basin and Range. Springer-Verlag Berlin Heidelberg. New York, NY. p .375.

*Partsh J.*, 1911. Schlesien, eine Landeskunde fur das deutsche Volk.II, S.586, Breslau.

*Pearson R.N.*, 1968. Physical geography. Barnes and Noble, New York, NY. p.242.

*Peddle D.R., Duguay C. R.*, 1995. Incorporating topographic and climatic GIS data into satellite image analysis of an alpine tundra ecosystem, Front Range, Colorado Rocky Mountains. *Geocarto International* 10(4), pp. 43-60.

*Péguy C.P.*, 1942. Principes de morphométrie alpine. *Revue de Géographie Alpine* 30, pp. 453–486.

*Péguy C.P.*, 1948. Introduction à l'emploi des méthodes statistiques en géographie physique. *Revue de Géographie Alpine* 36, pp. 5–101.

*Peitgen H. O., Jurgens H., Saupe D.*, 1992. Chaos and Fractal: New Frontiers of Science. Springer, New York, p.984.

*Peucker T. K., Fowler R.J., Little J.J., Mark D.M.*, 1979. The triangulated irregular network. *Proc. AutoCarto* 4, vol 2, pp. 96-103.

*Peucker T.K.*, 1980. The use of computer graphics for displaying data in three dimensions. *Cartographica* 17, pp. 59-72.

*Peucker T.K., Douglas D.H.*, 1974. Detection of surface specific points by local parallel processing of discrete terrain elevation data. *Computer Graphics and Image Processing*, 4, pp. 375-387.

*Peucker T.K., Tichenor M. and Rase W. D.*, 1975. The computer version of three relief representations. Davis, J. C. and M. McCullagh (eds.). *Display and Analysis of Spatial Data*. New York: John Wiley and Sons. pp. 187-197.

*Pfaltz J.*, 1976. *Surface networks*. *Geographical Analysis*, vol. 8, pp. 77-93.

*Pike, R.J.*, 1995. Geomorphometry-process, practice and prospects, *Zeitschrift f. Geomorphologie N.F. suppl. Bd.*, pp. 221-238.

*Pike, R.J.*, 2000. Geomorphometry – diversity in quantitative surface analysis. *Progress in Physical.*

*Pilesjö P.*, 1994. Estimation of drainage directions – A new method. *Proceedings of the 7th Australasian Remote Sensing Conference*, 1-4 March, Melbourne, pp. 328-332.

*Pilesjö P., Zhou Q.*, 1996. A multiple flow direction algorithm and its use for hydrological modelling, Geoinformatics'96 Proceedings, April 26–28, West Palm Beach, FL, pp. 366-376.

*Pilesjö P., Zhou Q.*, 1997. Theoretical estimation of flow accumulation from a grid-based digital elevation model, Proceedings of GIS AM/FM ASIA'97 and Geoinformatics'97 Conference, 26–29 May, Taipei, pp. 447–456.

*Pilesjö P., Zhou Q., Harrie L.*, 1998. Estimating flow distribution over Digital Elevation Models using a Form-Based Algorithm. Geographic Information Science, pp. 44-51.

*Pogorelov A.V., Doumit J.A.*, 2007. Morphometry of the Kuban River basin relief: some results of numerical modeling. Geographical studies of Krasnodar region: Sat scientific. tr. Vol. 2. - Krasnodar: Kuban State University. pp. 7-23. (In Russian).

*Pogorelov A.V., Doumit J.A.*, 2008. Classification and allocation of the discrete morphological elements of the digital elevation model //Actual problems of ecology and conservation of ecosystems of southern regions of Russia and adjacent areas: Proceedings of the twentieth inter-republic scientific-practical conference. - Krasnodar: Kuban State University, pp. 107-109. (In Russian).

*Pogorelov A.V., Doumit J.A.*, 2009. Relief of the Kuban river basin: Morphometrical analysis. GEOC. Moscow. P. 208. (In Russian).

*Polidori, L., Chorowicz, J., and Guillande, R.*, 1991. Description of Terrain as a Fractal Surface and Application to Digital Elevation Model Quality Assessment, Photogrammertic Engineering and Remote Sensing, Vol. 57, No. 10, pp. 1329-1332.

*Quinn P., Beven K., Chevallier P., Planchon O.*, 1991. The Prediction of Hillslope Flow Paths for Distributed Hydrological Modelling Using Digital Terrain Models, Hydrological Processes, Vol. 5, pp. 59-79.

*Quinn P., Beven K., Lamb R.*, 1995. The ln(a/TanB) index: how to calculate it and how to use it within the TOPMODEL framework. Hydrological Processes, Vol. 9, pp. 161-182.

*Rehfeld G. E.*, 1993. Genetic variation in the Ponderosae of the Southwest. Amer. J. Botany 80(3), pp. 330-343.

*Renard K., Foster G.R., Weesies G.A. Porter J.P.* 1991. RUSLE Revised universal soil loss equation. Journal of Soil and Water Conservation, 46, pp.30-33.

*Reuter H. I.; Nelson A.; Jarvis A.*, 2007. An evaluation of void-filling interpolation methods for SRTM data International Journal of Geographical Information Science, Volume 21, Issue 9 January 2007, pp. 983 – 1008

*Richardson L.F.*, 1961. The problem of contiguity: an appendix of statistics of deadly quarrels. General Systems Yearbook, 6, pp. 139-187.

*Rieger J. H.*, 1997. Topographical properties of generic images. International Journal of Computer Vision, 23(1), pp. 79–92.

*Rieger W.* 1993. Hydrological terrain features derived from a pyramid raster structure. K Kovar and H P Natchnebel (eds), Application of Geographical Information

Systems in hydrology and water resources management, IAHS Publication num. 211, Oxfordshire.

*Riley C and Moore McM.*, 1993. Digital elevation modelling in a study of the neotectonic geomorphology of the Sierra Nevada, southern Spain. *Zeitschrift fur Geomorphologie N. F.*, Suppl.-Bd. 94, pp. 25-39.

*Ritter P.*, 1987. A vector-based slope and aspect generation algorithm. *Photogrammetric Eng. and Remote Sensing* 53, pp. 1109-1111.

*Rodriguez, E.; Morris, C.S.; Belz, J.E.*, 2006. A Global Assessment of the SRTM Performance. *Photogramm. Eng. Remote Sens.* 72, pp. 249–261.

*Rothe Z.R.*, 1915. Problem des Talwegs. In *Sitzungsberichte der Berliner Mathematischen Gesellschaft*, volume XIV, pages 51–68, Leipzig, B. G. Teubner Verlag.

*Ruhe R.V., Walker P.H.*, 1968. Hillslope models and soil formation. I. Open systems. *Trans 9th Int Congr Soil Sci (Adelaide, Australia) IV*, pp.551–560.

*Rutter J. W.*, 2000. *Geometry of Curves*. Chapman & Hall/CRC.

*Ryder W. and Voyadgis D.*, 1996. Measuring the Performance of Algorithms for Generating Ground Slope. pp. 208-216, In: *Spatial Accuracy Assessment in Natural Resources and Environmental Sciences: Second International Symposium*, United States Department of Agriculture, Rocky Mountain Forest and Range Experiment Station, Fort Collins, CO, Report RM-GTR-277.

*Sakude M.T., Schiavone G.A., Morelos-Borja H., Martin G., Cortes A.*, 1998. Recent advances on terrain database correlation testing. *Proceedings of SPIE* 3369, pp. 364-376.

*Scarlatos L. L.*, 1989. An automated critical line detector for digital elevation matrices. *Proc. Auto-Carto 9*, pp.146-155.

*Schertzer D., Lovejoy S.*, 1995. Standard and advanced multifractal techniques in remote sensing. Wilkinson, G, Kanellopoulos, I. and Mégier, J. (eds). *Fractals in Geosciences and Remote Sensing*, Joint Research Centre, Report EUR 16092 EN. pp.11-40.

*Schmidt J., Evans I.S., Brinkmann J.*, 2003. Comparison of polynomial models for land surface curvature calculation. *International Journal of Geographical Information Science*, 17(8), pp.797-814.

*Schumm S.* 1956. Evolution of drainage systems and slopes in badland at Perth Amboy, New Jersey. *Bulletin of Geological Society of America*,67, pp. 597-646.

*Schumm S.A.*, 1965. Quantitative geomorphology of drainage basins and channel networks: *Handbook of applied Hydrology*. Ed. Ven Te Chow, pp. 4:39-4:76.

*Scribner J. M., Giebink B. L., Snider D.*, 1991. Reciprocal latitudinal clines in oviposition behavior of *Papilio glaucus* and *P. canadensis* across the Great Lakes hybrid zone: possible sex-linkage of oviposition preferences. *Oecologia* 14, pp. 360-364.

*Shary P.A.*, 1995. *Land surface in gravity points classification by a complete system of curvatures*. *Mathematical Geology*, 27(3), pp.373-390.

*Shary P.A., Sharaya L.S., Mitusov A.V.*, 2002. Fundamental quantitative methods of land surface analysis. *Geoderma*, 107(1-2), pp. 1-32.

*Shary P.A., Sharaya L.S., Mitusov A.V.*, 2005. The problem of scale-specific and scale-free approaches in geomorphometry. *Geografia Fisica e Dinamica Quaternaria*, 28(1), pp. 81-101.

*Shoulders E., Tiarks A. E.*, 1980. Predicting height and relative performance of major southern pines from rainfall, slope, and available soil moisture. *For. Sci.* 26, pp. 437-447.

*Shreve R.L.*, 1966. Statistical law of stream numbers. *J. Geol.*, 74, pp. 17-37.

*Simpson D.W., Anders M.H.*, 1992. Tectonics and topography of the Western United States - an application of digital mapping. *GSA Today*, 2 pp. 118-121.

*Sivapalan M., Beven K. J., Wood E. F.* 1987. On hydrologic similarity, 2, A scaled model of storm runoff production, *Wat. Resour. Res.*, 23(12), pp. 2266-2278.

*Skidmore A.*, 1989. A Comparison of techniques for Calculating Gradient and Aspect from A Gridded Digital Elevation Model. *International Journal of GIS*, Vol. 3, No. 4, pp. 323-334.

*Slater, J.A.; Garvey, G; Johnston, C.; Haase, J.; Heady, B.; Kroenung, G.; Little J.*, 2006. The SRTM Data “Finishing” Process and Products. *Photogramm. Eng. Remote Sens.*, 72, pp. 237-247. Finished SRTM data; [http://seamless.usgs.gov/website/seamless/faq/srtm\\_faq.asp](http://seamless.usgs.gov/website/seamless/faq/srtm_faq.asp), 2007.

*Smart J. S., Surkan A. J.*, 1967. The relation between mainstream length and area in drainage basins. *Water Resource. Res.*, 3, pp. 963-974.

*Smith K. G.*, 1950. Standards for grading texture of erosional topography. *American Journal of Science*, 248, pp. 655-668.

*Smith, B., and Sandwell, D.*, 2003. Accuracy and resolution of shuttle radar topography mission data. *Geophysical Research Letters*, 30(9), p.1467.

*Soille P.*, 1988. Modeles numeriques de terrain et morphologie mathematique : D’elimination automatique de bassins versants. Master’s thesis, Universite catholique de Louvain, Louvain-la-Neuve, Belgique

*Soille P.*, 2002. Advances in the analysis of topographic features on discrete images. *Lecture Notes in Computer Science*, 2301, pp.175–186.

*Soille P., Ansoult M.*, 1990. Automated basin delineation from digital elevation models using mathematical morphology. *Signal Processing*, 20, pp.171-182.

*Soille P., Vogt J., Colombo R.*, 2003. Carving and adaptive drainage enforcement of grid digital elevation models. *Water Resources Research*, 39(12), pp.1366.

*Spiridonov A.I.*, 1975. Geomorphologic cartography. Moscow: Nedra, 184 p. (In Russian).

*Stage A. R.*, 1976. An expression for the effect of aspect, slope, and habitat type on tree growth. *For. Science* 22(4), pp. 457-460.

*Stepanov*, 2006. in The theory of plasticity of relief and new thematic maps. Moscow: Nauka, 230. (In Russian).

*Stepinski T. F., Coradetti S.*, 2004. Comparing morphologies of drainage basins on Mars and Earth using integral-geometry and neural maps. *Geophys. Res. Lett.*, 31, L15604, doi:10.1029/2004GL020359.

*Stock, J. D., Bellugi, D., Dietrich, W. E., and Allen, D.*, 2002. Comparison of SRTM topography to USGS and high resolution laser altimetry topography in steep landscapes: Case studies from Oregon and California. *Eos Trans. AGU, Fall Meet. Suppl.*, Abstract H21G-09, 2002, Vol. 83(47).

*Strahler A. N.*, 1952. Hypsometric (area altitude) analysis of erosional topography. *Geological Society of America. Bulletin* 63, pp. 1117-1142.

*Strahler A. N.*, 1957. Quantitative analysis of watershed geomorphology. *Transactions of the American Geophysical Union* 8 (6), pp. 913-920.

*Sun, G., Ranson, K. J., Kharuk, V. I., and Kovacs, K.*, 2003. Validation of surface height from shuttle radar topography mission using shuttle laser altimeter. *Remote Sensing of Environment*, 88, pp. 401-411.

*Susam T.*, 2002. The Different use of Hillshade image an application in Tokat Province. *Gaziosmanpasa University, International Symposium on GIS, Istanbul-Turkey*.

*Swanson F. J.*, 1979. Geomorphology and ecosystems. pp. 159-169 in R.H. Waring ed. *Forests: fresh perspectives from ecological analysis*. Proc. of the 40th annual biology colloquium. Oreg. State Univ. Press, Corvallis, OR.

*Swanson D. N., Dyrness C. T.*, 1973. Stability of steep land. *J. Forest* 71, pp.264-269.

*Tang L.*, 1992. Automatic Extraction of Specific Geomorphological Elements from Contours. in *Proceedings of the 5th International Symposium on Spatial Data Handling* (ed E.C.a.D.C.P. Bresnahan), Vol. 2, pp. 554-566. *IGU Commission of GIS, Charleston*.

*Tarboton D.*, 1997. A new method for the determination of flow directions and upslope areas in grid digital elevation models, *Water Resources Research*, Vol. 33, No. 2, pp. 309-319.

*Tarboton D., Bras R., Rodriguez-Iturbe I.*, 1993. On the extraction of channel networks from digital elevation data. *Terrain Analysis and Distributed Modeling In Hydrology*, Edited By: K. Beven, I.D. Moore, John Wiley and Sons, New York, NY, pp. 85-104.

*Theobald, D.*, 1992. Chapter 9: Accuracy and Bias Issues in Surface Representation, In: *The Accuracy of Spatial Databases*, Edited by Michael F. Goodchild and Sucharita Gopal, Taylor and Francis, Bristol, PA, pp. 99-106.

*Tobler, W.R.*, 1976. Analytical cartography. *The American Cartographer* 3 (1), 21–31. *Geography* 24 (1), pp.1–20.

*Tobler, W.R.*, 2000. The development of analytical cartography – a personal note. *Cartography and Geographic Information Science* 27 (3), pp. 189-194.

*Trewartha G.T., Smith, G.H.*, 1941. Surface configuration of the Driftless Cuestaform Hill Land. *Annals Assoc. Am. Geogr.*, v.31, pp. 25-45.

*Troeh F.R., Hobbs J.A., Donahue R.L.*, 1991. Chapter Six: Predicting Soil Loss. *Soil and Water Conservation*, 2nd ed. Prentice-Hall, Englewood Cliffs, New Jersey, USA.

- Turner H.*, 1997. A comparison of some methods for slope measurement from large-scale air photos. *Photogrammetria*, 32, pp.209–237.
- Turner L. M.*, 1936. Factors influencing the rate of growth of pine in Arkansas. *Ecology* 17, pp.227-240.
- Turner L. M.*, 1937. Growth of second-growth pine on the coastal plain soils of Arkansas. *Arkansas Agr. Exp. Sta., Bull.* 342. Fayetteville, AK. p. 52.
- Turner L. M.*, 1938. Some profile characteristics of the pine-growing soils of the coastal plain region of Arkansas. *Arkansas Agr. Exp. Sta., Bull.* 361. Fayetteville, AK. p. 52.
- United States Geological Survey (USGS)*, 1997. Standards for Digital Elevation Models, Part 1: General, Part 2: Specifications, Part3: Quality Control. Department of the Interior, Washington, DC.
- Verstappen H. T.* 1983. Applied geomorphology. Elsevier Science Publishing Co. New York, NY. p. 437.
- Vincent L., Soille P.*, 1991. Watersheds in digital spaces: An efficient algorithm based on immersion simulations. *IEEE Transactions on Pattern Analysis and Machine Intelligence*, 13(6), pp. 583–598.
- Walsh S. J., Lightfoot D. R., Butler D. R.*, 1987. Recognition and assessment of error in geographic information systems. *Photogrammetric Eng. and Remote Sensing* 53, pp. 1423-1430.
- Warner, T.A., Levandowski, D.W., Bell, R. and Cetin, H.*, 1994. Rule-based Geobotanical Classification of Topographic, Aeromagnetic and Remotely Sensed Vegetation Community Data. *Remote Sensing of Environment*, No.50. pp. 41-51.
- Warntz W.*, 1966. The topology of a socio-economic terrain and spatial flows. *Papers, Regional Science Association*, 17, pp. 47-61.
- Wathen S. A.*, 1977. Maximum insolation on a surface as an estimator of site quality. M.S. Thesis. VPI and SU, Blacksburg, VA. p. 41.
- Way D. S.*, 1973. Terrain analysis: a guide to site selection using aerial photographic interpretation. Dowden, Hutchinson, and Ross Inc., Stroudsburg, PA. p. 392.
- Wentworth C.*, 1930. A simplified method for the determining the average slope of land surface. *American Journal of Science*, 20, pp. 184–194.
- Whipple K.X., Tucker G.E.*, 1999. Dynamics of the stream-power river incision model: Implications for height limits of mountain ranges, landscape response timescales, and research needs. *Journal of Geophysical Research*, v. 104, pp. 17 661–17 674.
- Willgoose G., Hancock G.*, 1998. Revisiting the hypsometric curve as an indicator of form and process in transport-limited catchment. *Earth Surf. Processes Landforms*, 23, pp.611–623,doi:10.1002/(SICI)1096 9837(199807)23:7<611:AIDESP872>3.0.CO;2-Y.
- Wilson J.P., Gallant J.C.*, 2000. Digital terrain analysis. In: Wilson, J.P., and Gallant, J.C. (Eds.), *Terrain Analysis: Principles and Applications*. Wiley, New York, pp. 1-28.
- Wilson T.H., Dominic. J.*, 1998. Fractal Interrelationships between Topography and

Structure. *Earth Surface Processes and Landforms*, vol.23, pp. 509-525.

*Wischmeier W.H., Smith D.D.*, 1978. Predicting rainfall erosion losses – A guide to conservation planning. Agricultural Handbook no. 537, Sci. and Educ. Admin., U.S. Dept. Agr., Washington, D.C.

*Wolock D., McCabe G.*, 1995. Comparison of single and multiple flow direction algorithms for computing topographic parameters, *Water Resources Research*, Vol. 31, No. 5, pp. 1315-1324.

*Wood J.*, 1996. Morphometric Characterization in The Geomorphological Characterization of Digital Elevation Models. PhD Thesis, University of Leicester.

*Wood, J.*, 1996. The Geomorphological Characterization of Digital Elevation Models. Ph.D. Dissertation, Department of Geography, University of Leicester, Leicester, UK, 1996.

*Wu I. P., Delleur J. W., Diskin M. H.*, 1964. Determination of peak discharges and design hydrographs for small watersheds in Indiana. School of Civil Engineering, Purdue University, Indiana.

*Yoeli P.*, 1976. Computer-aided relief presentation by traces of inclined planes. *The American Cartographer* 3(1), pp. 75-85.

*Zahner R.*, 1958. Site quality relationships of pine forests in southern Arkansas and northern Louisiana. *Forest Sci.* 4, pp. 162-176.

*Zevenbergen L., Thorne C.*, 1987. Quantitative Analysis of Land Surface Topography, *Earth Surface Processes and Landforms*, Vol. 12, pp. 47-56.

*Zhilin Li., Qing Zhu, Chris Gold*, 2004. Digital terrain modeling: principles and methodology, Library of Congress. pp. 1-318.

*Zukowskyj P., Teeuw R., Munro O.*, 2000. Interpolated Digital Elevation Models, Differential Global Positioning System Surveys and Digital Photogrammetry: A Quantitative Comparison of Accuracy from a Geomorphological Perspective. Environmental Sciences Department, University of Hertfordshire, College Lane, Hatfield, Herts. AL10 9AB, UK..<http://www.geocomputation.org/2000/GC002/Gc002.htm>

<http://srtm.cgiar.org/>

<http://technology.slashgeo.org/technology/09/08/17/1322244.shtml>

<http://www.ersdac.or.jp/GDEM/E/4.html>

<http://www.terrainmap.com/rm51.html>

# Table of Contents

	<i>pages</i>
Acknowledgements	3
Preface	4
<b>Introduction</b>	<b>5</b>
<b>1. Digital Elevation Modeling</b>	<b>10</b>
1.01 Shuttle Radar Topography Mission (SRTM)	13
1.02 Global Digital Elevation Map (GDEM)	16
1.03 Data Set Comparisons	17
1.04 Errors in Digital Elevation Models	19
1.05 DEM Error Constitutes Uncertainty	20
1.06 Non-Spatial DEM Characterization	21
<b>2. Terrain Representation</b>	<b>24</b>
2.01 Analytical Hillshading	25
2.02 Slope	28
2.03 Estimation of Slope	33
2.04 Aspect	34
<b>3. Morphometric Characterization and Hydrological Assessment</b>	<b>40</b>
3.01 Fill Sinks	40
3.02 Flow Direction	43
3.02.1 The Single Flow – D8 Algorithm	43
3.02.2 The Rho8 Algorithm	46
3.02.3 Multiple-Direction Algorithms	46
3.02.4 Topographic Form-Based Algorithm	47
3.02.5 The DEMON Algorithm	47
3.02.6 GIS Applied Algorithm	48
3.03 Flow Accumulation	49
3.04 Stream Order	52
3.05 Watershed Basins	56
<b>4. Hypsometry</b>	<b>65</b>
4.01 Geographical Characteristics and Data Sets	65
4.02 Hypsometry of Lebanon	66
4.03 The Hypsometric Curve	70
<b>5. Terrain Structure Lines</b>	<b>75</b>
5.01 Main Channel and Valley Lengths	75
5.02 Bifurcation Ratio	76
5.03 Length Ratio	79
5.04 Watershed Eccentricity	81
5.05 Stream Orientation	82
5.06 Fractal Dimension	83

<b>6. Areal Morphometry</b>	<b>86</b>
6.01 Circularity Ratio ( $R_c$ )	92
6.02 Elongation Ratio ( $EL$ )	93
6.03 Lemniscate Ratio	94
6.04 Form Factor ( $F$ )	95
6.05 Unity Shape Factor ( $U$ )	95
6.06 Fractal Dimension ( $FD$ )	96
<b>7. Terrain Quantitative Analysis (Morphometry)</b>	<b>97</b>
7.01 Basin Relief	97
7.02 Local Relief	98
7.03 Relative Relief ( $Rh$ )	100
7.04 Relief Ratio ( $Rp$ )	101
7.05 Ruggedness Number ( $Rn$ )	101
7.06 Terrain Roughness	102
7.07 Anisotropy	104
7.08 Fractal Dimensions	107
<b>8. Curvature</b>	<b>114</b>
8.01 Inflexion Points	117
8.02 Plan and Profile Curvature	118
8.03 Terrain Convergence	123
8.04 Curvature Classification	123
8.05 Morphometric Features	126
<b>9. Terrain Indices</b>	<b>131</b>
9.01 Compound Topographic Index (CTI)	131
9.02 Stream Power	134
9.03 LS Factor	137
9.04 Conclusion of all Indices	139
<b>Conclusion</b>	<b>140</b>
<b>Reference</b>	<b>142</b>

*Scientific edition*  
**DIGITAL TERRAIN ANALYSIS OF LEBANON:  
A STUDY OF GEOMORPHOMETRY**  
*Печатается в авторской редакции*

---

Подписано в печать 30.03.2017 Формат 60×84 1/16.  
Печать цифровая. Уч-изд. л. 24,25. Тираж 150 экз.  
Заказ №

Кубанский государственный университет.  
350040, г. Краснодар, ул. Ставропольская, 149.  
Издательско-полиграфический центр КубГУ.



**Dr. Jean Albert Doumit** received his Ph.D. in Geo-Sciences from Kuban State University, in the Russian Federation. He has since worked as a part time faculty member at several universities throughout Lebanon. Currently, Dr. Doumit is a full-time Associate Professor in Geography, in the faculty of Literatures and Human Sciences, at the Lebanese University.

He teaches subjects in Remote Sensing and Geospatial Information Science and Technology. His research interests include Digital Cartography, Geospatial Data Analysis, Remote Sensing, and GIS among others.

Dr. Doumit is a recipient of multiple international awards for his success and findings in Scientific Research, and is an author/coauthor of several scientific books and publications.

